

Summer 2017

# Epikarst Hydrogeochemical Changes in Telogenetic Karst Systems in South-central Kentucky

Leah Jackson

Western Kentucky University, leah.jackson073@topper.wku.edu

Follow this and additional works at: <http://digitalcommons.wku.edu/theses>



Part of the [Geology Commons](#), and the [Speleology Commons](#)

---

## Recommended Citation

Jackson, Leah, "Epikarst Hydrogeochemical Changes in Telogenetic Karst Systems in South-central Kentucky" (2017). *Masters Theses & Specialist Projects*. Paper 2018.

<http://digitalcommons.wku.edu/theses/2018>

This Thesis is brought to you for free and open access by TopSCHOLAR®. It has been accepted for inclusion in Masters Theses & Specialist Projects by an authorized administrator of TopSCHOLAR®. For more information, please contact [topscholar@wku.edu](mailto:topscholar@wku.edu).

EPIKARST HYDROGEOCHEMICAL PROCESSES IN TELOGENETIC KARST  
SYSTEMS IN SOUTH-CENTRAL KENTUCKY

A Thesis  
Presented to  
The Faculty of the Department of Geography and Geology  
Western Kentucky University  
Bowling Green, Kentucky


In Partial Fulfillment  
of the Requirements for the Degree  
Master of Science

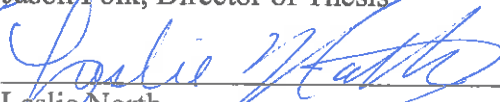
By  
Leah E. Jackson

August 2017

EPIKARST HYDROGEOCHEMICAL PROCESSES IN TELOGENETIC KARST  
SYSTEMS IN SOUTH-CENTRAL KENTUCKY

Date Recommended 4 July 2017

  
\_\_\_\_\_  
Jason Polk, Director of Thesis

  
\_\_\_\_\_  
Leslie North

  
\_\_\_\_\_  
Patricia Kambesis

  
\_\_\_\_\_  
Dean, Graduate School

7/13/17  
Date

## ACKNOWLEDGEMENTS

The decision to become a graduate student is not one made lightly. Graduate student life is an arduous and grueling, demanding, yet exciting experience, riddled with challenges that require dedication and fortitude to master.

I jumped into graduate school head first, with eyes open, eager, and ready and willing to face whatever obstacles stood in my way. Like most other new recruits, I was naive about the reality of graduate student life - a life that requires sacrifice, extreme hard work, perseverance, and constant flexibility. Further, being a graduate student means consistently stepping out of preconceived comfort zones, pushing personal limits, raising the bar ever higher, and discovering one's true potential. I owe my survival and accomplishments to a great many people.

First and foremost, I want to thank my advisor Dr. Jason Polk. You ensured I gained the most comprehensive, measurable, and thorough graduate school experience possible. You pushed me consistently to work hard, taught me to reevaluate every aspect from multiple angles, and trained me to be the best Earth Scientist I can be. To my committee members, Dr. Leslie North and Dr. Pat Kambesis, I thank you for entertaining my concerns and helping me celebrate my achievements. I thank you for supporting my thesis topic switch at the 11<sup>th</sup> hour and working with me to ensure I completed my degree on time.

To Dr. Margaret Crowder, I thank you for taking me under your wing to demonstrate the finest methods toward delivering a university level education. I have learned so much from you about what makes a great professor. Your unsurpassed advice and ongoing support have helped me grow into a confident instructor.

To Pauline Norris at AMI and Dr. Suvankar Chakraborty at SIRFER: thank you for ensuring my samples were handled properly. Without your ongoing assistance, this thesis wouldn't exist.

To all the members at CHNGES: thank you for all your help conducting field work, processing mountains of data, and aiding me in putting all the pieces together. Without your assistance and guidance, I would not be writing this acknowledgements section, much less a thesis. To one of my most favorite follow graduate students, Jason Lively - I thank you for indulging my grievances and joining me on all those evening stomping sessions through the mall. I never would have survived my first year without your ear to bend.

To all the folks in the graduate student office: Autumn, Brita, CeCe, and the international ladies Dolly, Indu, and Anisha; you showed me the world through a universal lens, helping me to develop a deeper appreciation for cultures other than my own, while simultaneously bringing levity and enjoyment to otherwise stress-laden situations.

Last, but certainly not least, I thank my personal heroes: Mike and John. Mike, I thank you for all those long, multi-hour-length, late-night phone sessions where you helped me work out my concerns in a logical and rational manner. You offered sound advice, an objective perspective, and a palette of humor I'll never forget.

John, you have served as my best friend throughout this adventure. You have counseled me through issues both professional and personal, but always doing it with a witty style. Your words of encouragement, everlasting support, and eclectic humor have

reinvigorated this road-worn student to complete what seemed to be only a dream a mere two years ago.

# TABLE OF CONTENTS

Chapter 1: Introduction .....	1
Chapter 2: Literature Review .....	4
2.1 Karst Landscapes .....	4
2.2 Epikarst Theory.....	13
2.3 Carbon Processes in Karst .....	20
2.3.1 CO <sub>2</sub> Dissolution Kinetics.....	20
2.3.2 δ <sup>13</sup> C <sub>DIC</sub> Isotope Sourcing and Flux .....	26
Chapter 3: Study Area.....	33
3.1 Crumps Cave at Smith’s Grove, KY.....	34
3.2 Lost River Cave and Valley in Bowling Green, KY .....	38
Chapter 4: Methods.....	41
4.1 Site Selection and Instrument Installation .....	41
4.2 Field Data and Sample Collection .....	44
4.3 Sample Analysis.....	47
4.4 Data Manipulation and Processing .....	48
4.4.1 Hydrogeochemical Data Processing .....	48
4.4.2 Carbon Isotope Sourcing.....	51
4.4.3 LRS Hydrograph Generation .....	52
Chapter 5: Results .....	54
5.1 Epikarst Hydrogeochemistry .....	54
5.1.1 Site Geochemistry Results .....	54
5.1.2 δ <sup>13</sup> C <sub>DIC</sub> Isotopes Time Series Analysis .....	58
5.1.3 Mixing Model Study Period and Seasonal Results.....	61
Chapter 6: Discussion .....	69
6.1 Epikarst Hydrogeochemistry .....	69
6.1.1 Site Geochemistry Discussion .....	69
Precipitation .....	70
Surface and Water Temperature .....	72
Specific Conductivity (SpC).....	75
pH.....	78

Soil Temperature and Moisture Conditions .....	84
Carbon Dioxide (CO <sub>2</sub> ) .....	87
Saturation Index (SI <sub>calcite</sub> ).....	94
Dissolved Inorganic Carbon (DIC).....	99
6.1.2 Storm Event Hydrogeochemical Variability at WF1 and LRS.....	102
STE 1: August 20-August 23, 2016 (JD233-236) .....	102
STE 2: November 28-December 1, 2016 (JD333-336) .....	109
6.1.3 Influences on Epikarst $\delta^{13}\text{C}_{\text{DIC}}$ .....	114
Soil Respiration.....	116
Bedrock Dissolution.....	116
$\delta^{13}\text{C}_{\text{DIC}}$ Sourcing at Crumps Cave (WF1 and SF).....	117
$\delta^{13}\text{C}_{\text{DIC}}$ Sourcing at LRCV (LRS and LRWF).....	119
6.1.4 Conduit Dissolution and DIC Flux .....	121
6.1.5 Low-Resolution $\delta^{13}\text{C}_{\text{DIC}}$ , CO <sub>2</sub> , SI <sub>c</sub> , DIC Fluxes .....	126
6.2 Site Hydrogeochemical Comparisons.....	132
6.2.1 Regional Scope .....	132
Chapter 7: Conclusions.....	140
References.....	146
Appendices.....	160



## LIST OF FIGURES

Figure 2.1 Conceptual model for a well-developed carbonate aquifer .....	8
Figure 2.2 Hydrologic features of epikarst zones .....	14
Figure 2.3 Diagram expressing the global carbon cycle .....	26
Figure 3.1 Karst distribution in Kentucky .....	33
Figure 3.2 GIS rendering of the study area in Warren County, Kentucky .....	35
Figure 4.1 Location of the study sites at Crumps Cave .....	42
Figure 4.2 Lost River Cave and Valley and the surrounding city of Bowling Green.....	43
Figure 4.3 Rating curve for Lost River Spring (LRS) discharge .....	53
Figure 5.1 $\delta^{13}\text{C}_{\text{DIC}}$ Time Series Site Comparisons for CRUMPS-WF1 and SF.....	59
Figure 5.2 $\delta^{13}\text{C}_{\text{DIC}}$ Time Series Site Comparisons for LRCV-LRS and LRWF .....	60
Figure 5.3 Mean Contributions of Carbon Sourcing at CRUMPS-WF1 .....	62
Figure 5.4 Mean Contributions of Carbon Sourcing at CRUMPS-SF.....	63
Figure 5.5 Mean Contributions of Carbon Sourcing at LRCV-LRS .....	66
Figure 5.6 Mean Contributions of Carbon Sourcing at LRCV-LRWF .....	67
Figure 6.1 Time series of hydrogeochemical changes at Crumps Cave-WF1 .....	71
Figure 6.2 Time series of hydrogeochemical changes at Crumps Cave-SF .....	74
Figure 6.3 Time series of hydrogeochemical changes at LRCV-LRS .....	76
Figure 6.4 Time series of hydrogeochemical changes at LRCV-LRWF .....	79
Figure 6.5 Surface and Soil Changes at Crumps Cave-WF1 .....	82
Figure 6.6 Surface and Soil Changes at LRCV-LRS .....	83
Figure 6.7 DIC coefficient changes at Crumps Cave-WF1 .....	86
Figure 6.8 DIC coefficient changes at Crumps Cave-SF .....	89

Figure 6.9 DIC coefficient changes at LRCV-LRS .....	93
Figure 6.10 DIC coefficient changes at LRCV-LRWF .....	97
Figure 6.11 Crumps Cave-WF1 Storm Event JD233-236.....	104
Figure 6.12 LRCV-LRS Storm Event JD233-236.....	106
Figure 6.13 Crumps Cave-WF1 Storm Event JD333-336.....	110
Figure 6.14 LRCV-LRS Storm Event JD333-336.....	113
Figure 6.15 Time Series DIC Fluctuations at WF1 and LRS .....	123
Figure 6.16 Time series of CO <sub>2</sub> , DIC, and $\delta^{13}\text{C}_{\text{DIC}}$ at Crumps Cave-WF1.....	127
Figure 6.17 Time series of CO <sub>2</sub> , DIC, and $\delta^{13}\text{C}_{\text{DIC}}$ at Crumps Cave-SF .....	129
Figure 6.18 Time series of CO <sub>2</sub> , DIC, and $\delta^{13}\text{C}_{\text{DIC}}$ at LRCV-LRS.....	130
Figure 6.19 Time series of CO <sub>2</sub> , DIC, and $\delta^{13}\text{C}_{\text{DIC}}$ at LRCV-LRWF.....	131
Figure 6.20 Illustration of CO <sub>2</sub> exchange in the epikarst.....	133

## LIST OF TABLES

Table 5.1 Summary statistics of major hydrogeochemical and $\delta^{13}\text{C}_{\text{DIC}}$ parameters.....	56
Table 5.2 Seasonal trends of mixing model results for WF1.....	64
Table 5.3 Seasonal trends of mixing model results for SF.....	65
Table 5.4 Seasonal trends of mixing model results for LRS.....	68
Table 5.5 Seasonal trends of mixing model results for LRWF.....	68
Table 6.1 Summary stats for DIC flux, conduit enlargement, and dissolution rates.....	125
Table 6.2 Comparison of world epikarst and aquifer spring discharges to this investigation.....	137

## LIST OF APPENDICES

Appendix 1 CRUMPS-WF1 Mixing Model Results .....	160
Appendix 2 CRUMPS-SF Mixing Model Results.....	161
Appendix 3 LRCV-LRS Mixing Model Results .....	162
Appendix 4 LRCV-LRWF Mixing Model Results.....	163
Appendix 5 Low Resolution Geochemical Time Series.....	164
Appendix 6 Recharge versus Discharge at Each Site .....	167

EPIKARST HYDROGEOCHEMICAL PROCESSES IN TELOGENETIC KARST  
SYSTEMS IN SOUTH-CENTRAL KENTUCKY

Leah E. Jackson

August 2017

168 pages

Directed by: Jason S. Polk, Leslie North, Patricia Kambesis

Department of Geography and Geology

Western Kentucky University

Telogenetic epikarst carbon sourcing and transport processes and the associated hydrogeochemical responses are often complex and dynamic. Among the processes involved in epikarst development is a highly variable storage and flow relationship that is often influenced by the type, rate, and amount of dissolution kinetics involved. Diffusion rates of CO<sub>2</sub> in the epikarst zone may drive hydrogeochemical changes that influence carbonate dissolution processes and conduit formation. Most epikarst examinations of these defining factors ignore regional-scale investigations in favor of characterizing more localized processes. This study aims to address that discrepancy through a comparative analysis of two telogenetic epikarst systems under various land uses to delineate regional epikarst behavior characteristics and mechanisms that influence carbon flux and dissolution processes in south-central Kentucky. High-resolution hydrogeochemical and discharge data from multiple data loggers and collected water samples serve to provide a more holistic picture of the processes at work within these epikarst aquifers, which are estimated to contribute significantly to carbonate rock dissolution processes and storage of recharging groundwater reservoirs on the scale of regional aquifer rates. Data indicate that, in agricultural settings, long-term variability is governed by seasonal availability of CO<sub>2</sub>, while in urban environments extensive impermeable surfaces trap CO<sub>2</sub> in the soil, governing increased dissolution and conduit development in a heterogenous sense, which is often observed in eogenetic karst development, as opposed to bedding plane derived

hydraulic conductivity usually observed in telogenetic settings. These results suggest unique, site-specific responses, despite regional geologic similarities. Further, the results suggest the necessity for additional comparative analyses between agricultural settings and urban landscapes, as well as a focus on carbon sourcing in urban environments, where increased urban sprawl could influence karst development.

## Chapter 1: Introduction

Due to the complexity of karst systems, assessing the primary hydrogeochemical processes involved in dissolution kinetics and aquifer storage and flow can be extremely difficult. Hydrogeochemical processes that influence karst development and recharge and discharge often begin in the epikarst zone, or “skin,” of the karst system, and result from geochemical changes due to aggressive water-rock interactions (Bakalowicz 2004). The extent of epikarst dissolution processes are highly influenced by surface conditions such as soil and vegetation type and thickness, as well as storm event variability and associated frequency of recharge intensity (Williams 2008). Excess atmospheric carbon dioxide (CO<sub>2</sub>) derived from an increase in human industrialization over the past few centuries has generated interest among scientists. It has been suggested that karst systems can serve as an extensive carbon sink, due to their ability to absorb and utilize CO<sub>2</sub> in dissolution kinetics, which is the primary driver in karst development (Emblanch et al. 2003; Bakalowicz 2004; Palmer 2007a). Since the epikarst zone is where dissolution initially occurs, and often is fastest, it is within this upper layer of the karst system where special attention needs to be paid (Yang et al. 2012).

In the past, hydrogeochemical studies relied on low-resolution investigations to account for changes in karst properties in relation to dissolution rates of limestone; however, the need for higher-resolution examinations to capture speedy aquifer responses has become vital to deriving a clearer and more thorough understanding of the connective tissue which exists between the epikarst and the deeper-seated aquifer. One of the many ways these high-resolution examinations have been achieved is through the deployment of hydrogeochemical analyses in conjunction with current water monitoring technology.

Additionally, the sourcing of carbon by examination of carbon isotopes, as well as assessing the concentrations of dissolved inorganic carbon, can shed light on the extent of carbon dioxide's role in karst systems and, in particular, the epikarst zone. The employment of these types of investigations can further delineate the influence excess atmospheric CO<sub>2</sub> has on karst regions and their feasibility as carbon sinks (Zhang et al. 1995; Emblanch et al. 2003; Li et al. 2010; McClanahan et al. 2016; Huang et al. 2015).

In addition to carbon-based dissolution kinetics, understanding epikarst conduit development can help infer the rate at which carbon is fluctuating within the system, which can contribute to the karst system's ability to serve as a carbon sink; therefore, it is important to characterize epikarst storage and flow properties. Storage and flow rates may be highly dependent on epikarst thickness, permeability and porosity, and the existence of faults and fractures (Bakalowicz 2004). When recharge rates exceed discharge rates, extensive storage may be actively occurring. In addition to high water infiltration near the top of the epikarst zone, especially during storm inputs, a contrasting property of water storage may exist near the base of the epikarst, allowing for longer residence times and more extensive dissolution of the surrounding rock body (Aquilina et al. 2004; Bakalowicz 2004; Chemseddine et al. 2015).

Regional examinations into karst landscape processes, such as the extent and rate of water storage and flow velocities, and the evolution of karst conduit systems related to dissolution kinetics, are prevalent for south-central Kentucky (Crawford 1984a; Crawford 1984b; Crawford 1989; Crawford 2003; Crawford 2005; Brewer and Crawford 2005; Cesin and Crawford 2005; Nedvidek 2014); however, most of these investigations were constrained to a single, specific cave system and fail to examine how epikarst processes



change over a regional scale. Additionally, where most studies in the past focused on the primary underground rivers theorized to contain the majority of groundwater flow (Palmer 2007a) at relatively low resolution (seasonal to bi-weekly), few studies quantify the epikarst's role in depth at a high resolution as a means to capture hydrogeochemical variations with respect to carbon that occur in these systems, especially during storm events (Lawhon 2014; Nedvidek 2014).

This study characterizes epikarst processes in a well-developed telogenetic karst region at four individual epikarst-derived springs at two separate locations over the course of nine months to capture seasonal changes, storm-event influences, and hydrogeochemical responses. A combination of high-resolution hydrogeochemical parameters, carbon isotope analysis, and hydrologic evaluations were employed. This study addresses the following questions:

- How does the sourcing and fluctuation of dissolved inorganic carbon change in response to seasonal influences and storm events regionally in telogenetic epikarst systems?
- How do these fluctuations influence carbonate rock dissolution and carbon flux in telogenetic epikarst systems?

The collected data from this investigation have illuminated the importance of several key factors in karst processes, including a better understanding of the role of carbon flux by karst systems, the extent to which that carbon is utilized within the epikarst zone, and the feasibility of epikarst portions of karst systems to be referenced as impactful carbon sinks.

## Chapter 2: Literature Review

### 2.1 Karst Landscapes

Nearly 15% of all non-glaciated landscapes are karst landscapes and supply about 25% of the world's fresh drinking water supply (Veni et al. 2001; De Waele et al. 2009; Anaya et al. 2014). Karst is a term applied to any lithological landform that is capable of producing conduits or caves through chemical dissolution (LeGrand 1983; Veni et al. 2001; White 2007; Mylroie 2013; Anaya et al. 2014). Karst environments are characterized predominantly by limestones and dolomites, and less commonly by gypsum, marble, and other evaporites (LeGrand 1983; Veni et al. 2001). The evolution of a karst landscape is often governed by the interaction of five components: the type of bedrock; the fluid involved in dissolution; the presence of structural influences such as stratigraphic dip and tectonic deformation; the hydraulic gradient of subsurface flow; and changes within local and regional climates over long periods of time (Palmer 1991; Ritter et al. 2002; Palmer 2003a; Palmer 2003b; Palmer 2007a; Palmer 2007b). Since each karst system is a unique combination of these elements, it can be difficult to categorize fully the dominant processes within; often, individual case studies, where observations are based on the interaction of one or more of these principles, are employed when identifying aquifer properties and specific behaviors conducive to overall development.

Solution-derived karst systems can be divided into two main sections, with each section governed by its own chemical and physical properties. The top layer, or "skin," of the karst system is known as the epikarst, which has been suggested also to include the vadose or unsaturated zone (Bakalowicz 2004; Petrella et al. 2007; Trček 2007; Jacob et al. 2009). Directly beneath the vadose zone is the phreatic or saturated zone. It is within

this zone that the main aquifer is located (Aquilina et al. 2004; Bakalowicz 2004; De Waele et al. 2009). Because karst systems are governed by dissolution kinetics, which happen to be at their most impactful within the epikarst, it is this top layer of a karst system that requires special attention in research.

The epikarst can be thought of as a protective layer for the entirety of the karst system. Previous investigations have shown that the majority of chemical changes within the epikarst are driven by high concentrations of atmospheric and soil derived carbon dioxide (CO<sub>2</sub>) (Zhongcheng and Daoxian 1999; Bakalowicz 2004; Palmer 2007a; Petrella et al. 2007; Trček 2007; White 2007; Jacob et al. 2009; Liu et al. 2010; Yang et al. 2012; Peyraube et al. 2014; Milanolo and Gabrovšek 2015; Zhang et al. 2016). This carbon dioxide enters the karst system as dissolved CO<sub>2</sub> in meteoric water or in antecedent moisture in the topsoil.

The subsurface path that meteoric water follows is wrought with complexities because of the heterogenetic nature of the epikarst, which is usually a result of several processes including diagenesis, secondary and tertiary porosity and permeability, and post-depositional structural deformation (LeGrand 1983; Aquilina et al. 2004; Palmer 2007a; De Waele et al. 2009; Pu et al. 2014a; Pu et al. 2014b). Diagenesis derived variability originates from the unique mixture of deposited sediment before it undergoes lithification. Depending on the orientation, shape, and size of each individual grain, small gaps can form as the material is compressed. This is referred to as the rock's porosity, while frequency and proximity of void spaces, and thus the ability for the rock to transmit fluid through those spaces, is considered the rock's permeability. As the limestone undergoes temporal diagenesis, permeability reduces due to overburden pressure from

overlying sediment deposition compressing the material and shrinking the size of the void spaces within the matrix, reducing the rock's ability to transmit fluid; however, as temporal diagenesis serves to reduce primary porosity and permeability, it also allows time for infiltrating water to dissolve along vertical fractures and horizontal bedding planes, generating a condition known as secondary porosity resulting from dissolution kinetics. Under these new conditions, the extent of water storage reduces as well, as pipe-style conduits provide a means for secondary permeability and, thus, more efficient hydraulic conductivity, unless the flow encounters a clog within the conduit system or it enters the phreatic zone (Aquilina et al. 2004; Veni et al. 2001; Palmer 2007a; Worthington 2007; De Waele et al. 2009; Anaya et al. 2014). The phreatic zone often leads to springs and outlet systems, where discharge rates are governed by water table fluctuations and the amount of recharge the system receives over time (Aquilina et al. 2004; Palmer 2007a).

Post-diagenetic structural deformation is usually a result of tectonic processes, such as rifting or uplift. These processes can alter the stratigraphic dip of the region and generate fractures and fissures, which then influence the hydraulic conductivity within the system. Hydraulic conductivity is a more concise term applied to subsurface water flow, such as slow percolation through a permeable medium, and the rapid drainage of water through pipe-style conduits. Landscapes wrought with structural deformation will aid in karst development and, thus, the transition between primary and secondary porosity (Aquilina et al. 2004; Palmer 2007a). Hydraulic conductivity is also governed by the dip of the landscape. As water infiltrates the bedrock, its ultimate goal is to reach local base level; thus, water will follow the path of least resistance. Stratigraphic dip will serve to

govern the direction of water flow and the depth of conduit formation as surface rivers simultaneously incise the landscape, dropping base level to a new position (Aquilina et al. 2004; Palmer 2007a).

The fluid involved in the dissolution of bedrock is dependent on several factors, including the type of recharge (allogenic or autogenic), the amount of recharge (a function of climate), and time (Palmer 2007a; Pu et al. 2014a; Pu et al. 2014b). In epigenic cave development, the primary ingredients in soluble fluids are water and carbon dioxide. The processes involved in dissolution from these soluble fluids are as follows: water from precipitation absorbs carbon dioxide (CO<sub>2</sub>) from the atmosphere as it falls onto the surface. The water becomes supersaturated with CO<sub>2</sub> as it passes through soil that is heavily laden with respiration-derived CO<sub>2</sub> from vegetation, and infiltrates the epikarst. This supersaturation of CO<sub>2</sub> lowers the water's pH to around 4.7, turning it into carbonic acid (H<sub>2</sub>CO<sub>3</sub>). When the carbonic acid encounters calcium carbonate (CaCO<sub>3</sub>), it will cause the calcium (Ca<sup>+</sup>) and carbonate (CO<sub>3</sub>) to disassociate (Veni et al. 2001; De Waele et al. 2009). Furthermore, the additional hydrogen will join with the carbonate to form bicarbonate (HCO<sub>3</sub><sup>-</sup>). The dissociation of CaCO<sub>3</sub> into calcium and bicarbonate is shown in the following reaction (White and White 1989; Palmer 2007a):



The extent of dissolution is often contingent on recharge type, including allogenic and autogenic (Palmer 1991; Palmer 2003a; Palmer 2003b; Palmer 2007a; Palmer 2007b). Allogenic recharge is derived from surface runoff that starts on non-karst landscapes, but flows into karst landscapes. Allogenic recharge is often under-saturated with respect to calcium and saturated with carbon dioxide by the time it enters the karst

system. As a result, its propensity for dissolution is much higher. In contrast, autogenic recharge derived from runoff that immediately flows over a karst system, and is in constant contact with soluble bedrock, may be heavily saturated with calcium and carbon dioxide; however, its propensity for dissolution is much lower, due to its high calcium saturation (Palmer 1991; Veni et al. 2001; Palmer 2003a; Palmer 2003b; Palmer 2007a; De Waele et al. 2009; Mylroie 2013). In regions where the climate is more temperate or tropical, karst development is more extensive due to higher annual precipitation rates.

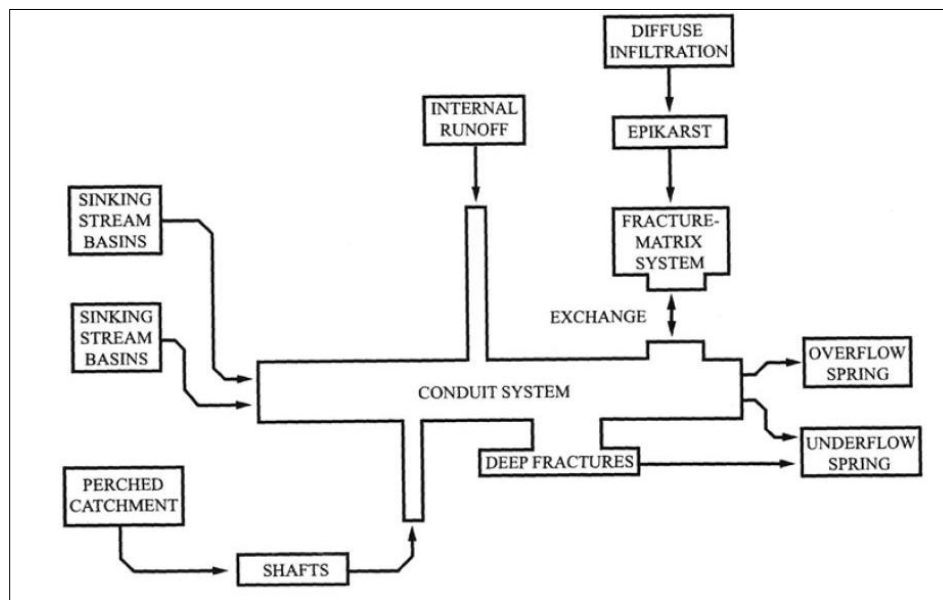


Figure 2.1 Conceptual model for a well-developed carbonate aquifer, illustrating the direction of water flow from input to output.

Source: White (2003).

De Waele et al. (2009) suggested that precipitation has the greatest influence on karst systems only within the first few meters of the epikarst where CO<sub>2</sub> concentrations are more abundant and dissolution generates common surface morphologies, such as dolines, poljes, and cenotes (Veni et al. 2001). These features tend to play a role in how easily water can enter the karst system. Using the hydraulic gradient as a driver, phreatic waters will dissolve through the subsurface, forming a maze of conduits that eventually

meet the current level of the water table (Figure 2.1). As the water table rises, existing caves and conduits will flood, and the processes will begin again at a different subsurface elevation. When the water table drops, the phreatic zone will follow suit. Given enough time, a series of intertwined conduits and caves develops in the subsurface, generating a cave system, provided that surface erosion does not supersede the rate of cave formation (Palmer 2007a; Palmer 2007b; De Waele et al. 2009).

Up to this point, the discussion of karst processes has been primarily through the lens of telogenetic karst, or karst that has undergone temporal diagenesis, uplift, and subsequent surface erosion; however, eogenetic karst has a hydraulic behavior and geologic evolution unique to its environmental conditions as well. Although mostly outside the scope of this study, it is important to touch on the primary differences between these two karst landscapes, with a focus on hydraulic conductivity as it relates to the storage and flow characteristics that are addressed in this study.

According to Worthington et al. (2000), Vacher and Mylroie (2002), and Florea and Vacher (2006), there are three different types of karst defined by stages of deposition influencing porosity of the limestone. Eogenetic karst is described as karst that has undergone deposition and early exposure to surface processes; mesogenetic karst is that which has experienced deep burial but not subsequent uplift; and telogenetic karst is karst that has undergone deep burial, subsequent uplift, and surface erosion processes. It is these three stages that result in telogenetic karst's matrix permeability becoming heavily altered. In eogenetic karst, permeable limestones having large volumes of interconnected pore spaces, allowing for matrix-dominated, diffuse flow, dominate the bedrock. On the other hand, deep burial of carbonates results in a reduction of porosity, due to

compression of overriding sediments, thus reducing permeability. Once the bedrock is uplifted and exposed to surface erosions processes, hydraulic conductivity becomes contingent on dissolution processes widening fractures and pore spaces between bedding planes, eventually providing for pipe-style transmission of fluids. It is this shift in the type of permeability, from matrix-dominated processes to conduit flow, which influences subsequent dissolution processes, aquifer development, and overall residence times.

Florea and Vacher (2006) compiled examinations of spring hydrographs from a variety of settings, including both eogenetic karst in Florida, and telogenetic karst in Kentucky. They discovered that the responses to aquifer discharges varied greatly depending on the type of karst, and attributed these varied responses to the type of flow within the limestone. Martin and Dean (2001) found through a hydrogeochemical study that the majority of flow within the Santa Fé River in Florida comes from matrix-dominated flow during low-flow conditions, and this suggested that diffuse flow processes are just as important to understanding karst landscape evolution as conduit-flow processes. This statement is in direct conflict with White (1988), who suggested that matrix permeability is negligible when examining spring response and, therefore, could be easily dismissed as a major player, especially in high flow events. Despite the conflict in the literature, Florea and Vacher (2006) submit that the type of karst will determine the influences on aquifer processes by flow type, and that neither can be easily dismissed. In fact, the authors suggested that matrix porosity cannot be dismissed as a significant player in eogenetic karst, while secondary porosity generated by the growth of solution-enlarged conduits in telogenetic karst plays a key role in hydraulic conductivity.



It is important to note, however, that White (1988) suggested that the primary distinctive difference between diffuse flow in eogenetic karst and conduit flow in telogenetic karst is in the spring response defined by a hydrograph. By using this tool, one can infer the dominant processes within any karst system with respect to hydraulic conductivity. According to Florea and Vacher (2006), White (1988) coined the term “flashiness” when describing the responses to discharge observed in a hydrograph, and describes this flashiness as a three-stage aquifer response: recharge, storage, and transmission. Should residence time contribute to storage without ample recharge causing a piston push effect, any rapid transmission of fluid discharged from the aquifer will be reflected in a “flashy” hydrograph (White 1988; Worthington et al. 2000; Florea and Vacher 2006; Worthington 2007). On the other hand, this flashiness could also be a reflection of rapid recharge and rapid transmission (White 1988), especially in telogenetic karst where water is easily transferred to the subsurface through sinking streams, with the possibility of that same water being discharged through the aquifer provided extensive storage is not taking place. The extent of storage in these cases, however, would need to be delineated by examining the differences in base-flow discharge versus high-flow discharge (Worthington et al. 2000; Worthington 2007). Additionally, Florea and Vacher (2006) proposed that these types of spring responses are more likely to occur in well-developed karst systems where flow has shifted from matrix-dominated diffuse flow to a combination of matrix, conduit, and fracture flow, with dissolution conduits formed from post uplift surface erosion and dissolution, leading to conduit flow becoming the dominant flow regime.

These studies demonstrate that the setting in which the aquifer exists will often determine the type of karst landscape, eogenetic versus telogenetic, which, in turn, will usually describe the flow regime: diffuse flow versus conduit flow. These same flow regimes are also observed in the epikarst (Petrella et al. 2007; Trček 2007; Williams 2008; Jacob et al. 2009); considering that the epikarst is more closely linked with surface process, and thus higher rates of dissolution, examinations of epikarst discharge can shed some light on just how different and unique are eogenetic and telogenetic karst, especially with respect to hydraulic conductivity. By analyzing the hydrological factors influencing subsurface geomorphology, an understanding of the timeline and key factors for formation of a particular cave or aquifer system can be gained. This is achieved through established methods, such as dye tracing, water sampling, and spatial and temporal analysis of specific input and output locations; however, since passages may be impassable for a variety of reasons, determining flow characteristics of an aquifer can be complicated and time consuming (White 2007).

Investigations into the role of the epikarst, where dissolution is suggested to be the most aggressive due to an open-system relationship with the surface, thus leading to a mixture of conduit and diffuse flow regimes, is still not thoroughly understood. The majority of investigations have shed some light on the abundant complexities of these systems and the roles they play with respect to aquifer processes, but, to date, only generalizations can be made about the influences that epikarst processes have on karst systems. Often, location-specific research is necessary to delineate effectively the epikarst's role in karst landscape development.

## 2.2 Epikarst Theory

The epikarst is defined as highly weathered rock immediately underlying the soil or present at the surface (Zhongcheng and Daoxian 1999; Aquilina et al. 2004; Bakalowicz 2004; Klimchouk 2004; Groves et al. 2005; Jiang et al. 2007; Palmer 2007a; Petrella et al. 2007; Trček 2007; White 2007; Williams 2008; Jacob et al. 2009; Liu et al. 2010; Yang et al. 2012; Peyraube et al. 2014; Milanolo and Gabrovšek 2015; Zhang et al. 2016). In the 1970s and 1980s, it was discovered that the uppermost layers of the karst system played an important role in overall karst development, prompting deeper investigations into the epikarst over the following decades (Williams 1983; Zhongcheng and Daoxian 1999; Bakalowicz 2004; Klimchouk 2004; Cheng et al. 2005). According to Klimchouk (2004), the term epikarst originated from the revelation that the upper part of karst systems acted as a recharge zone for the entire system (Figure 2.2). This zone is highly governed by the permeability and porosity of the bedrock, the type of recharge, and the presence of structural deformation. The employment of hydrochemical and isotopic analyses support the suggestion that these defining and governing characteristics are the dominant drivers in epikarst processes (Zhongcheng and Daoxian 1999; Bakalowicz 2004; Klimchouk 2004; Groves et al. 2005; Jiang et al. 2007; Petrella et al. 2007; Trček 2007; White 2007; Williams 2008; Jacob et al. 2009; Liu et al. 2010; Yang et al. 2012; Peyraube et al. 2014; Milanolo and Gabrovšek 2015; Zhang et al. 2016). Since the epikarst serves as a complex linkage with the surface and the deeply seated saturated zone, and is sensitive to surface environmental changes, it could potentially serve as a conduit for the percolation of polluted fluids as well as the transference of meteoric water to the aquifer (Cheng et al. 2005; Williams 2008). Bakalowicz (2004)

describes the epikarst as a shallow part of karst regions subjected to climate changes, vegetation interferences, such as tree roots generating cracks and enlarging rock joints, and serving as a permeable “gasket” to the underlying aquifer.

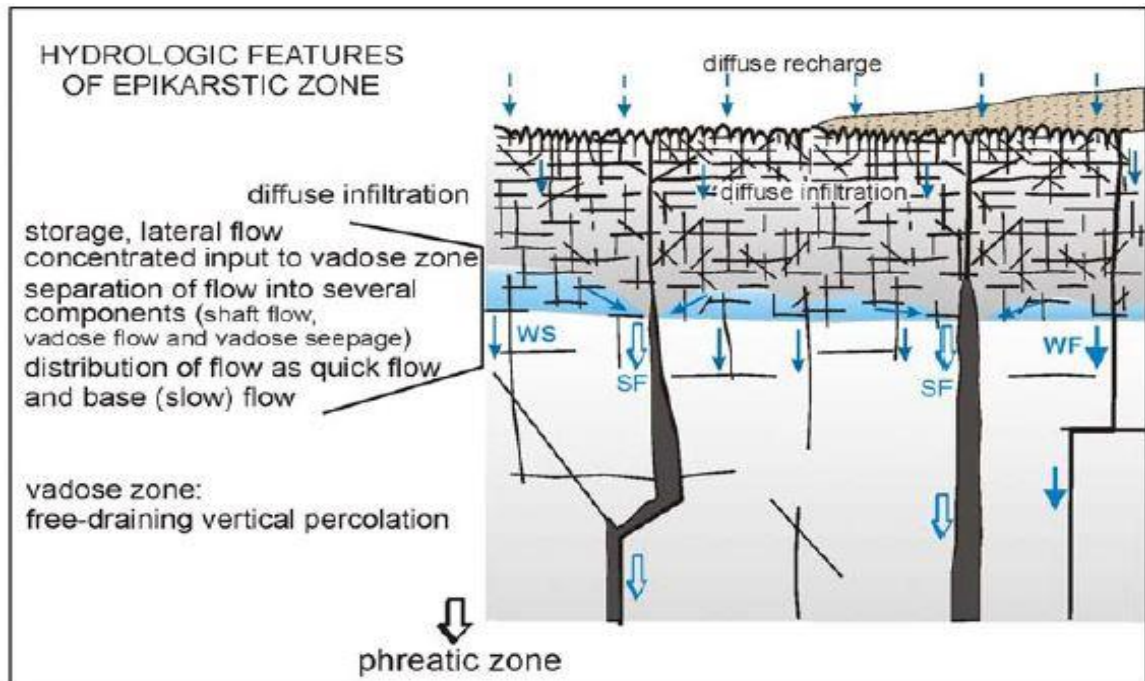


**Figure 2.2** Hydrologic features of epikarst zones, indicating the complexities involved with water infiltration and storage  
Source: Klimchouk (2004).

The epikarst is comprised of two sections, the immediate skin (or soil layer) and the transmission zone, which acts as connective tissue between the surface and the first emergence of the vadose zone. Some studies have suggested that the vadose zone should be included in the definition of an epikarst; however, geochemical reactions can be much different in the vadose zone compared to the current definition of the epikarst, and it is the geochemical evolution that delineates the epikarst from the rest of the karst system. In fact, it is suggested that the epikarst is primarily characterized by its hydraulic

capabilities in relation to dissolution kinetics (Clemens et al. 1999; Bakalowicz 2004; Klimchouk 2004; Groves et al. 2005; Jiang et al. 2007).

The epikarst can vary in thickness, depending on the particular region of karst being investigated and, as a consequence, its characteristics will follow suit. Williams (2008) suggested that the typical epikarst is between three and ten meters in depth and exhibits contrasting porosity and permeability. For example, permeability can be much greater near the surface of the epikarst, where the majority of fractures and faults have been found. As a result, water infiltration may be greater in these areas. Porosity, on the other hand, may be higher near the base of the epikarst where water is stored, forming conduits and allowing for increased hydraulic conductivity (Palmer 2007a). Additionally, if faults or fractures vertically transect part, or the entirety, of the epikarst, this can provide a means for epikarst water to flush immediately through the system with minimal to no storage time, generating high flow rates (Palmer 2007a; Williams 2008); however, this particular characteristic may not be representative of the entirety of the epikarst.

Where water storage in the epikarst occurs, it is more likely to be found near the base of the epikarst. In some respects, if the storage amount is great enough, it can be thought of as an epikarst aquifer and serves as an aquitard to the vadose and phreatic zones below (Clemens et al. 1999; Cheng et al. 2005; Groves et al. 2005; Aquilina et al. 2004; Jiang et al. 2007; Petrella et al. 2007; Trček 2007; Williams 2008; Jacob et al. 2009). As mentioned before, water storage in the epikarst is variable; therefore, it is also highly influenced by seasonal changes and storm surges. Klimchouk (2004) found that water within the epikarst could have various residence times, which are independent of water stored in the deep-seated aquifer. In essence, it takes significant amounts of

recharge to push significant amounts of water through the system, reflected in high rates of discharge. Due to the nature of water mixing within the solution-filled conduits, often water that initially infiltrates the system is not directly observed as being the same water that exits the system during the same storm event. In other words, freshly infiltrated water often tends to replace older storage water (Palmer 2007a), instead of being immediately discharged. In this respect, water storage in the epikarst allows time for limestone dissolution and potential CO<sub>2</sub> outgassing should that water enter the vadose zone, even in the form of drip water that slowly percolates to the saturated zone.

Williams (2008) emphasized the importance of ensuring that the epikarst and its functions are accurately identified as it may not always contain an active aquifer, suggesting alternative storage properties are at work, or that storage only occurs at a minimal level (Williams 2008); however, the presence of a perched aquifer in the epikarst may exist when there is a well-defined network of fractures and faults that intersect, or run perpendicular to bedding planes, thereby directly affecting water flow velocities and direction (Williams 1983). Dissolution along these joints and fractures can actually increase porosity and, thus, permeability as the rock undergoes temporal diagenesis. This increase in permeability will cause a shift from lateral flow to a more vertical flow direction; however, Williams (1983) noted that, with increasing depth, overburden pressure will actually cause the aperture of these vertical shafts to reduce, forming a cone-like shape near the base and creating a perched aquifer as water pools at these narrow constrictions. Flow velocity will tend to reduce to a simple percolation as it moves into the vadose zone. Consequently, water-flow direction may also shift to more lateral flow as the water seeks a less restrictive route. Most often, epikarst derived

waterfalls are simply a single main vertical shaft to which the water has migrated due to a reduction of flow-direction options. If the water cannot find its way toward these main shafts, it will remain stored within that perched aquifer until there is sufficient hydraulic head, often derived from storm events, to push it through the system (Williams 1983; Williams 2008).

Worthington (2007) suggested that contrasting characteristics exist governing mediums in which water will most likely be stored and/or transported. For example, in older rocks, conduits only serve as a transportation network for groundwater flow, while the majority of stored water occurs within the matrix, usually accompanied with long residence times. This seems to support the theory that telogenetic karst systems, and telogenetic epikarst specifically, are governed by a unique combination of matrix and conduit style storage and flow parameters. Fractures serve as the connecting medium between matrices and conduits, with low storage and moderate residence times. He also suggested that it is possible to use environmental tracers to delineate the mediums in which storage and residence times occur. For example, the author found that rapid flow from injection points (sinking streams) to discharge points (springs) is an indication of the presence of an extensive network of deep conduits with minimal storage and residence times. On the other hand, samples from shallow depth conduits indicated long residence times. Worthington (2007) also noted that the use of multiple environmental and injection based tracers yielded conflicting residence times, possibly hinting toward single, double, and triple porosity governing water flow and storage. He classified these varying porosities as a function of conduit numbers and sizes within the aquifer. Furthermore, it is possible these numbers will vary depending on the depth at which the

sample is collected. Epikarst permeability decreases with depth, according to Williams (1983; 2008), but porosity increases with dissolution (Palmer 2007a; Worthington 2007); therefore, storage, residence times, and flow rates will vary accordingly.

Williams (2008) suggested that dissolution propensity, which leads to this increase in permeability along joints and fractures and bedding planes, is higher near the surface, due to the abundant availability of atmospheric and soil derived CO<sub>2</sub>; thus, hydro-geochemical processes and changes to the karst system are more aggressive in the epikarst. This may not always be the case, as Chemseddine et al. (2015) claimed that deep waters in the saturated zone are more active when rich with CO<sub>2</sub>. This saturation at deep levels, however, may be a function of minimal epikarst thickness and/or storage, high porosity, and the piezometric position of the water table being close to the surface. In these cases, it may be that CO<sub>2</sub>-rich derived waters are immediately entering the saturated zone, suggesting that no or very minimal storage in the epikarst exists. Additionally, these phenomena may be local, in that this particular characteristic does not necessarily represent the entirety of epikarst functions everywhere.

Attempting to resolve epikarst storage rates can be a difficult pursuit. Often, the most common method is to calculate the difference between recharge and discharge rates at epikarst springs; however, these values may not always be an accurate representation of hydraulic conductivity, should the output exceed the input rate. To compensate for such occurrences, additional dye tracing, geochemical, and isotopic data can be collected at several points within a karst system to determine epikarst storage rates. Stable isotopes can be used as tracers, especially when their values are examined with respect to the fluctuation within different mediums as water moves from surface to subsurface.



Perrin et al. (2003) examined storage in a karst aquifer in the north of Switzerland to determine the extent and type of storage. The authors compared stable isotopic data of oxygen in spring discharge and underground river water samples to model the amount and type of storage occurring in the epikarst. The authors found that in diffuse flow environments, the epikarst exhibited the most dynamic storage properties, and that water transferred to the saturated zone was immediately transported via a conduit network to surface springs. They also identified two different types of water flow within the epikarst: base flow and quick flow, which are dependent on storm surges and subsequent recharge rates (Perrin et al. 2003).

The aforementioned studies highlight the importance of determining recharge and discharge properties to infer water storage capabilities, flow dynamics, and subsequent dissolution kinetics within the epikarst. It has been discovered that storage and flow, though dependent on seasonal variations and storm surges, are mostly constrained by the specifics of the locality of the karst system, such as lithology, geology, and latitude. Hydrogeochemical data, such as pH, water temperature, specific conductivity, total dissolved solids, alkalinity, and certain stable isotopes such as oxygen and carbon, can provide proxy measurements for water transference through karst systems. Since dissolution kinetics are most aggressive in the epikarst, and hydro-geochemical parameters greatly reflect the extent of those kinetics, then hydro-geochemical investigations are essential to delineating epikarst processes.

## 2.3 Carbon Processes in Karst

### 2.3.1 *CO<sub>2</sub> Dissolution Kinetics*

Due to the ever-increasing concerns regarding excess atmospheric CO<sub>2</sub> affecting the environment, multiple studies have suggested that karst systems can serve as carbon sinks (Li et al. 2008a; Cuezva et al. 2011; Gorka et al. 2011; Shin et al. 2011; White 2013; McClanahan et al. 2016; Jiang 2013; Zhang et al. 2015; Zeng et al. 2016). These studies attempt to delineate carbon fluctuations within karst systems to better understand carbon sequestration from the atmosphere. Additionally, as mentioned before, carbon is a primary constituent in karst-dissolution kinetics and can serve as a practical tracer for carbon flux. Therefore, by examining carbon isotope values with respect to carbon sourcing, carbon fluctuations from surface to discharge point can be resolved. Further, since the epikarst plays such a vital role in dissolution processes within karst systems, it is within this zone that special attention to carbon processes is paid.

Karst dissolution processes are heavily dependent on the presence of dissolved carbon dioxide in infiltrated waters. This CO<sub>2</sub> is responsible for increasing the aggressive nature of infiltrating waters, which, in turn, increases the rate by which carbonate bedrock may be dissolved, and thus the rate at which water is either stored or discharged from the system. Atmospheric CO<sub>2</sub> is considered in equilibrium with precipitation and is usually expressed as parts per million. According to the National Oceanic and Atmospheric Administration (NOAA 2016), the rate of CO<sub>2</sub> in the atmosphere, as of March 2017, was roughly 409 parts per million, while the average global carbon dioxide level in soil is significantly higher, at around 1,500 Pg (Hursh et al. 2017).

Most karst systems are considered open, wherein a continuous supply of CO<sub>2</sub> from the surface dissolved within infiltrating meteoric waters contributes to ongoing dissolution kinetics, even at great depths within the karst system. Several studies indicate that epikarst heterogeneity, as well as the subsurface elevation of the saturated zone, can greatly influence the point at which dissolution tends to cease (Hess and White 1992; Baldini et al. 2006; Blecha and Faimon 2014a; Blecha and Faimon 2014b). Dissolution kinetics lead to calcite and magnesium dominance in karst waters; therefore, karst water is often considered to be in one of three states: under-saturated, or aggressive; saturated, or chemically equilibrated; or supersaturated, at which point it is likely to precipitate the dissolved minerals it carries. These values can be delineated mathematically and expressed numerically, with any water value less than zero considered aggressive; any water value at zero at equilibrium, and any water value greater than zero considered supersaturated. In this sense, dissolution rates are considered a derivative of the saturation index of water with respect to CaCO<sub>3</sub> (Palmer 2007a).

In open systems, increased vegetation growth on the surface can contribute to a rise in CO<sub>2</sub> concentrations within the topsoil. This is primarily due to plant root respiration and subsequent microbial activity converting organic matter into carbon dioxide. Likewise, with increases in agriculturally based vegetation, soil CO<sub>2</sub> concentrations can increase in response to the presence of agriculture. When those crops are harvested, however, depletion in soil CO<sub>2</sub> concentrations can occur, due to a severe reduction in root respiration. Further, when natural vegetation shifts into the dormant state during the winter months, an even greater depletion in soil CO<sub>2</sub> can be observed; thus, water containing reduced concentrations is transferred to the epikarst. Additionally,

these seasonal fluctuations in CO<sub>2</sub> concentrations resulting from a change in vegetation cover can have an impact on δ<sup>13</sup>C values, where depletion occurs resulting from fractionation as plants utilize <sup>12</sup>C. During the inert months, <sup>13</sup>C enrichment occurs because less <sup>12</sup>C is utilized. Peyraube et al. (2014) suggests that equilibrium partial pressure of CO<sub>2</sub> can be used to account for the amount of dissolved CO<sub>2</sub> in the system, which, consequently, infers the extent of potential dissolution. To calculate the partial pressures of CO<sub>2</sub> (pCO<sub>2</sub>), the following equation (2.2) from Drever (1997) is used:

$$P_{\text{CO}_2} = \frac{K_1 K_{\text{CO}_2}}{10^{-\text{pH}} [\text{HCO}_3^-]} \quad (\text{Eq. 2.2})$$

where K<sub>1</sub> is the temperature dependent dissociation constant of H<sub>2</sub>CO<sub>3</sub> and K<sub>CO<sub>2</sub></sub> is the solubility product of CO<sub>2</sub> gas in water (Drever 1997; Lawhon 2014).

Studies on epikarst-dissolved CO<sub>2</sub> concentrations, as well as the direct influence from soils and in-cave air CO<sub>2</sub> concentrations, have been conducted worldwide (Zaihua et al. 1997; Baldini et al. 2006; Shen et al. 2013; Faimon et al. 2012a; Faimon et al. 2012b; Yang et al. 2012; Peyraube et al. 2013; Blecha and Faimon 2014a; Blecha and Faimon 2014b). Baldini et al. (2006) examined potential sources of CO<sub>2</sub> as it percolates through the epikarst using drip water from two caves in Ireland. The authors found that, in conjunction with soil CO<sub>2</sub>, seasonal fluctuations play a major role in total CO<sub>2</sub> concentrations and variability. Peyraube et al. (2013) developed a methodology for examining the concentrations of carbon and pCO<sub>2</sub> in cave air after it infiltrates the epikarst. They discovered that seasonal fluctuations are a key agent in pCO<sub>2</sub> content. Faimon et al. (2012a; 2012b) examined cave drip water for CO<sub>2</sub> concentrations in a cave in the Czech Republic. The authors found that their data correlated with previous investigations of the same nature conducted in other parts of the world, which claim soil

CO<sub>2</sub> rates and seasonal fluctuations are key agents in CO<sub>2</sub> and HCO<sub>3</sub> concentrations in the epikarst and, subsequently, in the vadose and phreatic zone (Zeng et al. 2016). Zaihua et al. (1997), Vesper and White (2004), Yang et al. (2012), and Blecha and Faimon (2014a; 2014b) all had similar findings in their investigations; however, those investigations examined the extent of dissolution resulting from influxes of CO<sub>2</sub> content. In fact, Peyraube et al. (2014) found that unsaturated zone CO<sub>2</sub> baseline measurements are extremely high and, thus, have a direct consequence on the CO<sub>2</sub>-saturation index factors for calcium and magnesium. This discovery further supports the suggestion that high concentrations of CO<sub>2</sub> in the epikarst are directly responsible for increased rates of dissolution during certain times.

Investigations conducted in Kentucky and Tennessee examined CO<sub>2</sub> influences on karst environments with the intent of determining the extent that CO<sub>2</sub> concentration has on dissolution kinetics (Hess and White 1992; Vesper and White 2004; Vanderhoff 2011; Hatcher 2013; Lawhon 2014; Salley and Groves 2016). For example, Hatcher (2013) investigated sources of CO<sub>2</sub> controlling carbonate chemistry at Logsdon River at Mammoth Cave. Three sites were chosen for that study: one feeding from the epikarst, one with direct interaction from the vadose zone, and another from a spring. Hatcher (2013) discovered that the vadose zone and spring exhibited minimal CO<sub>2</sub> concentrations with respect to the samples taken directly from the epikarst. This suggests that epikarstic storage of CO<sub>2</sub> is greater than in any other part of the karst system, furthering the hypothesis that CO<sub>2</sub> saturation is greatest where proximity or connection through permeability to soils is highest.

Vesper and White (2004) examined CO<sub>2</sub> from springs in a cave system near the Kentucky/Tennessee border during storm events and found that changes in CO<sub>2</sub> were a direct result of flushing from the system associated with conduit-dominated karst experiencing a pulse of water for the duration of the storm. The results suggest that CO<sub>2</sub> levels in the karst system are higher during base flow, which allows the system time to “compile” CO<sub>2</sub> from various sources (Vesper and White 2004). One of the earliest studies is by Hess and White (1992), who examined the hydrogeochemistry of several springs in the Mammoth Cave region over one year during 1972. The authors suggested that fluctuations in soil CO<sub>2</sub> values, primarily due to seasonal changes, have the greatest effect on the karst system. More localized and recent investigations of hydrogeochemical influences were conducted in Bowling Green (Lawhon 2014) and Smith’s Grove, Kentucky (Vanderhoff 2011), to ascertain the extent of storage and flow propensity, especially with respect to storm events and contaminant transport. Both of these investigations used CO<sub>2</sub> concentrations as a proxy with respect to the nature of the aquifers and their ability to transfer water from surface to spring. Although these investigations did not directly ascertain sourcing of CO<sub>2</sub> and direct effects of CO<sub>2</sub> storage and utilization, the work did reflect similar findings.

Dissolved CO<sub>2</sub> concentrations in meteoric water are directly linked to bedrock dissolution due to CO<sub>2</sub>’s ability to reduce pH to an acidic state (Zhongcheng and Daoxian 1999; Bakalowicz 2004; Palmer 2007a; Petrella et al. 2007; Trček 2007; White 2007; Jacob et al. 2009; Liu et al. 2010; Yang et al. 2012; Peyraube et al. 2014; Milanolo and Gabrovšek 2015; Zhang et al. 2016). The extent of dissolution from CO<sub>2</sub> contributions can be measured numerically by calculating the extent of water saturation, which is

referred to as the saturation index (SI) with respect to calcium and/or magnesium. In terrestrial meteoric water, the saturation index of a particular mineral ( $\text{Ca}^{2+}$  or  $\text{Mg}^{2+}$ ) is calculated by first determining the ion activity product (IAP). For example, the ion activity product for calcite is:

$$(\text{Ca}^{2+})(\text{CO}_3^{2-}) = K_{\text{Calcite}} \quad (\text{Eq. 2.3})$$

where  $(\text{Ca}^{2+})$  equals the calcium ion activity,  $(\text{CO}_3^{2-})$  equals the carbonate ion activity, and  $K_{\text{calcite}}$  is the equilibrium constant for the reaction (a temperature dependent value). Multiplying their values renders the IAP. If the IAP is less than K, then the solution is considered under-saturated. If this is the case, dissolution of that particular mineral will continue until the concentration of ions in solution supersaturates the solution. If the IAP is greater than K, then the solution is considered oversaturated and dissolution of that particular ion will cease and, in some cases, cause precipitation of that mineral (Palmer 2007a; Chemseddine et al. 2015). To determine the extent of solution saturation with respect to a particular mineral, in this case calcite, the saturation index can be calculated using the following formula from Palmer (2007a):

$$\text{SI}_c = \text{IAP}/K \quad (\text{Eq. 2.4})$$

The extent of dissolution is a product of  $\text{CO}_2$  concentrations in infiltrated waters. The  $\text{CO}_2$  is often derived from multiple sources, including atmospheric  $\text{CO}_2$ , soil derived  $\text{CO}_2$ , and carbonate water-rock interactions. Determining the source of  $\text{CO}_2$  can delineate which source is contributing the greatest amount of  $\text{CO}_2$  to the overall system, which, in turn, can help better explain dissolution kinetics in epikarst systems, as well as the role that anthropogenic forces play in natural systems.

### 2.3.2 $\delta^{13}C_{DIC}$ Isotope Sourcing and Flux

One of the primary ways in which  $CO_2$  sources can be delineated is by examining the isotope signatures of  $\delta^{13}C$  in water. As carbon fluctuates through the system, carbon isotope values will tend to become enriched or depleted, depending on environmental conditions and seasonal shifts. One of the greatest factors influencing the depletion or enrichment of  $^{13}C$  is soil-derived microbial activity (Telmer and Veizer 1999; White 2013; Zhang et al. 2015).

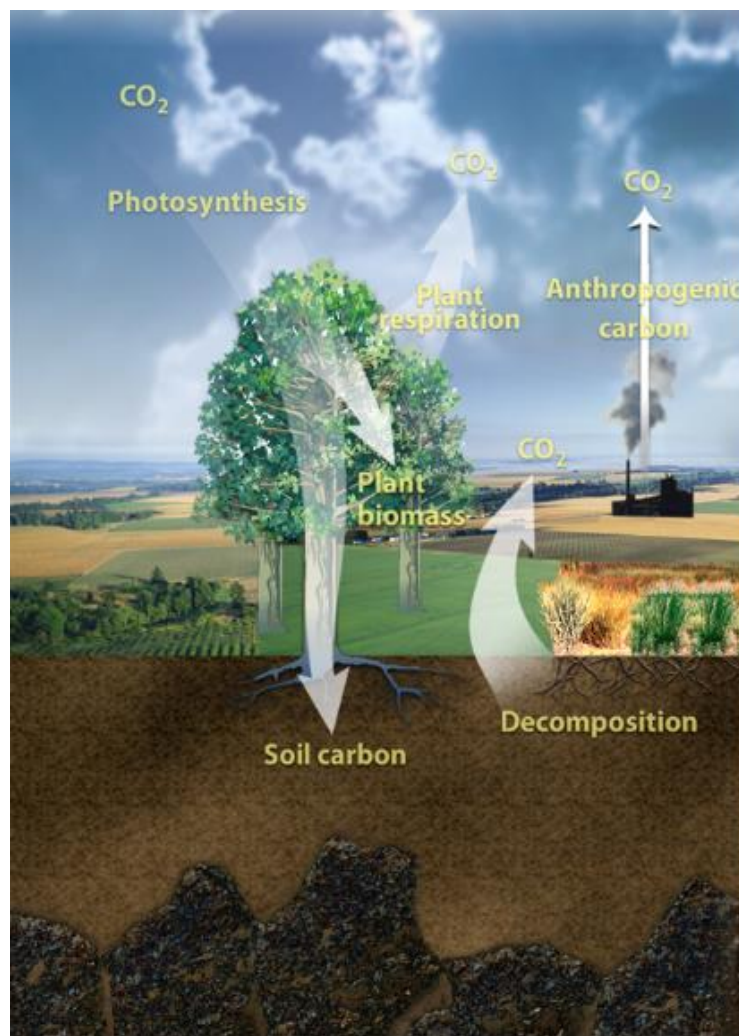


Figure 2.3 Diagram expressing the global carbon cycle, and the exchanges that occur. Source: USDOE (2008)



This variance is primarily due to the type of plant vegetation (C<sub>3</sub> vs C<sub>4</sub>) that has a direct bearing on the fractionation of carbon isotopes (<sup>12</sup>C vs <sup>13</sup>C) being used by the vegetation (Drever 1997; Li et al. 2008a; Hoefs 2010; Lambert and Aharon 2010; Gorka et al. 2011; Shin et al. 2011; Florea 2013; White 2013; McClanahan et al. 2016).

Carbon isotopic ratios are expressed as δ<sup>13</sup>C values and ascribe to the stable isotope theory as outlined by Drever (1997), Allen (2004), Palmer (2007a), and Hoefs (2010). Some elements on the periodic table include their isotopes, which are usually categorized by the number of protons and neutrons within their nucleus. All forms of stable isotopes exist within nature, but it is the ratio of each of these isotopes that is calculated when analyzing a sample. This process of selective abundance of one isotope relative to another, is called fractionation, and often occurs when there is a physical change of state. During plant root respiration, carbon undergoes fractionation processes, which shifts the ratio of heavy versus light isotopes, expressed by the δ symbol, and be calculated via the following equation from Drever (1997):

$$\delta^{13}\text{C} = \frac{(^{13}\text{C}/^{12}\text{C})_{\text{sample}} - (^{13}\text{C}/^{12}\text{C})_{\text{standard}}}{(^{13}\text{C}/^{12}\text{C})_{\text{standard}}} \times 1000 \text{ ‰} \quad (\text{Eq. 2.5})$$

where δ<sup>13</sup>C represents relative difference in parts per thousand (referred to as per mil, ‰) between the ratio in the sample and the ratio in the standard. These values are reported as a reference to marine calcite (a belemnite from the Pee Dee Formation in South Carolina) and expressed as PDB (Drever 1997; Allen 2004; Palmer 2007a; Hoefs 2010).

As mentioned before, there are six commonly identified sources of δ<sup>13</sup>C in terrestrial waters which can be delineated through carbon isotope investigations and contribute to overall carbon processes within karst systems: 1) dissolution of CO<sub>2</sub> in soil; 2) carbonate rock weathering; 3) the amount of CO<sub>2</sub> rich meteoric water infiltrating the

system; 4) exchange of bicarbonate and atmospheric CO<sub>2</sub>; 5) photosynthesis and respiration of aquatic plants; and 6) silicate rock weathering (Li et al. 2008a; Li et al. 2008b; Li et al. 2010; Liu et al. 2007; Liu et al. 2010; Jiang 2013; Zhang et al. 2015).

In the case of one and three, the most influential parameters on  $\delta^{13}\text{C}$  values, the concentration of dissolved CO<sub>2</sub> in soil is often a product of the season in which it is measured, the type of surface vegetation, and the amount and type of topsoil (permeable soils will be more likely to transmit fluid containing dissolved gases such as CO<sub>2</sub>, while, at the same time, soils high in microbial activity have higher concentrations of CO<sub>2</sub> which provide for increased CO<sub>2</sub> transmission). In the case of two, carbonate rock weathering is highly governed by the rate in which solutionally aggressive water enters, and is stored, in the system versus how often and how much water is immediately discharged. Increased storage rates increase residence times and, thus, the ability for dissolution to occur and remain ongoing until saturation is achieved. Four, five, and six are often parameters heavily examined in riverine systems, which, while potentially contributing to overall karst processes, are outside of the scope of this study and usually indicative of minimal influences on carbon fluctuations compared to sources one and three (Hess and White 1992; Drever 1997; Baldini et al. 2006; Li et al. 2008a; Hoefs 2010; Lambert and Aharon 2010; Gorka et al. 2011; Shin et al. 2011; Florea 2013; White 2013; Blecha and Faimon 2014a; Blecha and Faimon 2014b; McClanahan et al. 2016).

Since carbon isotopes ( $\delta^{13}\text{C}$ ) are often used as tracers for both sourcing of carbon in karst systems as well as assisting in delineation of the major hydrogeochemical players influencing a specific karst system, understanding the relationship of CO<sub>2</sub> and various vegetation uptakes of CO<sub>2</sub> can help delineate the impact that microbial activity within the

soil has on CO<sub>2</sub> sourcing and, thus, <sup>13</sup>C enrichment and/or depletion. For example, higher CO<sub>2</sub> concentrations provide for an increased uptake of <sup>12</sup>C by plant roots, causing soil waters transferred to the epikarst to become depleted with respect to <sup>13</sup>C due to fractionation. The ratio of <sup>12</sup>C/<sup>13</sup>C is often expressed with a negative value, which decreases as <sup>13</sup>C depletion increases (Drever 1997; Amundson et al. 1998; Li et al. 2008a; Hoefs 2010; Lambert and Aharon 2010; Gorka et al. 2011; Shin et al. 2011; Florea 2013; Jiang 2013; White 2013; McClanahan et al. 2016). The uptake of CO<sub>2</sub> by plant vegetation is highly reliant on the pathway by which the plant chooses to metabolize the CO<sub>2</sub>. For example, vegetation species characterized by C<sub>3</sub> pathways and associated photosynthesis are less efficient at metabolizing CO<sub>2</sub>, and, therefore, are often observed with more enriched <sup>13</sup>C values (closer to zero) as opposed to plants with C<sub>4</sub> pathways, which are known to metabolize CO<sub>2</sub> more efficiently and produce more depleted carbon isotopic values with respect to <sup>13</sup>C (further from zero).

In addition to using δ<sup>13</sup>C to trace the route which the water has taken to enter the system and its fluctuation through the system (Jiang 2013), δ<sup>13</sup>C can be useful in understanding the role of the global carbon cycle in specific systems. Epikarst water often is heavily laden with dissolved CO<sub>2</sub>, which is influenced by seasonal changes and storm events, thus δ<sup>13</sup>C values are often reflective of these same principles (Hunkeler and Mudry 2007; Knierim et al. 2015). Doctor et al. (2008) observed significant changes in δ<sup>13</sup>C values at a spring discharge during seasonal changes from snowmelt in early spring to summer rainfall. Their observations indicated changes related to both outgassing in the unsaturated zone as well as recharge flushing the system of shallow water saturated with CO<sub>2</sub> from topsoil during high vegetation growth periods. Drever (1997) and Hoefs (2010)

suggested that carbon fractionation factors reach equilibrium within seconds, making experimental determination rather challenging; thus, delineating sources of  $\delta^{13}\text{C}$  in conjunction with derived values of total dissolved inorganic carbon (DIC) can provide insight into how carbon is used by the system, as well as which source of carbon has the most influence.

Dissolved inorganic carbon (DIC) is considered a primary product of carbonate dissolution. This value is representative of several different carbon-based species including  $\text{H}_2\text{CO}_3$ ,  $\text{CO}_2$ ,  $\text{HCO}_3^-$ , or  $\text{CO}_3^{2-}$  (Li et al. 2008a) found in karst waters, which are fractionation factors of the dissolved carbon species; therefore, if the isotopic value of the carbon ( $\delta^{13}\text{C}_{\text{DIC}}$ ) in the soils and the limestone is known, then the equilibrium isotopic species of DIC currently dominating the system can be calculated (Zhang et al. 1995; Zhongcheng and Daoxian 1999; Drever 1997; Palmer 2007a; Li et al. 2008a; Li et al. 2008b; Hoefs 2010; Lambert and Aharon 2010; Liu et al. 2010; Gorke et al. 2011; Shin et al. 2011; Schulte et al. 2011; Faimon et al. 2012a; Faimon et al. 2012b; Singh et al. 2012; Florea 2013; White, 2013; Peyraube et al. 2013; Peyraube et al. 2014; Pu et al. 2014a; Pu et al. 2014b; McClanahan et al. 2016; Zhang et al. 2016).

According to Emblanch et al. (2003),  $\delta^{13}\text{C}_{\text{DIC}}$  can be used as a tracer to determine the extent of water mixing with respect to carbon sequestration within both the saturated and unsaturated zones of a karst system. The authors suggested that soil influences will be a primary adjuster to DIC content, since this relates to whether the DIC is being measured from an open or closed system (Emblanch et al. 2003). The authors further explained that exposure to soil compositions in open systems can heavily influence DIC totals, as opposed to systems that have a limited amount of soil derived carbon. In the

case of epikarst environments, it is important to remember that direct influences from soil derived carbon is common considering the type of infiltration and diffusion occurring near the surface.

Despite what seems to be an extensive understanding of CO<sub>2</sub> fluctuations and subsequent carbon isotope variations in the epikarst, Gorka et al. (2011) and Faimon et al. (2012a; 2012b) suggested that scientific understanding of epikarstic sources of CO<sub>2</sub> and changes with respect to  $\delta^{13}\text{C}_{\text{DIC}}$  is still in its relative infancy. The quantitative understanding of these processes increases with advances in monitoring technology. Liu et al. (2007) suggested that better developed, high-resolution sampling studies can potentially yield greater insight into the carbon uptake in epikarst systems. Zhang et al. (2015) and Zeng et al. (2016) discovered that carbonate weathering and surface runoff (river discharge versus subterranean sources) in karst catchments in China play vital roles in carbon source flux. Further, Zeng et al. (2016) proposed that soil type, lithology, and vegetation also play key roles in carbon fluxes. Due to the drastic need for quantitative understanding of the effects of anthropogenic CO<sub>2</sub> emissions on the environment, recognizing the role karst landscapes play with respect to potential carbon sequestration and utilization is imperative.

Ongoing examinations in the southcentral Kentucky region have been constrained to individual caves, inadvertently overlooking the importance of understanding regional CO<sub>2</sub> uptake and, thus, storage and flow properties, which may be at work within multiple cave systems. This research aims to fill a gap in the literature, with a comparative assessment of epikarst hydrogeochemical influences on dissolution and storage and flow dynamics, by examining the extent of carbon fluctuations with respect to CO<sub>2</sub> and  $\delta^{13}\text{C}$

variability through a nine-month, high-resolution study. It is hoped that this study will further support the findings of previous investigations that suggest CO<sub>2</sub> is one of the most vital ingredients in epikarst dissolution kinetics, and that δ<sup>13</sup>C values can shed light on the sourcing of this CO<sub>2</sub>.

## Chapter 3: Study Area

Kentucky is comprised of a well-developed karst landscape that underlies most of the state. In southcentral Kentucky, the karst area is known as the Western Pennyroyal Karst region and is divided into two parts, the Mammoth Cave Plateau and the Pennyroyal Sinkhole Plain, which are separated by the Dripping Springs Escarpment (Figure 3.1). The region is home to one of the longest mapped cave systems in the world, Mammoth Cave, with a total surveyed length of 629.25 km and counting.

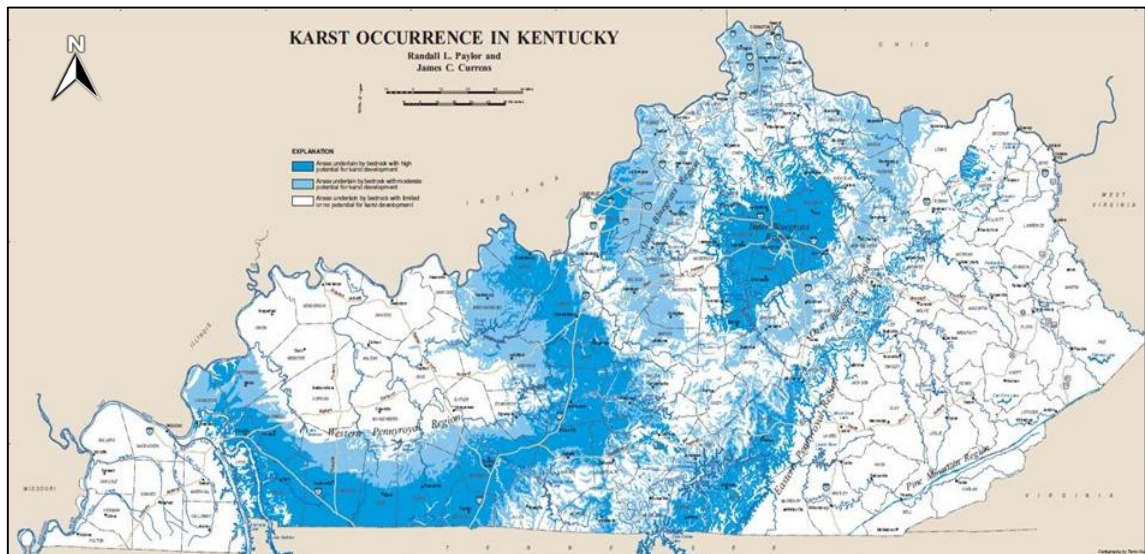


Figure 3.1 Karst distribution in Kentucky.

Source: Adapted from Paylor and Currens (2002).

Cesin and Crawford (2005) and Lawhon (2014) described the region as being one of the best examples of a complex karst environment in the northeastern United States. The dominant carbonate rocks include flat-lying, Mississippian-aged Girkin, Ste. Genevieve, and St. Louis limestones (Cesin and Crawford 2005; Palmer 2007a; Lawhon 2014). A distinct, but thin, layer of Lost River Chert lies within the upper portion of the St. Louis limestone and the lower portion of the Ste. Genevieve limestone. It is within

these lower bed layers (the St. Louis and the Ste. Genevieve) where the primary study sites are located. Due to weathering and erosion processes, these limestones are covered by thin, permeable clay soils in the sinkhole plain, while partially concealed beneath soils and a sandstone cap within the Mammoth Cave Plateau.

Southcentral Kentucky exhibits the characteristics of a broad, low-relief sinkhole plain and it is within this area that the primary study sites are situated (Figure 3.2). The limestones in this area have undergone a long period of temporal diagenesis, transforming the bed layers to telogenetic karst overlain by thin, clay rich soils. The sinkhole plain lies atop a well-defined aquifer, recharged via autogenic recharge through numerous sinkholes and sinking streams, as well as infiltration through fractures and matrix flow (Palmer 2007a; Cesin and Crawford 2005; Lawhon 2014). Both study locations (Crumps Cave and Lost River Cave and Valley) selected for this research are located within this sinkhole plain and, as such, share similar geology, hydrology, and soil type. Additionally, both systems eventually drain to the Barren River, with one draining from the north (Crumps Cave) and the other from the south (Lost River Cave and Valley). The primary differences between locations include surface land use (agricultural at Crumps Cave and urbanization at Lost River Cave and Valley) and epikarst thickness (Crumps Cave epikarst is roughly nine meters thicker than Lost River Cave and Valley). The study locations are approximately 22 km apart.

### **3.1 Crumps Cave at Smith's Grove, KY**

Crumps Cave offers a unique study location suited to investigate epikarst characteristics. The cave is situated beneath agricultural lands, away from the interference derived from large urban centers. Crumps Cave is located in Smith's Grove,





(Groves et al. 2005; Vanderhoff 2011; Groves et al. 2013). Land use in this region of the sinkhole plain is a mixture of agricultural and urban developments, with several population centers of varying sizes scattered throughout Warren County.

Temperatures range between 31 °C in the summer and 7 °C in the winter, classifying this region as humid subtropical in nature. Precipitation rates in this location average around 1,294 millimeters annually, with about 56% of this precipitation occurring between the months of April and October (Vanderhoff 2011). The recharge area for Crumps Cave lies within the Graham Springs groundwater basin, roughly 316 km<sup>2</sup>, and discharges into the Barren River ~17 km to the southwest (Ray and Blair 2005; Vanderhoff 2011). Annual baseflow at Graham Springs (Wilkins Bluehole) from this catchment is 0.56 m<sup>3</sup>/s. Previous work at Crumps Cave by Groves et al. (2005) suggested continuous flow through most epikarst springs in the cave, indicating extensive storage, while nearly immediate responses during storm events indicate the existence of a highly fractured and well developed epikarst conduit network. The cave sits under moderately permeable, well-dispersed soils that overlie the bedrock surrounding the sinkhole, and there is about 18 meters of limestone from the soil surface to the cave ceiling (Groves et al. 2005; Vanderhoff 2011; Groves et al. 2013). Access to Crumps Cave is obtained through a partially collapsed sinkhole. The entrance consists of a large, nearly horizontal passage 12 meters tall and 18 meters wide (Vanderhoff 2011; Groves et al. 2013). Crumps Cave is comprised of upper Mississippian-aged St. Louis limestone with a local dip of about 1-2° to the north. The Lost River Chert, an interbedded layer of silicified limestone, lies between the surface and the cave ceiling.

Crumps Cave contains two waterfalls along a relatively straight stretch of accessible cavern. Each of these waterfalls serves as an epikarst drain, which provides the opportunity to evaluate local hydrology and hydrochemistry. The first waterfall, located roughly 30 meters from the entrance and designated as Waterfall One (WF1), has an average drop of about four meters from the cave ceiling to the floor. WF1 drains from the epikarst and disappears into the cave floor as it passes through the vadose zone and joins the water table 40 meters below (Vanderhoff 2011; Groves et al. 2013). As part of the current investigation, a water catchment tarp, 189-litre barrel and two EXO II data loggers, combined with two HOBO pressure transducers and one HOBO temperature gauge, were installed near the waterfall to take measurements related to cave chemistry, waterfall discharge, and internal atmospheric conditions. The second waterfall, located 152 meters from the entrance, and designated Sed Falls (SF), is roughly six meters tall from ceiling to cave floor and drains into the water table some 25 meters below. This waterfall is primarily used for isotopic sampling, though plans for a more detailed water sampling station in the form of a 189-litre barrel and datalogger setup are in discussion.

On the surface, an Onset HOBO weather station exists to provide high-resolution temperature ( $^{\circ}\text{C}$ ), relative humidity (% RH), precipitation amount (mm), and barometric pressure data (mB). A four-litre rain gauge to trap precipitation is located next to the weather station. Two water table wells, one shallow (~15 m) and one deep (~50 m), provide continuous 10-minute measurements on current local and regional aquifer levels. Three soil lysimeters and one  $\text{CO}_2$  soil gas collector exist in the topsoil at various depths to analyze soil saturation and carbon dioxide concentrations.

### **3.2 Lost River Cave and Valley in Bowling Green**

Lost River Cave and Valley (LRCV) represents the primary drainage system for the Lost River Basin. The final discharge point, the Lost River Rise, represents roughly 152 km<sup>2</sup> (Ray and Blair 2005) of urban and agricultural landscape runoff (Crawford 1984a; Crawford 1984b; Crawford 1989; Crawford 2003; Crawford 2005; Brewer and Crawford 2005; Cesin and Crawford 2005; Palmer 2007a; Nedvidek 2014). The Lost River basin is part of the Pennyroyal Sinkhole Plain and is comprised of Mississippian-aged St. Louis and Ste. Genevieve limestones. Soils in the area cover 70% of the basin and are permeable silt and clay type soils (Lawhon 2014). Bowling Green, Kentucky, is built completely over the Lost River Cave system. Remediation efforts in the 1970s and 1980s to clean the cave environment after years of its use as a dump led to extensive studies to understand the hydrology and spatial extent of the drainage basin (Lawhon 2014); however, because the catchment incorporates runoff from both agricultural and urban activities, the possibility of having high major ionic concentrations is greater in this watershed than at the Smith's Grove Crumps Cave location.

One of the primary investigators to delineate the extent of the Lost River drainage basin was Crawford (1984a; 1984b; 1989; 2003; 2005) with others (Crawford et al.1999; Brewer and Crawford 2005; Cesin and Crawford 2005), who conducted a wide range of dye tracing examinations to delineate the subsurface flow paths in relation to sinkhole flooding and contaminant transport. Crawford (2005) also conducted electro-resistivity and microgravity investigations in conjunction with cave mapping to determine the overall length and extent of the Lost River. With these results, Crawford (1984a; 1989; 1999; 2003; 2005) generated reports for the City of Bowling Green to create new

stormwater treatment policies, protection from storm runoff pollutants (Crawford 1984a; Crawford 1984b), and characteristics of the effect of urban development over an unstable sinkhole plain (Crawford 1984a; Crawford 2005; Brewer and Crawford 2005).

The headwaters of the Lost River originate about 19 km south of the Bowling Green city limits, near the town of Woodburn, where several surface streams sink into the Ste. Genevieve limestone (Crawford 1984a; Crawford 1984b; Crawford 1989; Crawford 2005). The streams then converge, along with regional recharge, into a single river system trending northward toward Bowling Green (Nedvidek 2014). As the stream enters Bowling Green, it reemerges at the surface four times at multiple blue holes within the Lost River Valley, a collapsed cave passage roughly 2.41 km long, before it disappears into Lost River Cave. The stream continues northward through the subsurface strata until it finally resurges at Lost River Rise in Lampkin Park. Annual average discharge at the Lost River Rise is calculated to be roughly 0.35 m<sup>3</sup>/s, ranking it at number eight on the list of twenty largest springs in Kentucky (Ray and Blair 2005).

High discharge volumes, combined with a large catchment basin and increased incidences of cave flooding at the mouth of the Lost River Cave, suggest that the karst beneath Lost River has an extensive subsurface conduit flow network that is highly responsive to flood events. In fact, Lawhon (2014) discovered that the discharge at Lost River Blue Hole #4 would respond to rain events that occurred kilometers outside the Bowling Green city limits. These studies suggest that there may be extensive storage occurring that prevents water build up within the system, and that high levels of discharge are an indication of subsurface water replenishment through piston push style responses during large volume recharge events. This piston push response could also be

an indicator of extensive conduit development. After the river discharges at Lost River Rise, it continues as a surface stream before joining Jennings Creek, where it eventually discharges into the Barren River (Crawford 1984a, Crawford 1984b; Crawford 1989; Crawford 2003; Crawford 2005; Brewer and Crawford 2005; Cesin and Crawford 2005; Lawhon 2014; Nedvidek 2014).

Within the Bowling Green city limits, Lost River emerges on the surface at four blue holes. Each of these features are located within the valley, which is a remnant of subsequent cave collapse that now make up the valley. Adjacent to these blue holes is an epikarst spring, though its origins are unknown. The spring may be a tributary to the primary flow of Lost River, and thus may be incorporated within the overall Lost River groundwater basin; however, this suggestion has not been supported in the literature. The spring is located along the northeastern flank of the valley near the head. Flow from the spring is constant. The water emerges from the bedrock, pours over breakdown toward the base of valley, and then flows as a surface stream through the valley for about 111 meters before joining with Blue Hole #1. Subsequently, Blue Holes #2-4 are located periodically within a 0.80 km long length of the valley. At Blue Hole #4, the Lost River emerges on the surface and flows for roughly 30.48 meters before draining into Lost River Cave. Roughly 61 meters from the entrance of Lost River Cave is a three-meter-tall epikarst-fed waterfall that drains directly to the water table. It is one of the known epikarst waterfalls to exist within Lost River Cave, and is accessible year-round as part of an in-cave boat tour, which functions as a tourist site for Bowling Green visitors and locals. Western Kentucky University owns the land, which is managed by the Friends of Lost River, a non-profit organization dedicated to karst preservation and education.

## Chapter 4: Methods

This study employed a wide variety of field, laboratory, and data processing and analysis tools and methods. Field methods included automated data logging (YSI 2013), metrological based recharge measurements, velocity and bucket based discharge measurements, water sample collection for stable isotopes (Hess and White 1992; Wilde et al. 2015) and cation/anions (Huang et al. 2015), and the collection of grab samples for supplementary hydrogeochemical parameter analysis (Hunkeler and Mudry 2007). Laboratory analysis included Cavity Ring-Down Mass Spectrometry for carbon isotope ratio analysis (Godoy et al. 2012; Gebbinck et al. 2014), ion chromatography (IC) analysis for major anion concentrations, inductively coupled plasma emission spectroscopy (ICP-OES) for major cation concentrations, and manual titrations for bicarbonate alkalinity. Data analyses were conducted using SigmaPlot and *IsoSource* software, with Excel spreadsheets used to conduct simple calculations and for data organization. SigmaPlot software was used to generate complicated data analyses and graphical representation of all data. *IsoSource* software was used to determine carbon isotope sourcing.

### 4.1 Site Selection and Instrument Installation

Two locations containing two sample sites each were chosen at both Crumps Cave (WF1 and SF) and at Lost River Cave and Valley (LRWF and LRS) based on relatively unrestricted access to epikarst derived water and the ability to install (or use existing) scientific equipment.

At Crumps Cave Waterfall One (WF1), the sampling site coincides with a site being used for current hydrogeochemical investigations; thus, existing scientific instruments already on location were utilized for this research, including HOBO pressure/temperature and relative humidity transducers and YSI EXO II high-resolution hydrogeochemical data loggers. At Sed Falls (SF), a four-litre bucket was used to determine discharge at the falls by calculating the number of minutes and seconds it took for the bucket to fill to four litres. Figure 4.1 is a plan view of Crumps Cave, with the designated waterfalls marked as red dots.

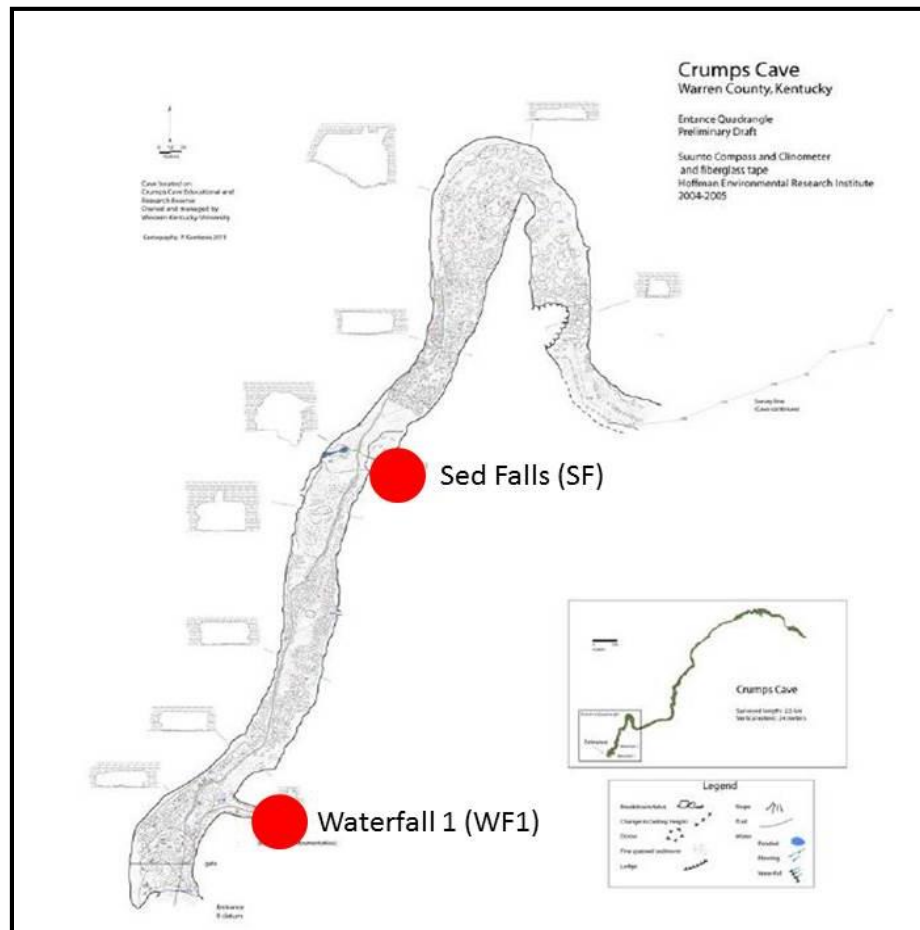


Figure 4.1 Location of the study sites at Crumps Cave. The locations of Waterfall One (WF1) and Sed Falls (SF) are indicated by red dots.

Source: Modified from Vanderhoff (2011).



## Lost River Cave and Valley

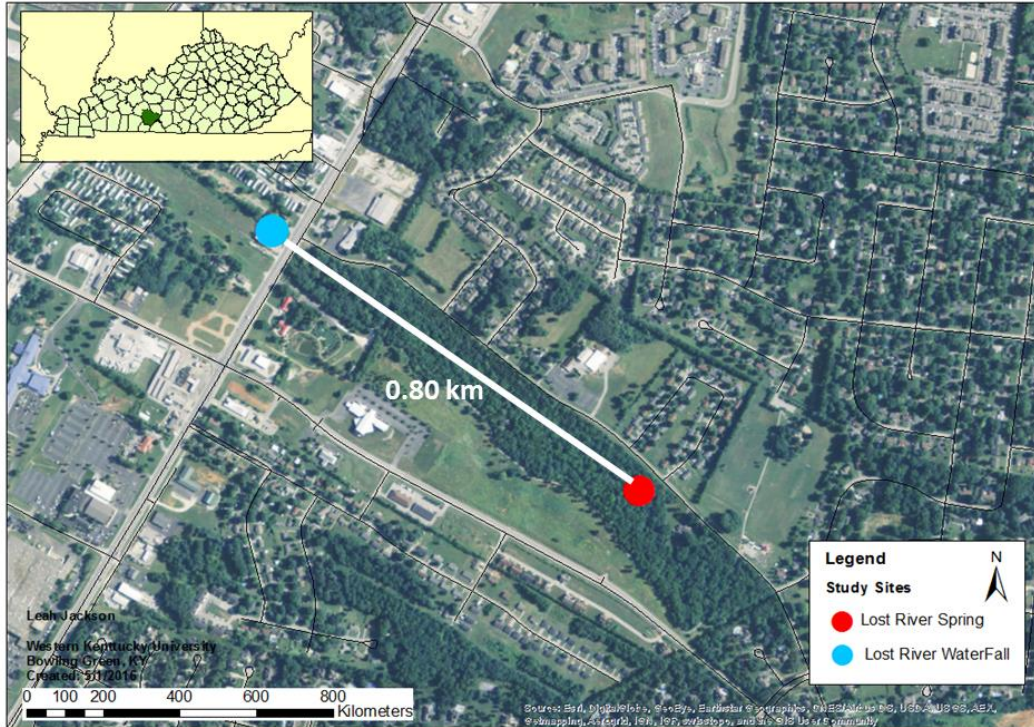


Figure 4.2 Lost River Cave and Valley and the surrounding city of Bowling Green. The locations of LRS and LRWF are identified by red and blue markers, respectively (with the extent of the LRCV identified by the mass of trees in the center of the image). The study sites are roughly 0.8 km apart.

Source: created by the author.

Lost River Cave sampling sites were divided geographically (Figure 4.2). Lost River Spring is located at the head of the valley, while Lost River Waterfall is located roughly 18 meters inside the mouth of the cave. Both sites are roughly 0.80 km apart, separated by natural vegetation within a collapsed karst valley. Lost River Spring is identified as a shallow epikarst spring at the origin of the valley and designated as LRS. The spring consists of a 2.13-meter waterfall that drains into a narrow and shallow surface stream, which flows for about 111 meters until it empties into Blue Hole #1. Close to the base of the falls is a wooden bridge constructed by the management of Lost River Cave and Valley. Placement of a HOBO pressure transducer and a YSI 600 Series

high-resolution data-logging sonde was adjacent to the bridge and housed in 3.81-cm diameter, 0.60-meter-long PVC stilling wells with fitted caps and secured with key locks to avoid theft and/or vandalism. Small holes were drilled in the pipes at random spots along their lengths to allow for water flow. A plastic screen was placed at the bottom of the pipe to ensure that the logger and transducer placement inside the well did not vary.

Lost River Waterfall is located about 18 meters within the cave at an epikarst-derived flowstone and is designated as LRWF. Access to the base of the flowstone is through a narrow passage adjacent to the river and access to the waterfall portion of the flowstone is up a set of manmade stairs carved into the limestone to a platform overlooking the river. The falls is on the interior side of the flowstone, roughly three meters above the river and about two meters above the base of the flowstone. A plastic 36-liter rectangular shaped tub and four-liter bucket were placed directly beneath the point where the water emerges from the bedrock. The bin and bucket were used to channel water flow to calculate discharge and collect water samples. A YSI 600 series data-logging sonde was placed in a pool formed by a rimstone dam near the base of the flowstone and programmed for high-resolution (10-minute interval) data collection. The logger was secured to a nearby boulder with thick metal airline cable to prevent theft or loss during flood events.

#### **4.2 Field Data and Sample Collection**

Beginning on May 24, 2016, weekly water sample collection occurred at each site. A complete suite of water samples was collected in various-sized containers ranging from 125 mL Nalgene bottles to 10 mL glass vials. Alkalinity samples were collected in 125 mL Nalgene bottles; cation samples were collected in 60 mL Nalgene bottles

containing seven drops of nitric acid for preservation; anion samples were collected in 60 mL Nalgene bottles; and carbon isotope samples were collected in 10 mL glass vials. All water samples were filtered from 500 mL Nalgene bottles filled directly from the source site, using a 0.45 $\mu$ m filter paper and 60 mL syringe. Distribution into all bottles ensured zero headspace, and screw caps were covered with multiple layers of parafilm wax to prevent outgassing and further fractionation. All water samples were collected following guidelines in the USGS National Field Manual for the Collection of Water-Quality Data (Wilde et al. 2015). All samples were refrigerated at 4 °C, until they could be delivered to the proper facility for analysis (Hess and White 1992; Wilde et al. 2015).

In addition to water sampling, a YSI 556 Handheld Multiparameter Instrument was used to perform grab sample analysis of standard geochemical parameters to support logger results at all four sites. The handheld is equipped with probes designed to obtain data regarding pH ( $\pm 0.2$  units), specific conductivity ( $\pm 0.001$  mS $\cdot$ cm $^{-1}$ ), temperature ( $\pm 0.15^\circ$  C), dissolved oxygen ( $\pm 1\%$  saturation or  $\pm 0.1$  mg $\cdot$ L $^{-1}$ ), and turbidity ( $\pm 0.3$  NTU) (YSI 2013). Grab samples were obtained at all four sites each week, except for during times of high water, causing a lack of site access.

At WF1, high-resolution (10-minute) interval EXO II data logging collected hydrogeochemical parameters, while one HOBO pressure transducer collected pressure and temperature readings from inside the barrel. Additional HOBO barometric pressure and relative humidity sensors were placed several meters away from the falls to determine cave air conditions. Each of these sondes collected 10-minute resolution data throughout the course of the study, except when briefly pulled for maintenance.

Beginning on August 21, 2016, an automated high-resolution YSI 600 Series data logging sonde and a HOBO pressure/temperature transducer were installed at LRS. A second automated high-resolution YSI 600 Series data logger was installed in a rimstone dam pool one meter below LRWF. Each 600 Series sonde was programmed to record geochemical parameters (pH, SpC, and water temperature) every ten minutes. Each 600 Series sonde is equipped with a probe for pH ( $\pm 0.2$  units), specific conductivity ( $\pm 0.001 \text{ mS}\cdot\text{cm}^{-1}$ ), and temperature ( $\pm 0.15 \text{ }^\circ\text{C}$ ) (YSI 2013). The HOBO pressure transducer was programmed for high-resolution 10-minute sampling of water temperature and pressure.

Volumetric discharge measurements were taken to gauge the amount of water discharging from LRS using a wading rod and flow meter. The bucket and stopwatch method was used to determine discharge at SF using a four-liter bucket (Michaud and Wierenga 2005). The same bucket and stopwatch method was employed at LRWF, only with the addition of a 36-liter tub to channelize flow in order to ensure full collection of water. The amount of water being discharged at LRS, LRWF, and SF was measured once a week and whenever flow conditions changed.

Meteorological data, including precipitation rates (mm/10 mins), relative humidity (RH %), surface temperature ( $^\circ\text{C}$ ), barometric pressure (mB), and soil moisture and temperature at three (10cm, 30cm, and 50cm) depths, were obtained from weather monitoring stations located within 0.80 kilometers of Crumps Cave and Lost River Cave and Valley. Soil temperature and moisture data at Lost River Cave and Valley were obtained from the Kentucky Mesonet FARM monitoring station, and represented conditions at three depths (8cm, 20cm, and 40cm).

### 4.3 Sample Analysis

Stable isotope concentrations of dissolved inorganic carbon ( $\delta^{13}\text{C}_{\text{DIC}}$ ) were determined using a Cavity Ring-Down Mass Spectrometer as outlined in Godoy et al. (2012) and Gebbinck et al. (2014) at the University of Utah's Stable Isotope Ratio Facility for Environmental Research (SIRFER) laboratory for each week samples were collected at each site. Isotope ratios were calculated using the standard isotope ratio based on the Vienna standard calculation for that element (Drever 1997; Allen 2004; Palmer 2007a; Hoefs 2010). Carbon isotopes ratios were reported using the standard  $\delta$  notation with a precision of  $\pm 0.3\%$ . Results are referenced to the VPDB standard.

Anion concentrations of fluoride ( $\text{F}^-$ ); chloride ( $\text{Cl}^-$ ); bromide ( $\text{Br}^-$ ); nitrate ( $\text{NO}_3^-$ ); nitrite ( $\text{NO}_2^-$ ); phosphate ( $\text{PO}_4$ ); sulfate ( $\text{SO}_4^{2-}$ ) were determined using Ion Chromatography (IC) analysis conducted at WKU's Advanced Materials Institute (AMI) following EPA Method 9056 on a Dionex ICS-1500, and after Jackson (2000). Cation concentrations of potassium ( $\text{K}^+$ ), sodium ( $\text{Na}^+$ ), magnesium ( $\text{Mg}^{2+}$ ), and calcium ( $\text{Ca}^{2+}$ ) were determined using inductively coupled plasma emission spectroscopy (ICP-OES) and were performed at AMI following EPA Method 200.8 using a Thermo Scientific ICAP 6500 ICP-OES (Stefansson et al. 2007). These instruments provide concentrations in parts per million (ppm) (equivalent to mg/L).

Manual titration of bicarbonate ( $\text{HCO}_3^-$ ) alkalinity was conducted at the Center for Human GeoEnvironmental Studies (CHNGES) laboratory at Western Kentucky University (WKU). Samples were poured into 120 mL glass beakers and manually titrated to a pH of  $\sim 4.5$  using 0.205 N  $\text{H}_2\text{SO}_4$  from May 24, 2016, to December 7, 2016. A second 500 mL glass jar of 0.027 N  $\text{H}_2\text{SO}_4$  was mixed at the HydroAnalytical

Laboratory at Bowling Green on December 7, 2016, and used to titrate samples manually to a pH of ~4.5 from December 13, 2016, to March 14, 2017. The pH and temperature were measured using the YSI 556 handheld probe. The total volume (mL) of H<sub>2</sub>SO<sub>4</sub> used to reduce the pH of a 50-mL sample to ~4.5 was recorded and used to calculate the total carbonate alkalinity concentration in mg/L based on the methods outlined in Neal (2001).

#### **4.4 Data Manipulation and Processing**

All processed data were organized in SigmaPlot spreadsheet software for convenient record keeping. Mastersheets were created for each site and included a column for every measured parameter as well as those calculated as a function of other measured parameters.

##### *4.4.1 Hydrogeochemical Data Processing*

Recorded high-resolution data from the EXO II, YSI 600 Series hydro-geochemical loggers and HOBO pressure transducers were compiled into Sigma Plot spreadsheet software for each week that data were collected. Calibration offsets for high-resolution SpC and pH at WF1, LRS, and LRWF were corrected per the USGS method 1-D3 (Wagner et al. 2006). Cation and anion concentrations in ppm, titrated alkalinity concentrations in mg/L, water temperature values and pH values for all sites, were inserted into a designated Excel spreadsheet to determine charge balances and calculate bicarbonate concentrations in mg/L. Charge balances ranged between ±10-20% for all sites, indicating raw data were good. Weekly HCO<sub>3</sub> concentrations, SpC, pH, Ca<sup>2+</sup>, Mg<sup>2+</sup> and water temperature values for all sites were then transferred into SigmaPlot to calculate activity coefficients, including H<sub>2</sub>CO<sub>3</sub>, CO<sub>3</sub>, CO<sub>2</sub>, saturation index (SI) with respect to CaCO<sub>3</sub>, and dissolved inorganic carbon (DIC), for each week at each site that

data were available. The equations used to execute these calculations included modified versions of the following: partial pressure of CO<sub>2</sub> as outlined in Drever (1997) and expressed in Eq. 2.2, the Palmer equation to determine saturation index (Palmer 2007a) and expressed in Eq. 2.4; and dissolved inorganic concentrations (DIC) as outlined in White (1988) and expressed in Eq. 4.3. Concentrations of the partial pressure of CO<sub>2</sub> were calculated by normalizing calculated P<sub>CO2</sub> to atmospheric contributions, allowing to express the final calculated values in the results and discussion as concentrations of CO<sub>2</sub> in volumetric parts per million (ppmv).

Further, dissolution rates of limestone at varying timescales were calculated using the equations found in White (1988) and Palmer (1991) and expressed as:

$$R = k_1[H^+] + k_2[H_2CO_3] + k_3[H_2O] - k_4[Ca^{2+}][HCO_3^-] \quad (\text{Eq. 4.1})$$

where  $R$  is the rate of the dissolved calcite and expressed as millimoles per centimeter square per second,  $k_{1-3}$  are temperature dependent forward rate constants that describe the rate that calcite is dissolving, and  $k_4$  is the backwards rate constant dependent on temperature and dissolution rates that describes the potential for precipitation of dissolved calcite from solution. The rate of wall retreat in karst conduits can be calculated using the equation from Palmer (1991) and expressed as:

$$S = \frac{31.56 k (1-SI_{\text{Calcite}})^n}{Pr} \quad (\text{Eq. 4.2})$$

where  $S$  is the rate of conduit wall retreat in cm/year,  $k$  is the temperature dependent rate constant,  $SI_{\text{Calcite}}$  is the saturation index of the mineral calcite (a ratio of the concentration of calcite in solution to the saturation concentration of calcite in solution),  $n$  is the reaction order of the dissolution reaction, and  $Pr$  is the density of the rock (2.7 g/cm<sup>3</sup>).

Dissolved inorganic carbon (DIC) concentrations in mg/L were derived from the following formula from White (1988):

$$\text{DIC} = \text{HCO}_3 + \text{CO}_3 + \text{H}_2\text{CO}_3 \quad (\text{Eq. 4.3})$$

Mass flux of dissolved species, including DIC, at WF1 and LRS, were computed by multiplying the concentration of the species of DIC by the discharge. Once a continuous record of DIC fluctuations was generated, a mass flux of DIC in mg/9 months for the study period was calculated by summing the total DIC concentrations. Likewise, once high-resolution data were generated for dissolved calcite, an estimated volume of rock dissolved at WF1 and LRS was determined by summation of the dissolution rate in mg/L over the entirety of the study period.

Regression analyses were conducted on high-resolution SpC and weekly  $\text{Ca}^{2+}/\text{Mg}^{2+}$  and  $\text{HCO}_3$  for WF1, LRS, and LRWF to determine statistical robustness, as well as their associated  $R^2$  values. As an additional statistical check, weekly resolution hydrogeochemical samples for SpC and pH were plotted against high-resolution logger data for the same date and time. No statistical difference was observed between both data sets, indicating that field equipment was operating within specific parameters. Regression equations from high resolution SpC, pH, and water temperature and weekly collected  $\text{Ca}^{2+}/\text{Mg}^{2+}$  and  $\text{HCO}_3$  concentrations were inserted into SigmaPlot to calculate high resolution  $\text{Ca}^{2+}/\text{Mg}^{2+}$  and  $\text{HCO}_3$  concentrations, and DIC activity coefficients of  $\text{CO}_2$ , Saturation indices, and DIC concentrations at WF1, LRS, and LRWF for the dates of May 24, 2016, to March 13, 2017, for WF1, and August 18, 2016, to March 13, 2017, for LRS and LRWF. Due to a logger malfunction at LRS, data are missing for a period of three weeks (December 28, 2016, to January 11, 2017) at that site. The  $R^2$  values



representing the relationship between high-resolution measured variables and weekly resolution ion constituents for WF1 and LRWF proved to be relatively robust, and thus using the slope equation derived from regression analysis to extrapolate certain high resolution was a simplified method to characterize shorter changes. This particular method to extrapolate data is commonly used in other studies (Groves and Meiman 2001; Groves et al. 2005; Liu et al. 2007; Groves et al. 2013; Pu et al. 2014a), but it is important to note that it is not without some limitation of error, especially when  $R^2$  values aren't as strong as hoped for, as was the case at LRS. At that particular site, extrapolation measures could potentially yield results subject to additional calculation error as described in Osterhoudt (2014). To ensure robustness of the extrapolated data, despite the low  $R^2$  value, weekly resolution data for LRS were compared with LRS high-resolution data collected at the same date and times. No significant statistical difference exists.

#### *4.4.2 Carbon Isotope Sourcing*

Raw collected weekly carbon isotope data were organized in Excel spreadsheets by site and date. A mixing model was run to determine exact source contributions (atmosphere/soil/carbonates/etc.) over the entire course of the study and seasonally. *IsoSource* software (v1.3) created by Don Phillips at the U.S. Environmental Protection Agency was employed for this study (Phillips and Jillian 2003). Data for each week were analyzed independently. The model was run with a 1.0% increment and mass balance tolerance of 0.5% (Phillips and Jillian 2003). Data parameters covered one isotope system with three possible isotopic end members (atmosphere, soil water, and carbonate bedrock). Values for the mixture were input based on collected weekly waterfall samples. The atmosphere value was assumed constant at -7‰ and based on established literature

(Clark and Fritz 1997; Shin et al. 2011; Zhang et al. 2015). Soil water values for Crumps Cave (WF1 and SF) were obtained by analyzing soil water collected from three soil lysimeters installed at varying depths (10cm, 30cm, and 50cm) to characterize soil CO<sub>2</sub> inputs to the cave. The three lysimeters are located directly above WF1 and varied each week they were available. During weeks that soil samples were not available at Crumps Cave (WF1 and SF), a calculated value of -16‰ was obtained by averaging values for soil carbon isotopes generated by Clark and Fritz (1997) for C<sub>3</sub> vegetation (-23‰) and C<sub>4</sub> vegetation (-9‰). Likewise, a soil sample value of -16‰ was used to process all collected samples from Lost River Cave and Valley (LRS and LRWF) (Clark and Fritz 1997; Shin et al. 2011; Zhang et al. 2015). Carbonate bedrock values were derived from powdered bedrock obtained from solid samples collected at each location (Crumps Cave and Lost River Cave).

#### *4.4.3 LRS Hydrograph Generation*

Atmospheric pressure data collected from the LR HOBO weather station were combined with the LRS HOBO pressure transducer data to determine high-resolution water level in feet at the spring. Water level data were then transferred to a separate Excel spreadsheet, which contained an embedded formula determined by regression analysis to generate a rating curve. Units for water level were converted from feet to meters during the rating curve generation phase of data processing. Average values calculated from collected data from velocity Q discharge measurements conducted at LRS were compiled in Excel spreadsheet software to generate a rating curve (Figure 4.3). Regression analysis was conducted to determine an R<sup>2</sup> value of 0.89 (p<0.001), which indicates a strong statistical significance between the parameters.

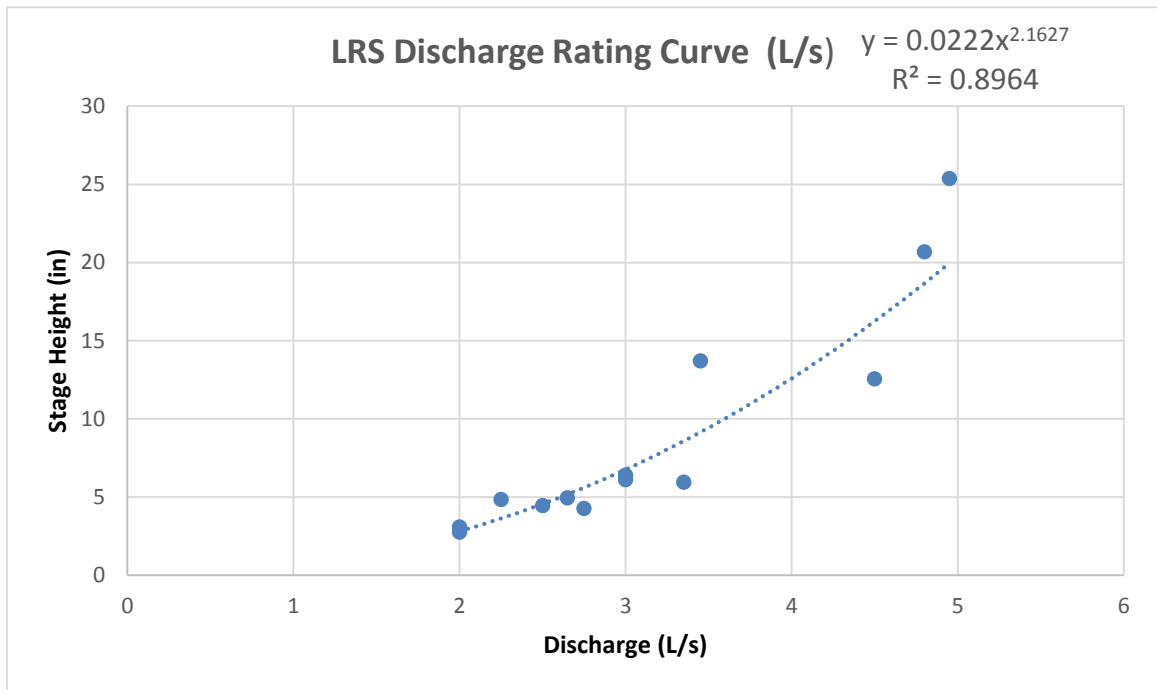


Figure 4.3 Rating curve for Lost River Spring (LRS) discharge. The Rating curve was generated from measured state height (in) and calculated discharge (L/s).

Source: Created by the author.

The slope equation generated from the regression analysis, in conjunction with the high-resolution water level data, was used to calculate high-resolution 10-minute discharge at LRS, in L/s, from August 18, 2016, to March 13, 2017. Final calculated discharge data were then transferred into the SigmaPlot mastersheet for LRS and plotted graphically over time.

## Chapter 5: Results

The hydrogeochemistry and carbon flux of four epikarst-derived waterfalls within the Pennyroyal Sinkhole Plain in southcentral Kentucky was examined from May 24, 2016, to March 13, 2017, to determine the impact of seasonal and storm event variability. A multi-parameter approach was employed to collect 10-minute resolution data for pH, SpC, water temperature, and meteorological changes, including precipitation, surface temperature, and influences on soil moisture and temperature. Weekly sampling for cations, anions, alkalinity, and carbon isotopes served to complete the study and address carbon sourcing and fluctuations. These data show variations at each of the four sampling sites (WF1, SF, LRS, and LRWF) with respect to the geochemistry and carbon fluctuations, which can be attributed to epikarst development and surface input, while carbon sourcing at each site seemed to show similar fluctuation responses. This suggested that contributions from land use, vegetation cover, and soil microbial activity are present and geochemical responses to these factors are relatively similar in a regional sense, yet exhibit site specific differences.

### 5.1 Epikarst Hydrogeochemistry

#### *5.1.1 Site Geochemistry Results*

High-resolution hydrogeochemical basic statistical results for WF1, LRS, and LRWF, and weekly resolution hydrogeochemical basic statistical results are presented in Table 5.1. Study period precipitation at Crumps Cave (WF1 and SF) was 994.8 mm. Crumps Cave-WF1 pH values range from 6.64 to 8.39, with an average of 7.43 (Table 5.1) during the study period. Specific conductivity values range from 144  $\mu\text{s}/\text{cm}$  (January) to 438  $\mu\text{s}/\text{cm}$  (July), with an average of 305  $\mu\text{s}/\text{cm}$ . Water temperature for WF1

range from 5.78 °C in December to 15.5 °C the following day in December. The average water temperature at WF1 was 11.5 °C. Discharge at WF1 is variable, but responds to high precipitation events (Table 5.1). Baseflow at WF1 was recorded at 0.013 L/s during the fall, while peak flow in discharge occurred in July and was recorded at 11.5 L/s. Average discharge at WF1 was calculated to be 0.07 L/s. Concentrations of CO<sub>2</sub> at Crumps Cave-WF1 range from 0.67 ppmv during the winter and early spring to 147 ppmv during the month of September, with an average of 43.9 ppmv. SIC at WF1 shows seasonal influences, with a minimal saturation index of -1.05 during the month of September and a maximum saturation index of 0.33 during the month of November. The average saturation index at WF1 was -0.31. DIC at WF1 showed similar seasonal fluctuations, with high concentrations during the summer and low concentrations during the winter. Minimum DIC in January was calculated at 127 mg/L while maximum DIC was calculated at 1,455 mg/L during September, with an average value of 734 mg/L (Table 5.1). DIC fluctuations varied during the study period, with a peak maximum loading of 536 mg/L/s during the month of July and a minimum loading of 0.2110 mg/L/s during the month of March.

Crumps Cave-SF (Table 5.1) collected geochemical and discharge data were at a weekly resolution, and were plotted in conjunction with high-resolution precipitation and surface temperature. Values for pH range between 6.12 and 7.81, with an average of 6.95. Specific conductivity values range from 175 µs/cm (January) to 580 µs/cm (September), with an average of 368 µs/cm. Water temperature for SF ranged from 8.52 °C in December to 17.5 °C in July. The average water temperature at SF was 13.7 °C.

Table 5.1. Summary statistics of major hydrogeochemical and  $\delta^{13}\text{C}_{\text{DIC}}$  parameters, at all sites.

Site		Water Temp (°C)	SpC ( $\mu\text{s}/\text{cm}$ )	pH	$\text{Ca}^{2+}$ (mg/L)	$\text{Mg}^{2+}$ (mg/L)	$\text{HCO}_3^-$ (mg/L)	$\text{CO}_2$ (ppmv)	$\text{SI}_{\text{CALCITE}}$	DIC (mg/L)	$\delta^{13}\text{C}_{\text{DIC}}$ (‰)	Discharge (L/s)
CRUMPS-WF1**	Min	5.78	144	6.64	19.6	4.0	41.3	0.67	-1.05	127	-14.8	0.013
	Max	15.5	438	8.39	67.5	12.9	312	147	0.33	1,455	-3.00	11.5
	Avg	11.5	305	7.43	45.8	8.8	189	43.9	-0.31	734	-9.49	0.07
CRUMPS-SF*	Min	8.52	175	6.12	25.3	3.8	72.0	2.96	-1.28	227	-15.9	0.06
	Max	17.5	580	7.81	90.9	15.8	385	604	0.27	3,204	-3.73	0.46
	Avg	13.7	368	6.95	54.2	9.2	217	117	-0.61	1,051	-9.60	0.16
LRCV-LRS**	Min	10.3	180	6.88	25.4	5.1	74.4	0.98	-0.91	15.0	-13.7	0.01
	Max	22.9	473	8.65	111	21.0	562	82.61	1.11	78.0	-1.60	3.84
	Avg	17.0	359	7.82	55.0	10.6	242	9.53	0.43	49.0	-11.4	0.06
LRCV-LRWF**	Min	11.4	237	3.95	34.7	6.8	127	0.21	-3.70	30.9	-14.5	0.009
	Max	17.9	673	9.53	106	19.9	529	63,162	2.32	13,209	-4.20	0.93
	Avg	15.5	505	7.52	78.4	14.9	375	1,077	0.40	298	-11.4	0.39

\*Weekly resolution

\*\*High Resolution

Source: Created by the author.

Discharge at SF was calculated every week and ranged from 0.06 L/s in baseflow conditions during November to peak flow conditions recorded at 0.46 L/s during August. Average discharge at SF was calculated to be 0.16 L/s. At Crumps Cave-SF, CO<sub>2</sub> concentrations ranged from 2.96 ppmv during February to 604 ppmv during the month of October, with an average of 117 ppmv. SIC at SF shows seasonal influences, but with less degree of variability than at WF1. Minimal saturation occurred during the month of May at -1.28 and a maximum saturation of 0.27 during the month of November. The average saturation index at SF was -0.61. DIC at SF showed similar responses, with a minimum value of 227 mg/L during February and a maximum value of 3,204 mg/L during October, with an average value of 1,051 mg/L (Table 5.1).

Study period precipitation at LRCV was 1019.6 mm. Lost River Cave and Valley-LRS pH values range from 6.88 to 8.65, with an average of 7.82 (Table 5.1). Specific conductivity values range from 180 µs/cm (August) to 473 µs/cm (December), with an average of 359 µs/cm. Water temperatures for LRS ranged from 10.3 °C in December to 22.9 °C in September. The average water temperature at LRS was 17.0 °C. Discharge at LRS ranges from 0.01 L/s in baseflow conditions during the fall to peak flow conditions recorded at 3.84 L/s in December. Average discharge at LRS was calculated to be 0.06 L/s. CO<sub>2</sub> concentrations at LRS range from 0.98 ppmv during August and 82.61 ppmv during the month of December, with an average of 9.53 ppmv. SIC values at LRS fluctuated, with minimal saturation occurring during the month of August at -0.91 and a maximum saturation of 1.11 during the month of November. The average saturation index at LRS was 0.43. DIC at LRS show similar responses, with a minimum value of 15 mg/L during August and a maximum value of 78 mg/L during December, with an

average value of 49 mg/L (Table 5.1). DIC fluctuations showed study period variability, with a maximum loading peak of 208 mg/L/s during the storm event in December, a minimum loading of 0.0 mg/L/s, and an overall study period average of 2.75 mg/L/s.

Lost River Cave and Valley-LRWF pH values range between 3.95 and 9.53, with an average of 7.52 (Table 5.1). Specific conductivity values range from 237  $\mu\text{s}/\text{cm}$  (December) to 673  $\mu\text{s}/\text{cm}$  (October), with an average of 505  $\mu\text{s}/\text{cm}$ . Water temperatures for LRWF range from 11.4 °C in November to 17.9 °C in the same month. The average water temperature at LRWF is 15.5 °C. Discharge at LRWF was calculated weekly and ranged from 0.009 L/s in baseflow conditions during November, to peak flow conditions recorded at 0.93 L/s in January. Average discharge at LRWF was calculated to be 0.39 L/s. The CO<sub>2</sub> concentrations range from 0.21 ppmv during the fall to 63,162 ppmv during the month of January, with an average of 1,077 ppmv. SIC at LRWF fluctuated, with minimal saturation occurring during the month of January at -3.70 and a maximum saturation of 2.32 during the month of November. The average saturation index at LRWF was 0.40. DIC at LRWF show similar responses, with a minimum value of 30.9 mg/L during December and a maximum value of 13,209 mg/L during January, with an average value of 298 mg/L (Table 5.1).

#### *5.1.2 $\delta^{13}\text{C}_{\text{DIC}}$ Isotopes Time Series Analysis*

A time series analysis of  $\delta^{13}\text{C}_{\text{DIC}}$  isotope data for Crumps Cave and LRCV is displayed in Figures 5.1 and 5.2 for all samples when they were available. Missing data at LRWF are the result of the site being inaccessible during high water periods. Missing data at WF1, SF, and LRS are the result of broken bottles during transport to the SIRFER lab. The  $\delta^{13}\text{C}_{\text{DIC}}$  values exhibit clear seasonal trends with depletion during the summer



months and enrichment during the winter months. Values at WF1, SF, and LRWF are close to zero at the onset of the study. Depletion in  $\delta^{13}\text{C}_{\text{DIC}}$  values occurred shortly after the study began, dropping from  $-11.9\text{‰}$  to  $-14.5\text{‰}$ , respectively, between sites on June 7, 2016.

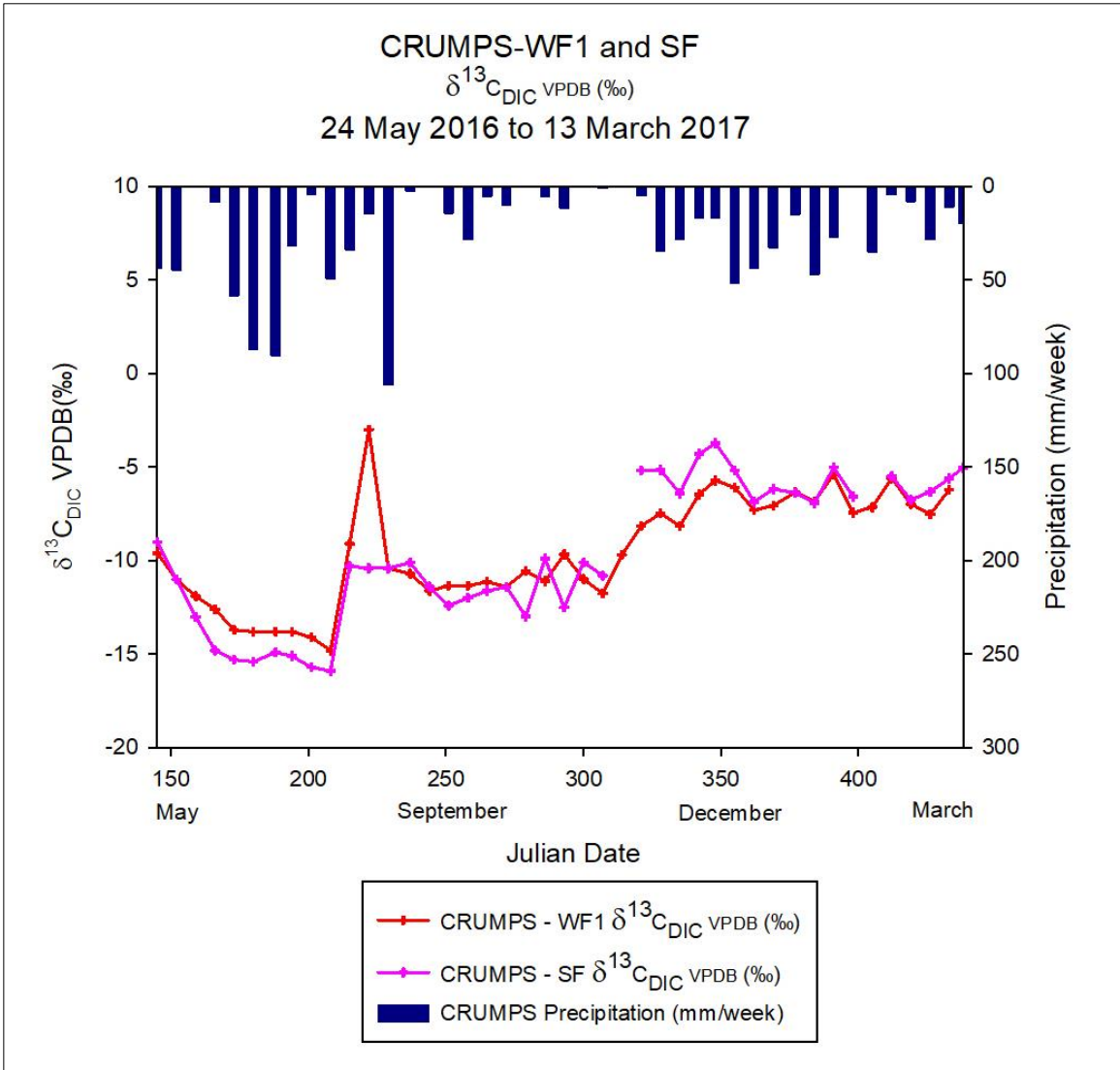


Figure 5.1  $\delta^{13}\text{C}_{\text{DIC}}$  Time Series Site Comparisons for CRUMPS-WF1 and SF. Note the summertime depletion followed by sudden enrichment at the fall transition at both sites. Source: Created by the author.

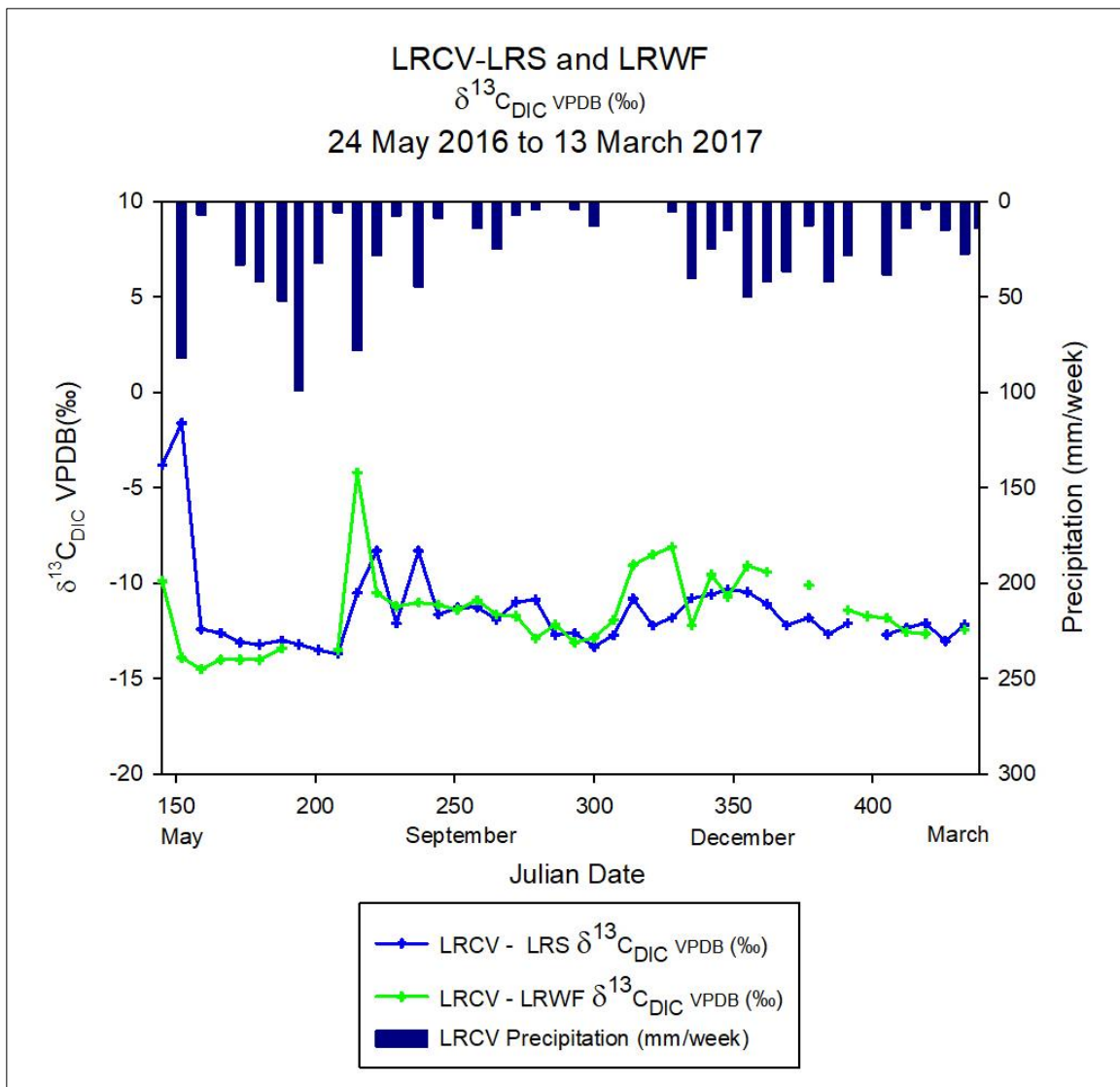


Figure 5.2  $\delta^{13}\text{C}_{\text{DIC}}$  Time Series Site Comparisons for LRCV-LRS and LRWF. Note the summertime depletion followed by sudden slight enrichment at the fall transition at both sites, and the general trend toward increased depletion over the remaining study period. Source: Created by the author..

Values remained in this depleted range at all sites until the end of July, when  $\delta^{13}\text{C}_{\text{DIC}}$  values enriched by  $-13\text{‰}$  at all sites, respectively. A distinct, minor depletion of  $\sim -8\text{‰}$  in  $\delta^{13}\text{C}_{\text{DIC}}$  values is visible around mid-August (JD 225) at all sites, which corresponds with the beginning of the fall transition. At that point,  $\delta^{13}\text{C}_{\text{DIC}}$  values at all sites remained within a range of  $-9\text{‰}$  to  $-13\text{‰}$  until late November (JD 328), when WF1

and SF  $\delta^{13}\text{C}_{\text{DIC}}$  values enriched to  $-3\text{‰}$  and  $-5\text{‰}$ , respectively, and remained in that range for the rest of the study period. LRS and LRWF remained relatively depleted within the range of  $-10\text{‰}$  to  $-12\text{‰}$  for the rest of the study period.

### 5.1.3 Mixing Model Study Period and Seasonal Results

The data for each sample collection date that samples were available were inserted into *IsoSource* software program designed to determine isotope sourcing of individual elemental compositions. Data for the mixtures and soil water at Crumps Cave varied each week. When at least two of the three soil lysimeters at Crumps Cave produced a sample, the values were averaged. When soil water sample values were not available, mixtures were processed using an assumed constant value of  $-16\text{‰}$ , drawn from the literature using the averaged values of both  $\text{C}_3$  ( $-23\text{‰}$ ) and  $\text{C}_4$  ( $-9\text{‰}$ ) vegetation contributions to soil (Clark and Fritz 1997). Values for the bedrock obtained from samples collected at Crumps Cave and Lost River Cave and Valley were  $3.9\text{‰}$  and  $3.6\text{‰}$ , respectively, and averaged to  $3.8 \pm 0.2\text{‰}$ . The value for the atmosphere were assumed constant from the literature and entered as  $-7\text{‰}$  VPDB (Zhang et al. 1995; Clark and Fritz 1997; McClanahan et al. 2016).

Time series analysis of the model results are presented in Figures 5.3 to 5.6, which show noticeable seasonal dependence in carbon sourcing at Crumps Cave, but not as much at LRCV. Due to the fact that the model reported all possible contribution sources and frequencies, mean contributions from each source, along with their possible ranges and standard deviations, were recorded and are presented in Appendices 1 to 4.

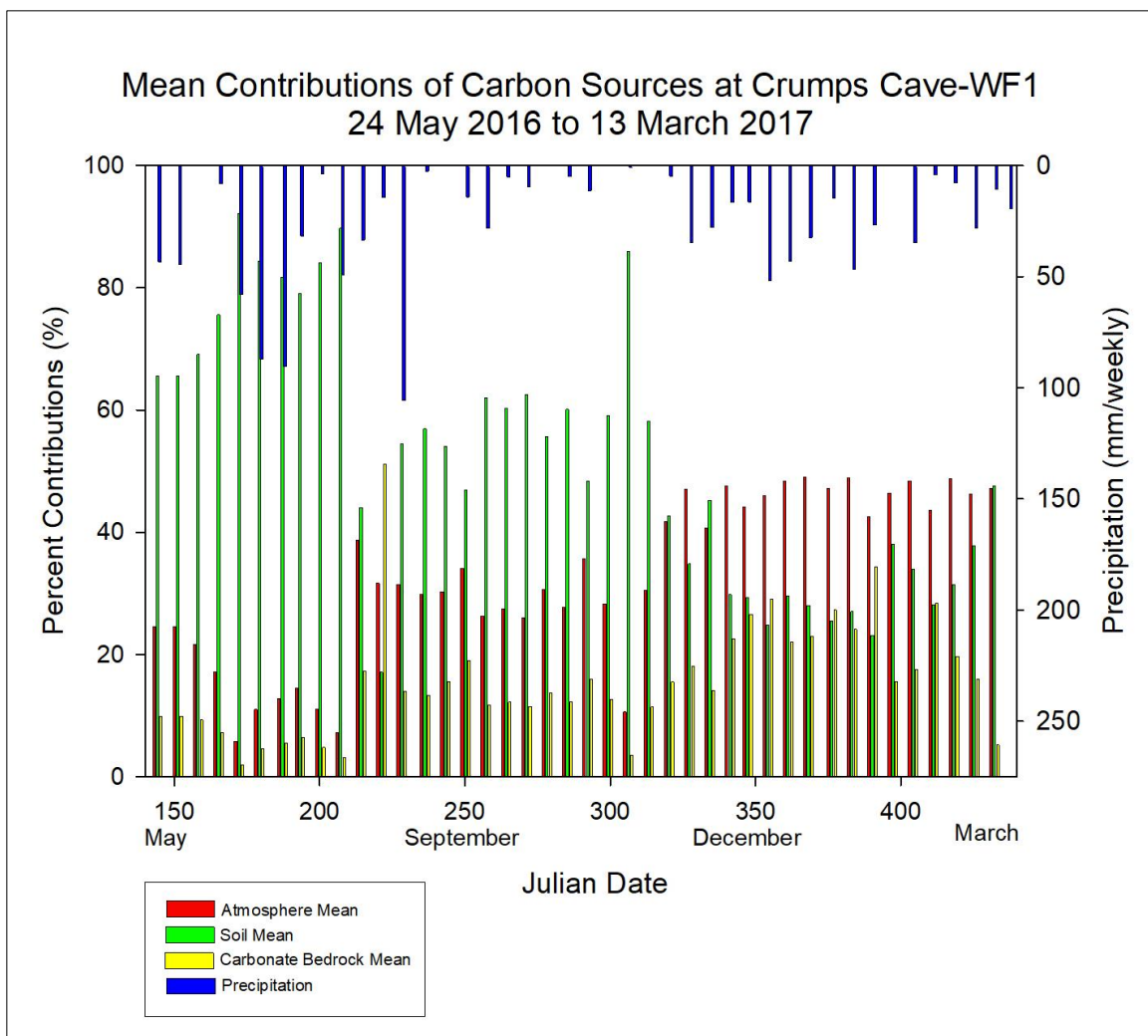


Figure 5.3 Mean Contributions of Carbon Sourcing at CRUMPS-WF1. Note the seasonal shift in carbon sourcing, from soil dominance during the summer months to atmospheric dominance during the winter months. Conversely, bedrock contributions are reduced at the start of the study, but increase during the winter months.

Source: Created by the author.

Mean contributions by percentage from each source are presented in Figures 5.3 to 5.6, which represent a study period time series analyses of carbon sourcing at WF1, SF, LRS, and LRWF, respectively. The majority of carbon samples were derived from the soil during the summer months at Crumps Cave and LRCV sites, while carbon was primarily derived from the atmosphere during the wintertime at Crumps Cave. Soil

contributions dominated throughout the year at LRCV. Seasonal variability at Crumps Cave sites would seem to coincide with both a reduction in photosynthesis during the winter, as well as a minimal amount of fractionation effects after the water had entered the epikarst.

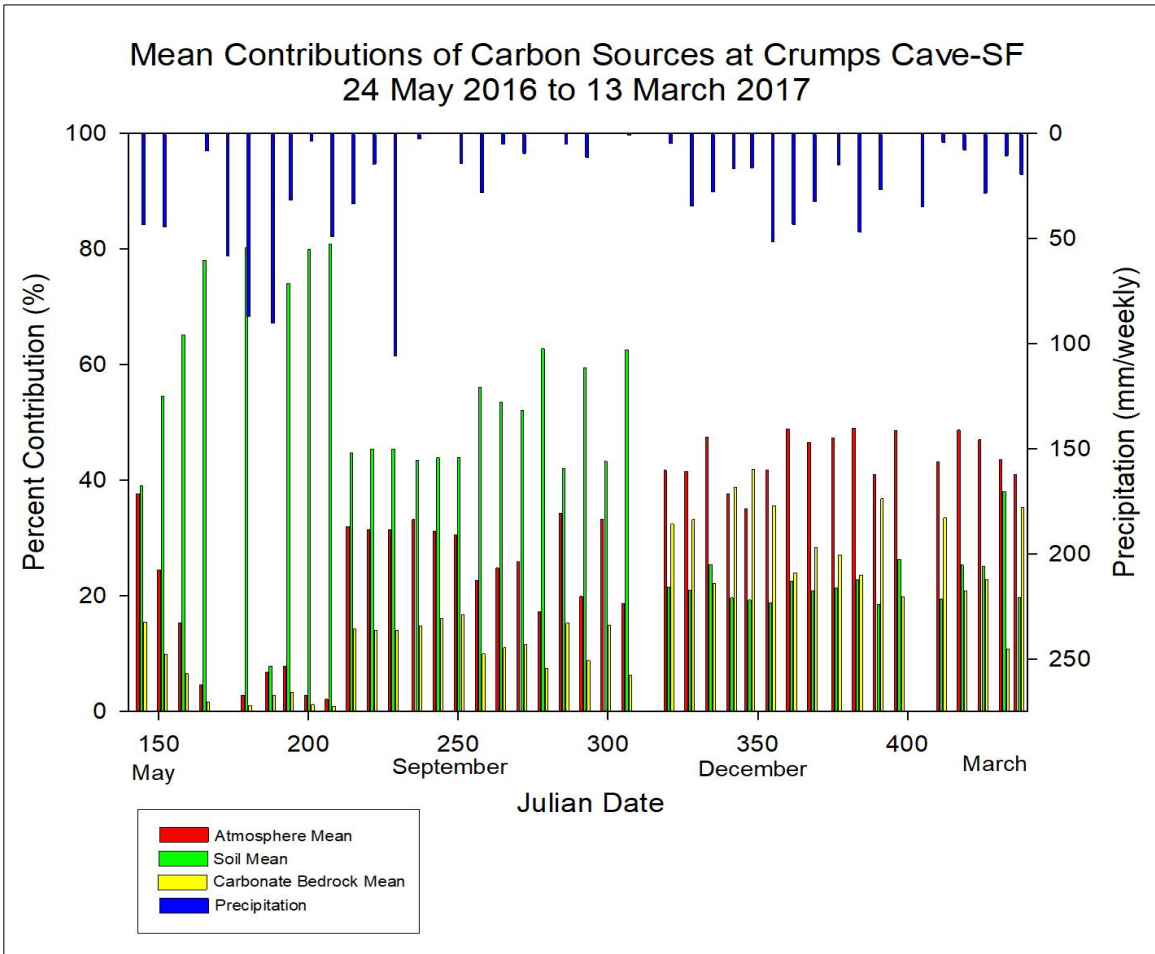


Figure 5.4 Mean Contributions of Carbon Sourcing at CRUMPS-SF. Note the similar responses to WF1 in seasonal shifts of sourcing. Likewise, water-rock interaction seems to increase over the progression of the study period

Source: Created by the author.

For seasonal results, median contributions and their standard deviations and possible ranges of each source were computed from the mean contributions to prevent any degradation in data reporting (Phillips and Jillian 2003) and are presented in Tables

5.2 to 5.5. Contributions to DIC at Crumps Cave WF1 and SF indicate clear seasonal transitions as dominating carbon sources shift from soil to atmospheric origins over the course of the study. The mixing model suggests that at WF1 the soil mean value is 51.3%  $\pm$ 20.9% over the course of the study period, with a range of 17.1% to 92.2%.

Atmospheric mean contributions are 31.6%  $\pm$ 13.4%, with a minimum of 5.8% and a maximum of 49%. Bedrock mean contributions are 14.1%  $\pm$ 9.5% with a range of 2% to 51.2% (Figure 5.3).

Table 5.2 Seasonal trends of mixing model results for WF1.

		Crumps Cave-WF1 DIC Contributions by Source (%)					
		Atmosphere		Soil		Bedrock	
		Value	Median Std	Value	Median Std	Value	Median Std
Spring	Median	35.4	12.8	56.6	13.8	9.9	4.4
	Min	24.5		37.8		5.2	
	Max	47.2		65.6		16.0	
Summer	Median	17.2	10.9	75.6	21.6	7.2	12.8
	Min	5.8		17.1		2.0	
	Max	38.7		92.2		51.2	
Fall	Median	30.5	9.1	58.1	12.6	12.6	3.8
	Min	10.6		34.8		3.5	
	Max	47.1		85.9		19.0	
Winter	Median	47.4	2.2	28.7	4.1	23.5	5.3
	Min	42.6		23.1		15.5	
	Max	49.0		38.1		34.3	

Source: Created by the author.

Seasonally, the values shift, with soil median contributing 75.6%  $\pm$ 21.6% in the summer, most likely from soil microbial activity and root respiration, and atmospheric median contributing 47.4%  $\pm$ 2.2% in the winter when minimal vegetation cover exists (Table 5.2). At SF, soil mean values contribute similar concentrations of carbon as observed at WF1, with 51.1%  $\pm$ 24.9% from soil, with a minimum of 9.4% and a maximum of 97%. Atmospheric mean values contribute 33.2%  $\pm$ 14.6, with a range of

2.1% to 49%. Bedrock mean contributions are 15.1%  $\pm$ 11.7, with a range of 0.9% to 41.9% (Figure 5.4). Seasonally, soil median contributions accounted for roughly 66.4%  $\pm$ 27.1% during the summer, while atmospheric median contributions accounted for 46.6%  $\pm$ 4.9% during the winter (Table 5.3).

Table 5.3 Seasonal trends of mixing model results for SF.

		Crumps Cave-SF DIC Contributions by Source (%)					
		Atmosphere		Soil		Bedrock	
		Value	Median Std	Value	Median Std	Value	Median Std
Spring	Median	41.0	8.7	45.7	16.3	15.5	10.5
	Min	24.5		23.7		9.9	
	Max	47.0		65.5		35.3	
Summer	Median	11.6	13.7	66.4	27.1	4.9	6.5
	Min	2.1		9.4		0.9	
	Max	33.2		97.0		16.1	
Fall	Median	28.2	10.0	57.7	18.5	13.2	9.1
	Min	17.2		25.2		6.3	
	Max	47.5		75.3		33.2	
Winter	Median	46.6	4.9	25.1	3.2	28.4	7.6
	Min	35.0		22.2		19.8	
	Max	49.0		31.6		41.9	

Source: Created by the author.

At LRCV-LRS and LRWF, seasonal shifts in carbon sourcing were not as apparent. Soil contributions seem to dominate throughout the entire study. At LRS, study period median soil contributions accounted for roughly 68.2%  $\pm$ 14.6%, with a range of 13.6% to 81%. Atmospheric contributions accounted for 22%  $\pm$ 7.03%, with a minimum of 13.3% and a maximum of 43.1%. Bedrock contributions accounted for 9.8%  $\pm$ 10.0%, with a range of 5.7 to 61.2% (Figure 5.5). Seasonally, soil median contributions account for 72.2%  $\pm$ 14.8% in the summer and 68%  $\pm$ 7.19% in the winter. LRWF displayed similar soil dominance during the entire study period (Figure 5.6). Study period soil

contributions accounted for  $65.1\% \pm 15.3$ , with a range of 20.1% to 87.2%. Median atmospheric contributions accounted for  $24.2\% \pm 9.52\%$ , with a minimum of 9% and a maximum median contribution of 44.3%. Bedrock contributions are  $10.7\% \pm 6.69$ , with a range of 3.8% to 42.6% (Figure 5.6). Seasonally, soil contributions dominated the system throughout the entire study period, with median values of  $59.7\% \pm 10.6\%$  during the winter and  $78.5\% \pm 19.9\%$  during the summer (Table 5.5).

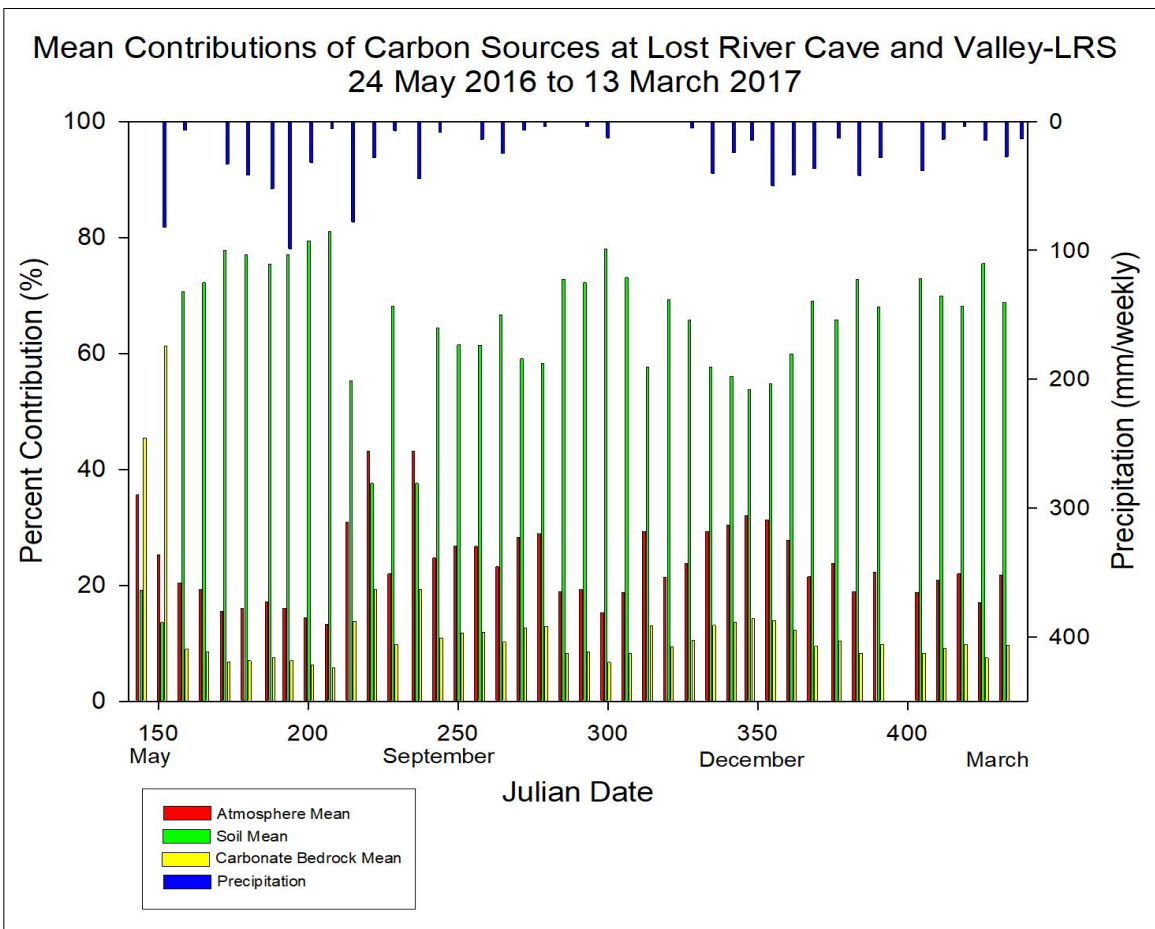


Figure 5.5 Mean Contributions of Carbon Sourcing at LRCV-LRS. Note that soil sourcing seems relatively uniform throughout the study.

Source: Created by the author.



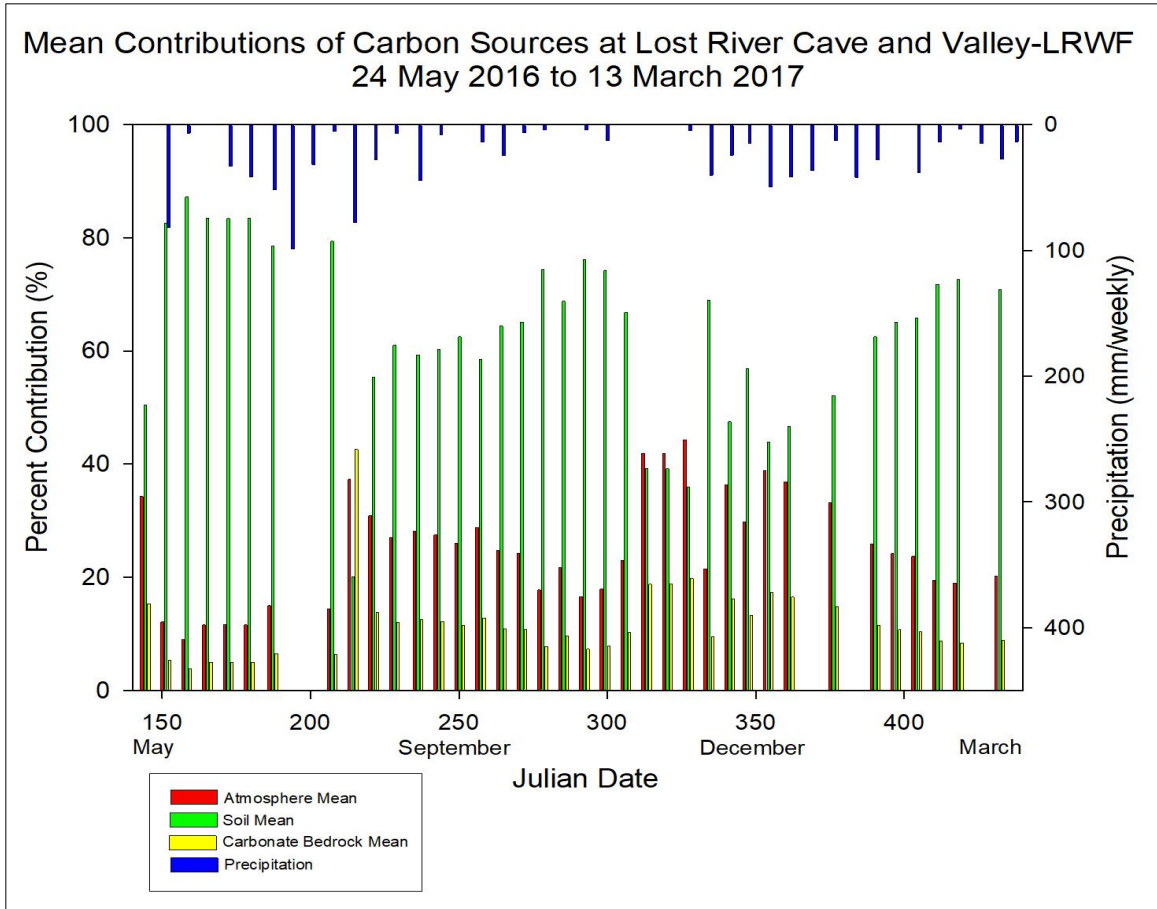


Figure 5.6 Mean Contributions of Carbon Sourcing at LRCV-LRWF. Note the similar responses to those observed at LRS, however, soil influences are increased at this site, especially during the summer months.

Source: Created by the author.

Table 5.4 Seasonal trends of mixing model results for LRS.

		LRCV-LRS DIC Contributions by Source (%)					
		Atmosphere		Soil		Bedrock	
		Value	Median Std	Value	Median Std	Value	Median Std
Spring	Median	23.5	7.9	43.95	32.41	27.5	26.6
	Min	17		13.6		7.5	
	Max	35.6		75.5		61.2	
Summer	Median	19.3	10.2	72.2	14.86	8.5	4.63
	Min	13.3		37.6		5.7	
	Max	43.1		81		19.3	
Fall	Median	23.8	4.76	65.7	6.93	10.5	2.17
	Min	15.3		57.6		6.7	
	Max	29.3		78		13.1	
Winter	Median	22.2	4.95	68	7.19	9.8	2.25
	Min	18.8		53.8		8.3	
	Max	32		72.9		14.3	

Source: Created by the author.

Table 5.5 Seasonal trends of mixing model results for LRWF.

		LRCV-LRWF DIC Contributions by Source (%)					
		Atmosphere		Soil		Bedrock	
		Value	Median Std	Value	Median Std	Value	Median Std
Spring	Median	20.2	11.2	70.9	16.3	8.9	5.1
	Min	12.1		50.4		5.3	
	Max	34.3		82.6		15.3	
Summer	Median	15.0	9.9	78.5	19.9	6.5	11.0
	Min	9.0		20.1		3.8	
	Max	37.3		87.2		42.6	
Fall	Median	24.2	9.6	65.1	14.0	10.7	4.4
	Min	16.6		35.9		7.3	
	Max	44.3		76.1		19.8	
Winter	Median	27.9	7.3	59.7	10.6	12.4	3.3
	Min	19.0		43.9		8.4	
	Max	38.8		72.6		17.3	

Source: Created by the author.

## Chapter 6: Discussion

### 6.1 Epikarst Hydrogeochemistry

#### *6.1.1 Site Geochemistry Discussion*

The data presented from this investigation suggest that open system conditions are present at both study locations (Williams 1983; White 1988; Palmer 1991; Clemens et al. 1999; Emblanch et al. 2003; Klimchouk 2004; Cheng et al. 2005; Palmer 2007a; Jiang et al. 2007; Williams 2008; Faimon et al. 2012a). Higher precipitation rates and warm surface temperatures during the summer months facilitate the interaction of CO<sub>2</sub> with the carbonate system by providing for surface conditions to encourage vegetation growth and CO<sub>2</sub> production in the soil at Crumps Cave sites, but less pronounced at Lost River Cave and Valley sites due to an urban landscape potentially interfering with CO<sub>2</sub> diffusion. High precipitation events transport accumulated soil CO<sub>2</sub> into the epikarst. During the dry, relatively warm months, CO<sub>2</sub> diffusion also occurs, but at a slower rate, because precipitation events are lacking. In this case, while diffusion to the epikarst does occur, CO<sub>2</sub> concentrations appear to accumulate in the soil at increased concentrations. During the colder, wet winter months, new soil CO<sub>2</sub> production seems to decrease, along with vegetation growth, while the remaining soil CO<sub>2</sub>, which has not diffused to the epikarst during the warm, drought season, is then dissolved in rainwater and carried to the bedrock below. Fluctuations in SpC and pH values throughout the study are representative of dissolution and/or precipitation, and seem to coincide with surface patterns. Likewise, CO<sub>2</sub> concentrations, SI<sub>c</sub>, and DIC fluctuations also support surface influences and, thus, open system conditions.

To delineate the extent of surface influences on epikarst responses, this study focused on two levels of scrutiny: a multi-month time series analysis, which reflects the seasonal changes occurring at each site (Figures 6.1 to 6.10), and two specific storm events to characterize epikarst changes at extremely high-resolution at three different intervals: baseflow conditions prior to the storm, storm responses at the site, and a return to baseflow conditions (Figures 6.11 to 6.14). Both storm events (one in the summer and one in the winter), spanned roughly three days and focus on the conditions at WF1 and LRS to represent changes observed at each location as a regional comparison of site responses. Due to the extremely large dataset, the most notable points within each time series at every site are presented in the hydrogeochemical discussions.

### *Precipitation*

Precipitation values at Crumps Cave (Figures 6.1 and 6.2) and LRCV (Figures 6.3 and 6.4) indicate wet and dry seasons. Distinctly higher precipitation rates and frequencies occur during the summer months, followed by reduced precipitation events during the fall, with increased precipitation events during the winter months and spring transition. Summer precipitation frequencies and rates appear to be contributing to epikarst water temperature, SpC, and pH conditions, reflecting distinct dilution effects as precipitation filters through the topsoil and enters the epikarst (Figures 6.1 to 6.4). Study period precipitation rates at Crumps Cave are higher than at LRCV (65% at Crumps Cave versus 34% at LRCV); however, recorded precipitation at Crumps Cave and LRCV is assumed the same for each study site within each location. Thus, the overall precipitation rates at Crumps Cave are considered the same for WF1 and SF; likewise, the overall precipitation rates at LRCV are assumed the same for LRS and LRWF.

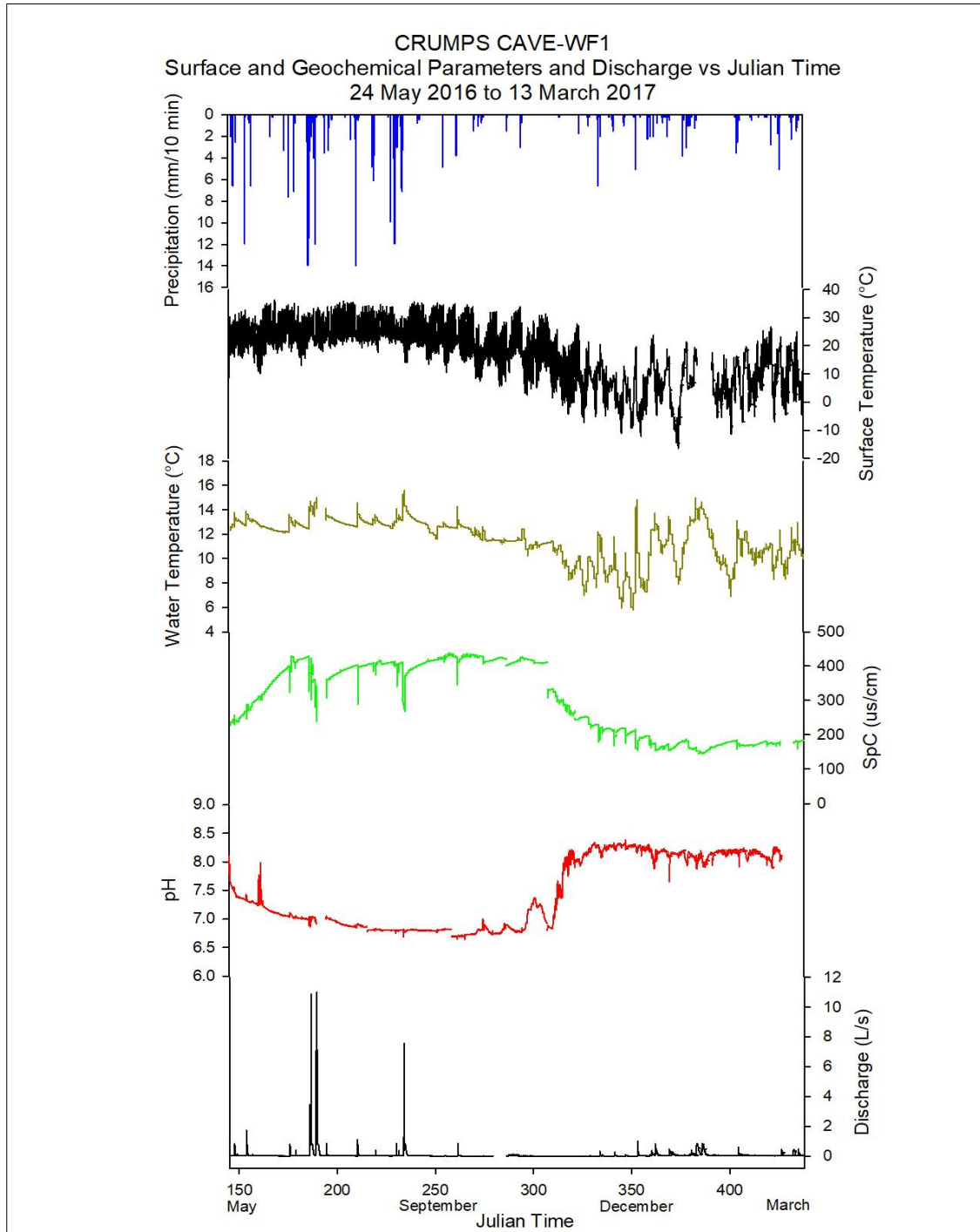


Figure 6.1 Time series of hydrogeochemical changes at Crumps Cave-WF1. Note the distinct seasonal changes in all respects, including the inverse relationship between SpC and pH during the summer and fall months. Water temperature trends closely with surface temperature, while discharge seems to respond rather quickly to precipitation inputs.

Source: Created by the author.

### *Surface and Water Temperature*

Surface and epikarst water temperature patterns at Crumps Cave (WF1 and SF) indicate clear seasonal, diurnal, and storm event responses, with an overall study period trend of warmer temperatures in the summer and colder temperatures in the winter. Diurnal inflections of warmer temperatures during the daytime and cooler temperatures during the night are also present, with sudden increases to precipitation, followed almost immediately by gradual decreases (Figures 6.1 and 6.2). During the summer months, minimal diurnal surface temperature fluctuations are observed. During the winter, diurnal surface temperature fluctuations are more pronounced and seem to coincide with heavy precipitation events. Water temperature behaves in a similar fashion, with a general seasonal trending from high temperatures to low temperatures, more pronounced influences from surface conditions during the winter months, and immediate responses to infiltrating precipitation, especially during high precipitation events (Figures 6.1 and 6.2).

At the LRCV (LRS and LRWF), surface temperatures indicate distinct seasonal responses, as evident by overall higher temperatures during the summer months, which trend to lower temperatures during the winter months (Figures 6.3 and 6.4). As with observations in surface temperatures made at Crumps Cave, winter variability in surface temperatures at LRCV is pronounced, diurnal fluctuations are distinct throughout the year, and responses to storm events indicate a decrease in surface temperatures immediately following the onset of rainfall. Water temperatures at LRS and LRWF seem to mirror surface temperature, both seasonally and during precipitation events, indicating an overall decrease in temperatures as summer transitions to winter, and immediate decreases in temperature following the onset of rainfall (Figure 6.3 and 6.4); however,

some very distinct differences in temperature responses from both storm events and seasonal variability occur at both sites. It is possible that these temperature differences are also contributing to CO<sub>2</sub> fluctuations, as increased water temperatures are less capable of holding dissolved CO<sub>2</sub>, while decreased water temperatures are more capable of holding higher concentrations of CO<sub>2</sub>, and thus, can contribute to ongoing dissolution.

While water temperatures at LRS (Figure 6.3) trend seasonally (high in the summer to low in the winter) and responses to storm events are clearly present (temperature dilutions at the onset of precipitation), the most pronounced effect is the diurnal fluctuation in water temperature. These fluctuations are representative of responses to water temperature, which is in relative equilibrium with surface temperature, thus mirroring surface temperature behavior of day and night fluctuations. Increased water temperature variability resulting from diurnal fluctuations in riverine systems have been observed in hydrogeochemical studies conducted by Hess and White (1992), Osterhoudt (2014), Pu et al. (2014a), McClanahan et al. (2016), and Salley (2016). At the LRWF (Figure 6.4), these diurnal fluctuations are less pronounced, possibly due to the water reaching equilibrium with cave temperature; thus, LRWF water temperature is more heavily influenced by precipitation events and overall seasonal trending versus daily cycles of day and night temperatures as observed at LRS.

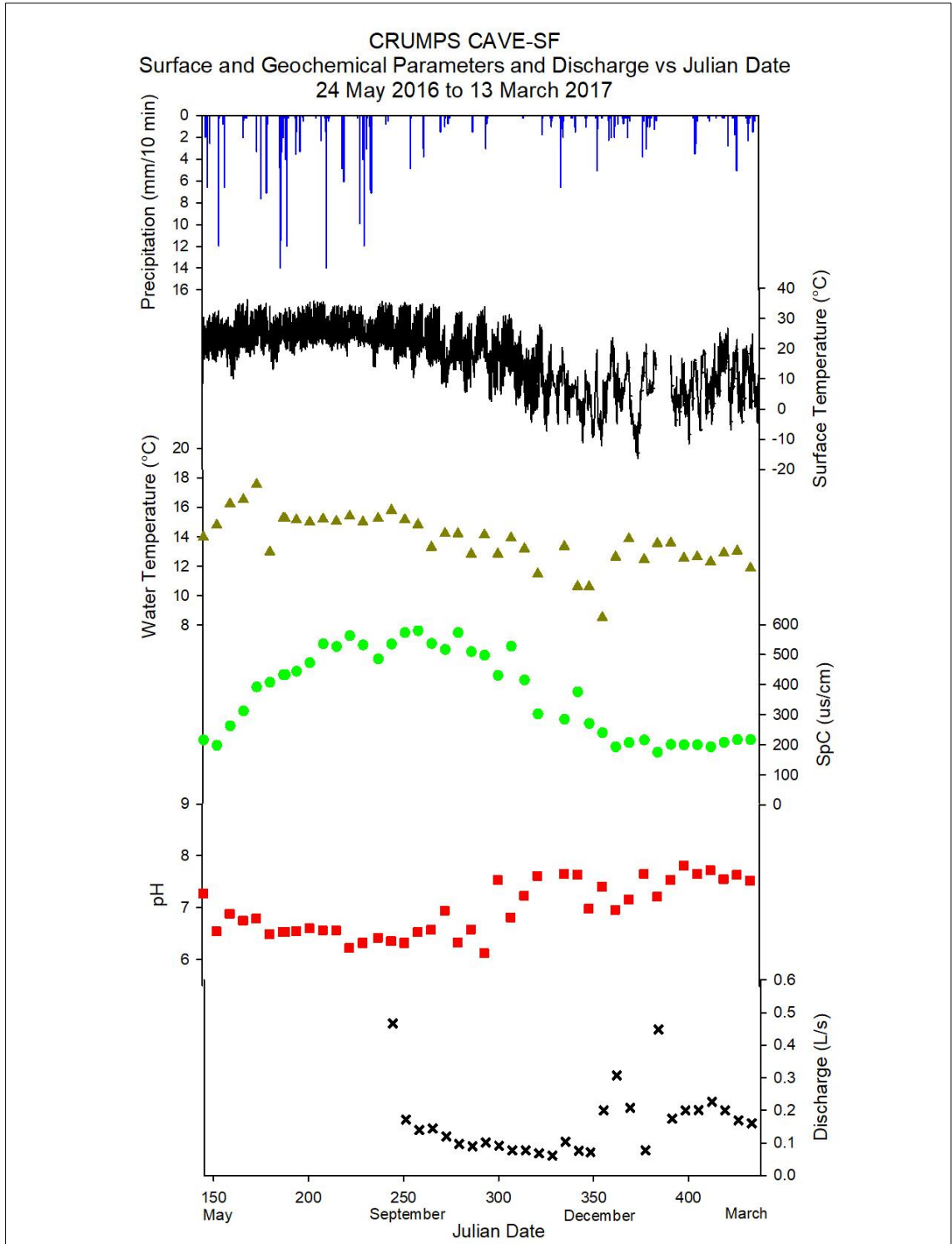


Figure 6.2 Time series of hydrogeochemical changes at Crumps Cave-SF, over the course of the study. Note the seasonal responses similar to those observed at WF1.

Source: Created by the author.



Similar responses are observed at Crumps Cave and LRCV with respect to seasonal, diurnal, and precipitation event temperature fluctuations and are common in epikarst studies. Cheng et al. (2005); Jiang et al. (2007); Liu et al. (2010) and Pu et al. (2014b) all found the same trends in karst regions in China. Likewise, investigations into eogenetic karst systems in Florida by Gulley et al. (2015) found that surface temperature and water temperature tend to mirror one another on all three scales. The studies suggest that temperature fluctuations, both seasonally and diurnally, are a result of normal surface influences on water temperature in open karst systems. Additionally, diurnal patterns are a consequence of absorbed solar radiation influencing the water, which eventually drains at the base of the epikarst. Lastly, during the summer months, solar output tends to heat precipitation, driving the subsurface water temperature upward upon initial infiltration as new water is mixed with older, more equilibrated water (Cheng et al. 2005; Liu et al. 2010; Yang et al. 2012; Pu et al. 2014a; Pu et al. 2014b; Gulley et al. 2015).

#### *Specific Conductivity (SpC)*

SpC values are an indicator of the number of free ions in water, usually caused by dissolution (White 1988; Palmer 1991; Hess and White 1992; Drever 1997; Palmer 2007a). With higher values, the increased concentrations of free ions are assumed to occupy the water. Since dissolution of limestone usually results in a combination of  $\text{Ca}^{2+}$  and  $\text{Mg}^{2+}$ , (and less commonly  $\text{K}^+$  and  $\text{Na}^+$ ) and  $\text{HCO}_3^-$ , then active dissolution, especially during the summer months, is occurring at all sites, as evident by seasonal oscillations, with higher values during the summer months and lower values during the winter months.

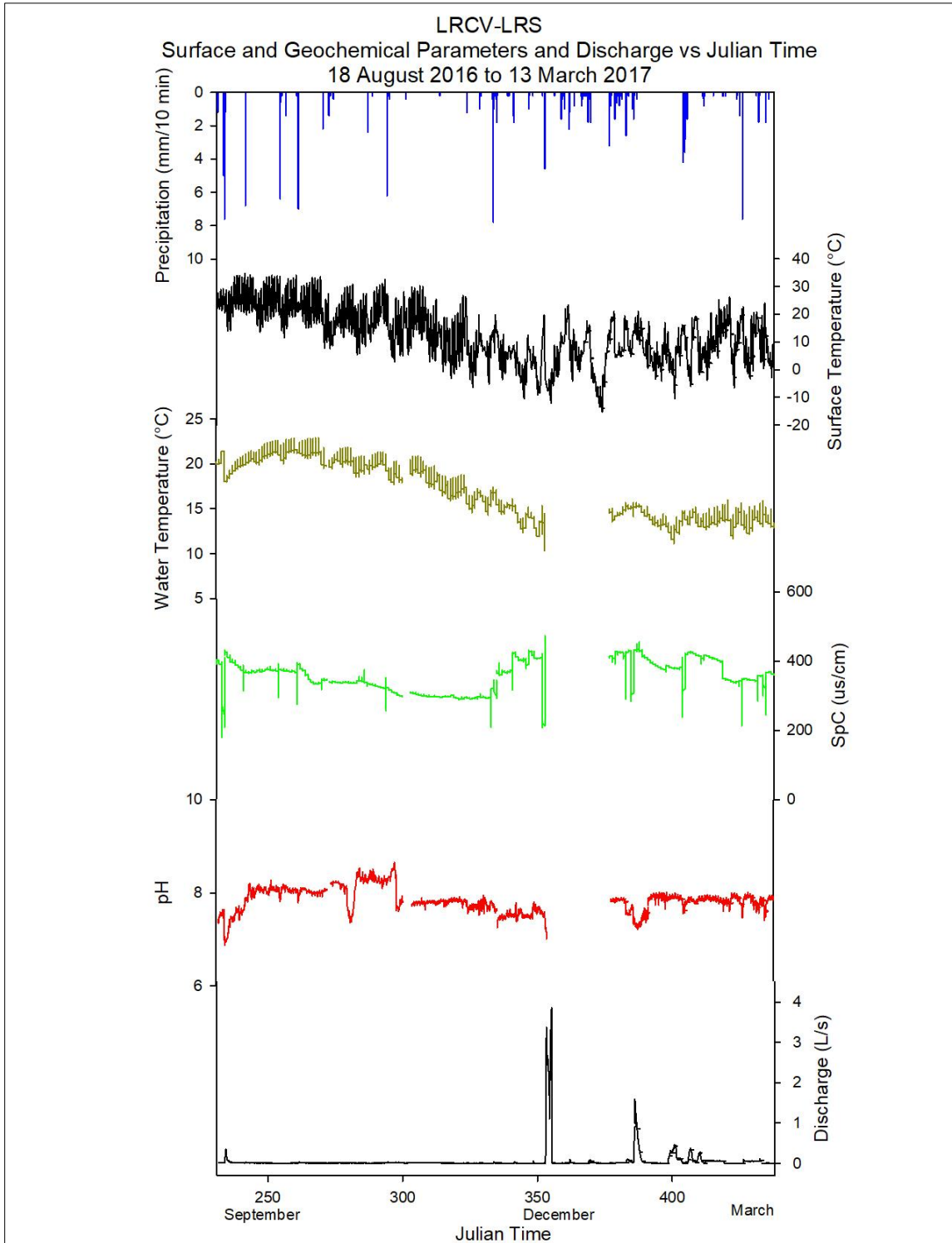


Figure 6.3 Time series of hydrogeochemical changes at LRCV-LRS. Note the seasonal trends in surface and water temperature; however, the SpC and pH exhibit little variation during the study period. A data gap for geochemical values is a result of mechanical failure of the logger.

Source: Created by the author.

Most pronounced are the near immediate decreases in values following the onset of precipitation events (Figures 6.1 to 6.4), which occur concurrently at all four sites with seasonal trends (higher overall values in the summer and lower overall values in the winter) (Cheng et al. 2005; Yang et al. 2012) (Figure 6.1 and Figure 6.2). Precipitation responses create a near immediate decrease in values resulting from infiltrating water with a low SpC, causing dilution effects resulting from the fast flush of fresh and storage water through the system. Despite the difference in resolution at WF1 and SF, these trends in both seasonal and storm event responses are very similar, suggesting that both waterfalls are influenced by similar epikarst conduit networks, as was discovered by studies conducted by Groves et al. (2005), Vanderhoff (2011), and Groves et al. (2013).

At the LRCV (LRS and LRWF), SpC values also show seasonal trends; however, that trend is the least pronounced at LRS (Figure 6.3). This could be the result of surface influences, such as exposure to the atmosphere, reducing the available CO<sub>2</sub> for dissolution reactions via degassing, causing precipitation of calcite and reduction of dissolved ions (McClanahan et al. 2016; Osterhoudt 2014); however, SpC values still show dilution responses to precipitation events, suggesting that SpC values in the spring are severely affected by infiltrating rainwater.

The accounted difference in SpC values between locations (Figures 6.1 and 6.4) could be a result of increased residence times at LRCV providing for additional water-rock interaction, as suggested by Liu et al. (2010), which would cause higher SpC and pH values, a higher saturation index, and lower CO<sub>2</sub> values. At Crumps Cave, higher volumes of discharge and near immediate responses to storm events in SpC values indicate that shorter residence times are occurring in conjunction with rapid infiltration of

rainwater during certain events. Likewise, concentrations of  $\text{Ca}^{2+}$  and  $\text{Mg}^{2+}$ , and  $\text{HCO}_3$  are greater at the LRCV sites versus the Crumps Cave sites, suggesting more dissolution is occurring at the LRCV sites, which supports the increased SpC values recorded at LRS and LRWF (Table 5.1; Figures 6.3 and 6.4).

### *pH*

Values of pH are highly contingent on the concentrations of dissolved  $\text{CO}_2$  in infiltrating waters (Palmer 2007a; Liu et al. 2010; Yang et al. 2012). Higher concentrations of  $\text{CO}_2$  can drive pH toward more acidic values, causing an increase in the aggressiveness of water and, thus, an increase in the extent and rate of dissolution. Over time, prolonged water-rock interaction will buffer pH as  $\text{CO}_2$  concentrations reduce. Concurrently, increased concentrations of dissolved  $\text{CaCO}_3$  may eventually increase pH values as well. Fresh infiltrations of lower pH rainfall (~ 5.5), as suggested by White (1988), Williams (1988), Palmer (1991), and Palmer (2007a), can serve to flush  $\text{CO}_2$  from the soil into the system and drive the pH lower (Liu et al. 2007; Li et al. 2008a; Li et al. 2008b; Yang et al. 2012; Pu et al. 2014a; Pu et al. 2014b).

The pH values at WF1 and SF (Figures 6.1 and 6.2) trend similarly to one another, indicating that differences in hydrogeochemical parameters are minimal between sites with respect to pH. Seasonal trends, where values are lower in the summer and higher in the winter, with a distinct increase around the beginning of the winter season, is indicative of ongoing surface influences. Surface influences impacting pH, especially during the winter months, can derive from several processes: a reduction in precipitation and surface temperature causing of the reduction in root respiration from vegetation and

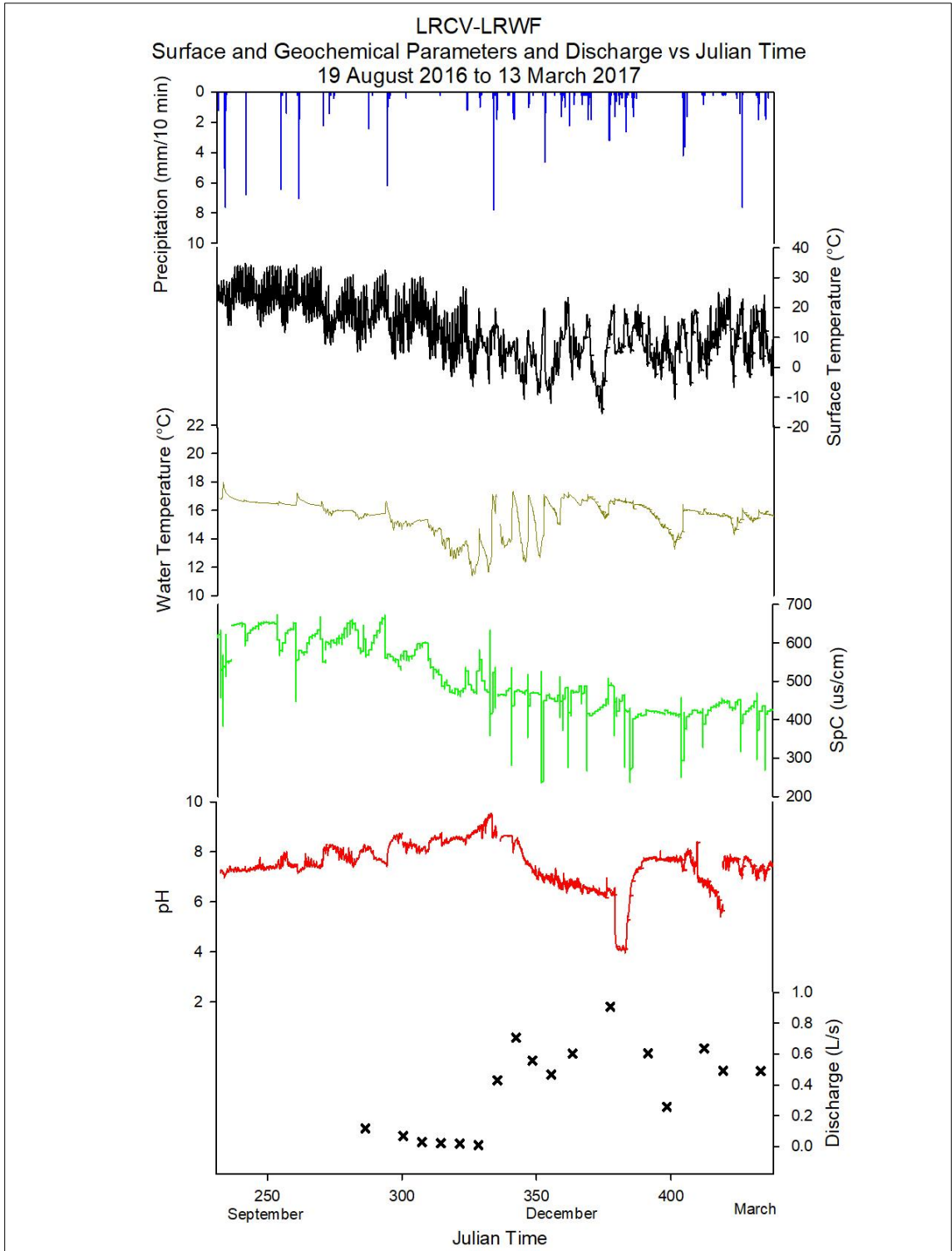


Figure 6.4 Time series of hydrogeochemical changes at LRCV-LRWF. Note the seasonal trends in all respects are more visible at this site, especially response to storm events  
 Source: Created by the author.

microbial activity in the soil, thus significantly dropping or cutting off the supply of CO<sub>2</sub> for utilization. This reduction in available CO<sub>2</sub> in epikarst waters will cause the pH to increase, while the SpC decreases, creating an inverse relationship, such as the one observed during the winter (Figures 6.1 and 6.2). Groves et al. (2005) and Vanderhoff (2011) discovered through investigations of contaminant transport during storm events at Crumps Cave that certain thresholds of precipitation exist in which CO<sub>2</sub> is more easily transported through the soil and into the epikarst as a dissolved constituent in rainwater. Similar responses were observed during this study, which suggest that, while diffuse infiltration occurs regardless of precipitation, increased precipitation allows for increased transport of dissolved CO<sub>2</sub>, such as the case observed during the summer and fall months (Figures 6.1 and 6.2).

The near immediate response in infiltrating water flushing through the system is reflected in all parameters, as well as in increased volumes of discharge observed at both sites in response to large precipitation events. This direct transference of surface flow to both waterfalls is an indication that the epikarst, while heavily influenced geochemically by surface variables, is developed to a point that contributes to a reduction in extended residence times and efficient water transference to the aquifer. Similar behaviors are observed in epikarst discharges and CO<sub>2</sub> responses related to pH in karst springs studied extensively in China and elsewhere (Williams 1983; White 1988; Palmer 1991; Hess and White 1992; Cheng et al. 2005; Groves et al. 2005; Palmer 2007a; Li et al. 2008a; Li et al. 2008b; Vanderhoff 2011; Liu et al. 2010; Pu et al. 2014a; Pu et al. 2014b; Knierim et al. 2015; Gulley et al. 2012; Gulley et al. 2015), where pH is heavily dependent on available CO<sub>2</sub> from the surface driving dissolution kinetics.

The pH values at the LRCV (LRS and LRWF) show minimal seasonal trends, such as distinct decreases during the summer months and increases during the winter months (Figures 6.3 and 6.4). Both sites indicate responses to storm events, suggesting that precipitation containing dissolved CO<sub>2</sub> may be a driving factor for pH, especially at the LRWF (Figure 6.4). Additionally, despite a seeming lack of seasonal responses in pH and SpC values, LRS (Figure 6.3) responds to influences from storm events as well. Distinct reductions in pH values in response to increased precipitation are observed throughout the study period during each rain event. These immediate decreases in epikarst pH values are a result of infiltrating rainwater driving down the pH (Figure 6.3).

At the LRCV LRWF, seasonally, pH values trend in reverse to what is observed at Crumps Cave (Figure 6.1 and 6.3). Values begin around 7.7 and steadily increase throughout the summer and into the winter transition, where a shift occurs, as increased precipitation seems to carry excess CO<sub>2</sub> into the system, causing a gradual decline in pH and an increase in dissolution. Reduced surface precipitation during the dry season may slow CO<sub>2</sub> diffusion, thus concentrations build in the soil zone. Stored epikarst water is then free to utilize all available CO<sub>2</sub> until the water becomes supersaturated, causing calcite precipitation. In January, a severe drop in pH seems to coincide with a large precipitation event. In this case, increased concentrations of CO<sub>2</sub> appear to infiltrate the system from the soil zone, driving the pH to extremely low levels. The excess CO<sub>2</sub> may derive from both soil CO<sub>2</sub> and decay of organic material (see Hatcher 2013), which found excess CO<sub>2</sub> flushing through the epikarst at Logsdon River near Mammoth Cave, which severely reduced the pH.

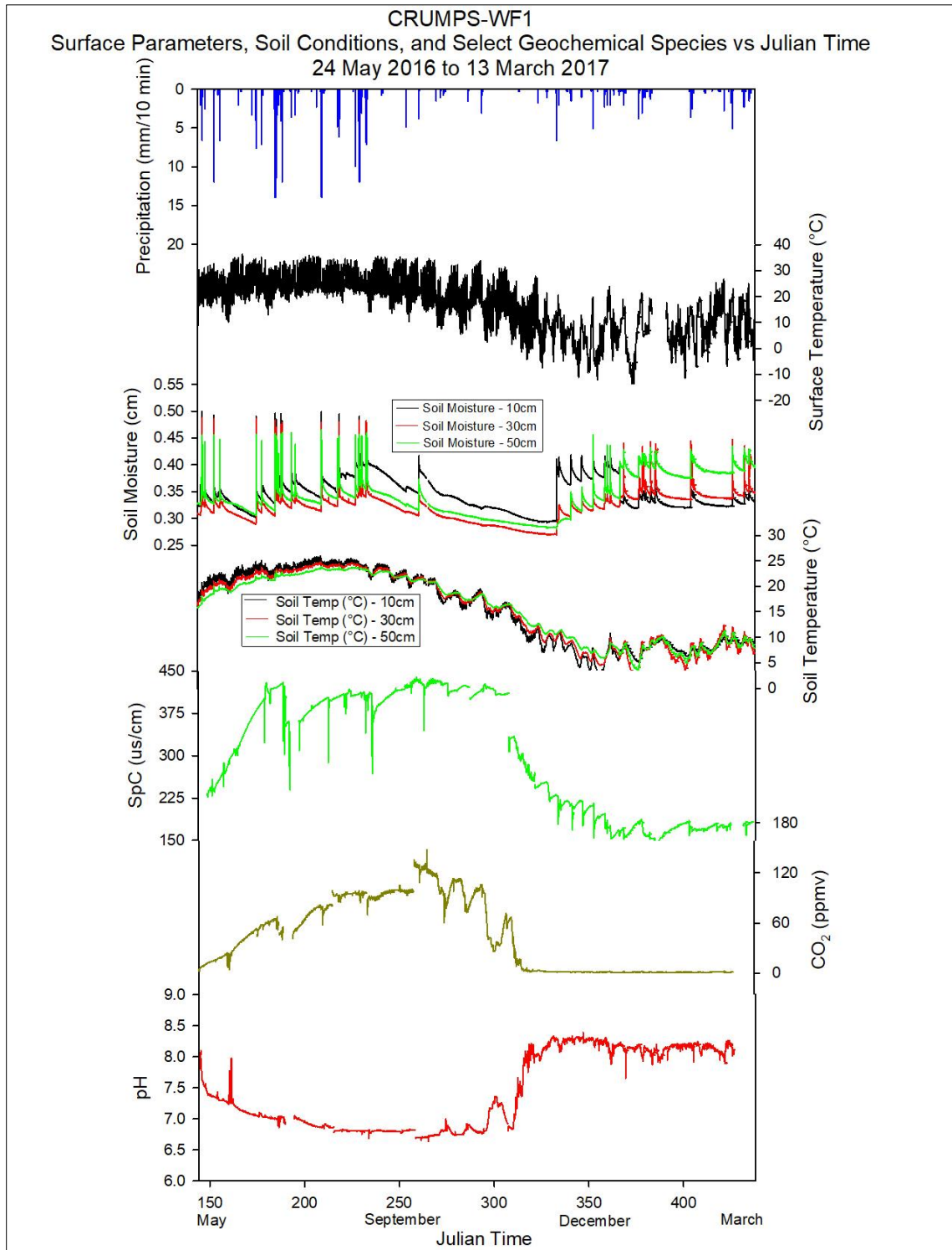


Figure 6.5 Surface and Soil Changes at Crumps Cave-WF1. Note the seasonal trends in all variables.

Source: Created by the author.





It is possible that, at the LRWF, certain precipitation thresholds need to be met before diffusion of CO<sub>2</sub> in high concentrations can move swiftly to the epikarst and transfer directly to the waterfall with minimal water-rock interaction. Responses in discharge during large storm events seem to support the suggestion that a certain threshold exists; however, when a threshold is not met, despite the continual flow of water at LRWF, extremely low baseflow suggests that during dry periods extensive water-rock interaction occurs. Increased SpC and Ca<sup>2+</sup>, Mg<sup>2+</sup>, and HCO<sub>3</sub> concentrations, as well as increased saturation index further support that concurrent ongoing dissolution and precipitation is occurring at LRWF (Table 5.1 and Figure 6.4).

#### *Soil Temperature and Moisture Conditions*

According to Yang et al. (2012), soil CO<sub>2</sub> originates from root respiration and microbial decomposition and is a function of temperature and antecedent moisture. The higher the temperature, the more root respiration and microbial activity observed, while, conversely, drier, colder soils tend to produce less CO<sub>2</sub> (Li et al. 2008a; Li et al. 2008b; Liu et al. 2010; Yang et al. 2012). On diurnal scales, CO<sub>2</sub> concentrations also fluctuate, due to the day/night switch, as root respiration for most C<sub>3</sub> and C<sub>4</sub> plants (except for a few row crop types) tends to slow during the night, with microbial activity in the soils following suit (Clark and Fritz 1997). During the winter season, these diurnal fluctuations are less pronounced, as most vegetation is dormant and, thus, microbial soil activity slows or ceases depending on temperature (Yang et al. 2012). Excess soil CO<sub>2</sub> is likely to dissolve in antecedent moisture, which then slowly percolates into the epikarst. Likewise, excess CO<sub>2</sub> will also dissolve and transfer to the epikarst during increased precipitation; however, if precipitation amounts supersede pre-existing antecedent moisture conditions,

it is possible that some soil CO<sub>2</sub> may be exposed to the atmosphere and degas before it is diffused to the epikarst. If antecedent moisture thresholds are not exceeded during precipitation events, the infiltrating precipitation may transfer large concentrations of dissolved CO<sub>2</sub> to the epikarst more quickly than under normal, relatively dry conditions.

Soil conditions at Crumps Cave (Figures 6.5) indicate seasonal trends, with increased temperatures during the summer months and decreased soil temperatures during the winter months. Additionally, diurnal fluctuations are present, indicative of solar radiation heating during the day and a reduction in solar radiation during the night. At Crumps Cave (WF1 and SF), soil moisture conditions show significant increases during large precipitation events, suggesting, especially during the summer months, that antecedent moisture levels are consistently higher, possibly due to a lag time between infiltration to the epikarst and the next storm event (Figure 6.5). A general decrease in moisture conditions is visible during the fall drought, followed by an increase in antecedent moisture during the winter storms (Figures 6.5). These distinct seasonal and precipitation driven changes in temperature and soil moisture conditions are more likely to produce CO<sub>2</sub> during the spring-summer and into the fall months during the growing period, while being less likely to produce soil CO<sub>2</sub> during the late fall and winter months due to vegetation loss and a reduction in soil microbial activity. More extreme fluctuations in surface temperatures during the winter months are met with multiple instances of fluctuations in both soil moisture and temperature, which suggest that soil microbial activity may be switching on and off, thus producing, even in small increments, higher concentrations of CO<sub>2</sub>.

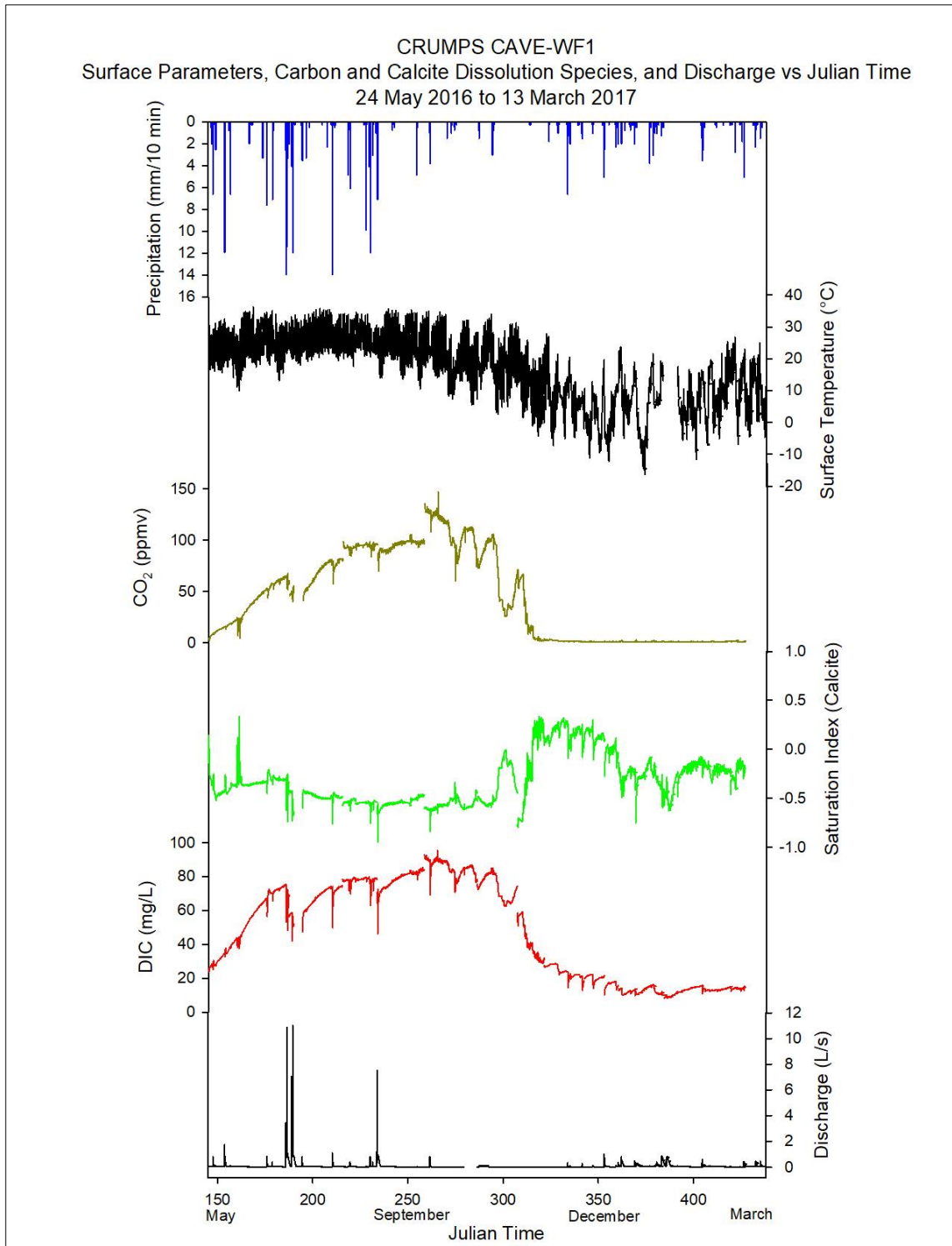


Figure 6.7 DIC coefficient changes at Crumps Cave-WF1. Note the seasonal responses in all respects, especially in DIC concentrations of CO<sub>2</sub>, as well as a seasonal trend in saturation index, indicating a strong relationship between each variable.

Source: Created by the author.

Similar soil responses in both temperature and moisture conditions, indicative of vegetation and microbial activity and, thus, correlative fluctuations in soil CO<sub>2</sub> concentrations, are observed in studies in China and elsewhere (Amundson et al. 1998; Clemens et al. 1999; Bakalowicz 2004; Klimchouk 2004). The nearby Kentucky Mesonet FARM Station recorded soil conditions for the LRCV, and the data were assumed to be similar enough to apply to both study sites (LRS and LRWF) (Figure 6.6). Soil temperature at the LRCV responds seasonally, with increased temperatures during the summer months and decreased temperatures during the winter months (Figure 6.6). As with observations made in soil temperature at Crumps Cave, LRCV soil temperature indicates increased fluctuations on diurnal scales to winter surface temperatures. Soil moisture conditions at the LRCV indicate more muted responses to seasonal changes, especially the shallower readings, but distinct responses to precipitation events, especially in the winter months (Figure 6.6). The difference in soil temperature and moisture conditions between locations could be due to data collection resolution. Crumps Cave collected data at ten-minute intervals while the FARM Station for LRCV collected data every 30 minutes. Additionally, soil extent is heavily impacted by the presence of large expanses of impermeable surfaces at LRCV, thus influencing the soil's ability to respond to seasonal changes (USDA 2017).

### *Carbon Dioxide (CO<sub>2</sub>)*

Carbon dioxide in groundwater is a major geochemical driving factor in dissolution kinetics (Williams 1983; White 1988; Palmer 1991; Drever 1997; Clemens et al. 1998; Veni et al. 2001; Palmer 2007a; Li et al. 2008a; Yang et al. 2012; Gulley et al. 2015). As waters move from areas of low CO<sub>2</sub> concentrations to high CO<sub>2</sub>

concentrations, pH levels decrease and dissolution occurs after the water becomes acidic. This CO<sub>2</sub> gradient is often spatially delineated (Gulley et al. 2012; Gulley et al. 2015) and is identified to be heterogeneous in nature throughout the landscape. Likewise, an investigation into the formation of phreatic caves in eogenetic karst by Gulley et al. (2012), suggested that CO<sub>2</sub> in a gaseous state may be responsible for increased cave formation as opposed to the mixing of fresh and saltwater resulting from sea level rise, which had been the assumed driver regarding eogenetic cave formation. Their study found that the heterogenic distribution of CO<sub>2</sub> is spatially dominant, in that cave formation is a direct result of CO<sub>2</sub>-driven dissolution in a spatial context. In telogenetic karst, dissolution is primarily a result of fluid dynamics and water-rock interaction, in that water percolating through the matrix and along fractures and bedding planes tends to form void spaces (Williams 1983; White 1988; Palmer 1991; Veni et al. 2001; Palmer 2007a). Further, CO<sub>2</sub> exchange with the atmosphere and the epikarst is heavily contingent on the presence of antecedent moisture in the topsoil and the surrounding temperature (Cuezva et al. 2011).

The diffusion of CO<sub>2</sub> at WF1 seems to occur in several ways. Firstly, as observed in epikarst studies in other regions of the world, CO<sub>2</sub> concentrations seem to vary seasonally, with highs during the summer and lows during the winter (Liu et al. 2007; Li et al. 2008a; Li et al. 2008b; Cuezva et al. 2011; Liu et al. 2010; Peyraube et al. 2012; Yang et al. 2012; Peyraube et al. 2014; Pu et al. 2014b; Gulley et al. 2015), while storm events result in high precipitation, which transports soil CO<sub>2</sub> into the epikarst. Initially, dilution effects are visible, followed by a relative lag before concentrations begin to rise.

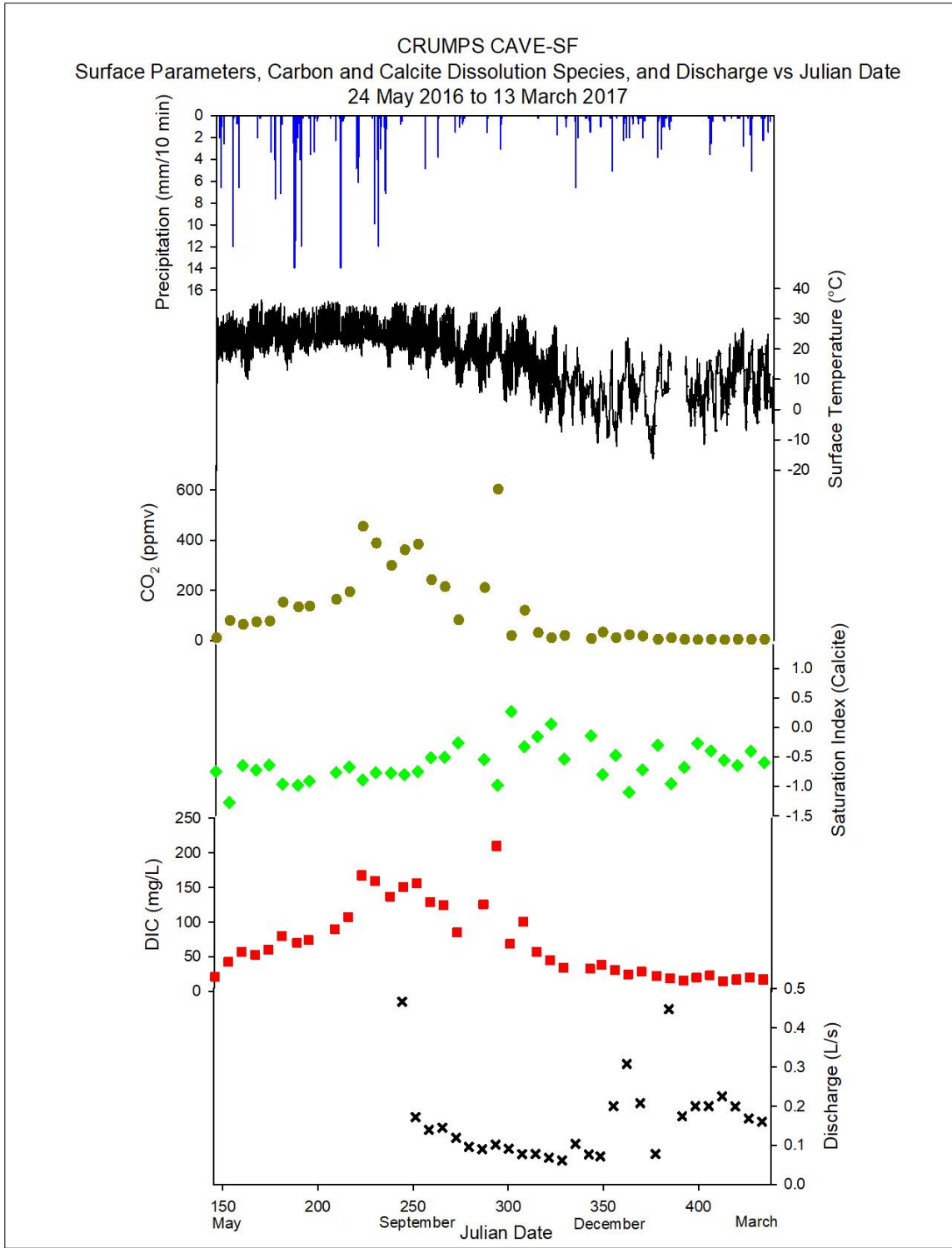


Figure 6.8 DIC coefficient changes at Crumps Cave-SF. Note that similar trends in all variables to those observed at WF1 exist.

Source: Created by the author.

Likewise, peak CO<sub>2</sub> concentrations during the months of September and October are most likely due to the onset of the dry season combined with the maturation state of surface vegetation, providing for the accumulation of increased soil CO<sub>2</sub> concentrations. At the onset of the late fall-early winter, when crops are harvested and natural vegetation begins to wither, CO<sub>2</sub> concentrations started to decrease to reach their lowest value (near zero) and remained at that level for the rest of the study (Figure 6.7 and 6.8). Despite the variability in precipitation, soil moisture, and soil temperature near the end of the winter months and transitioning into the spring, little response is observed in CO<sub>2</sub> concentrations. Minimal microbial activity and reduced root respiration may be the cause of minimal CO<sub>2</sub> concentrations in the epikarst, as no increases in CO<sub>2</sub> concentrations were observed in groundwater discharged from the spring. As a result of drastic diurnal surface temperature fluctuations ranging above 20 °C on some days during the winter, it is likely that microbial activity may have shifted between dormant and non-dormant phases in response. This shifting between phases generated higher concentrations of CO<sub>2</sub> in the soil. Studies regarding vegetation growth and microbial contributions to soil respiration and CO<sub>2</sub> production with respect to temperature and moisture fluctuations were conducted by Zogg et al. (1995), Davidson et al. (1998), and Fierer et al (2003). Zogg et al. (1995) found that fluctuations in soil temperatures can alter microbial communities in the soil, thus dominant communities at higher temperatures can increase their ability to metabolize nutrients more so than at lower temperatures.

Davidson et al. (1998) found that soil CO<sub>2</sub> fluctuations are a result of variations in soil temperature and moisture, especially over seasonal and diurnal scales. Fierer et al. (2003) discovered that concentrations of CO<sub>2</sub> from nutrient digestion by microbial



communities occurs at greater rates in the deeper substrate, influenced by a heightened sensitivity to soil temperature and moisture changes versus the surface layer, which appears less responsive. Despite these conditions, which should yield increased CO<sub>2</sub> concentrations at the springs, WF1 and SF have low CO<sub>2</sub> concentrations, which suggests that any soil derived CO<sub>2</sub> from the fluctuations in temperature was immediately utilized in bedrock dissolution, as evident by minimal changes to pH at the spring, fluctuations of SpC, and slight increases in DIC.

Trends of CO<sub>2</sub> at SF mirror that of WF1 (Figure 6.8), suggesting that similar influences in the epikarst are governing processes at both waterfalls. Seasonal responses can be delineated, despite the weekly resolution; however, diurnal and storm event variability at SF is not as easily identified and, in certain respects, impossible to determine based on lower resolution. Seasonal trends indicate increases during the growing season and decreases during the winter season. Additionally, SF exhibits overall higher concentrations of CO<sub>2</sub> relative to WF1. This difference in concentrations could be due to the difference in resolution between sites. Likewise, the dominant processes at each site, while similar, may be operating at different levels and intervals between sites.

Minimal seasonal variability is observed in CO<sub>2</sub> concentrations at LRCV-LRS, but increases in concentrations seem to coincide with storm events, suggesting that high precipitation events breach the threshold required to facilitate the rapid movement of dissolved CO<sub>2</sub> (which had not degassed to the atmosphere) from the soil to the epikarst (Figure 6.9). The lack of seasonal influence may be explained by land use in the region adjacent to LRS. Vegetation and soil cover at LRS exist in pockets, due to residential and commercial infrastructure and, thus, CO<sub>2</sub> that normally contributes to seasonal increases

and decreases may be reduced to those pockets where vegetation exists and where CO<sub>2</sub> production in the soil is still occurring. Likewise, any CO<sub>2</sub> that would normally degas to the atmosphere during the winter months under low antecedent moisture conditions could potentially be trapped by the presence of extensive impermeable surfaces, preventing that exchange with the atmosphere (Cuezva et al. 2011). Additionally, since CO<sub>2</sub> values are calculated from SpC and pH, which also indicate muted seasonal trends, it is likely that CO<sub>2</sub> measurements do the same. Lastly, discharge at LRS seems highly dependent on increased precipitation rates at high frequencies. Thus, certain volumes of water in the system must be met before any increase in discharge occurs, which suggests that longer residence times are occurring at the site. Longer residence times would result in the following conditions: reduction in CO<sub>2</sub> due to the ongoing water-rock interaction driving dissolution; an increase in pH due to a reduction in CO<sub>2</sub> used in dissolution, and an increase in SpC with high concentrations of calcium, magnesium, and bicarbonate, due to an increase in dissolution. These conditions have been observed and described in situations with similar soil and shallow epikarst springs in residential regions in other parts of the world (Cheng et al. 2005; Liu et al. 2007; Li et al. 2008a; Li et al. 2008b; Cuezva et al. 2011; Liu et al. 2010; Peyraube et al. 2012; Yang et al. 2012; Peyraube et al. 2014; Pu et al. 2014a; Pu et al. 2014b).

The aforementioned conditions at LRS (Figure 6.9) could be considered baseline conditions for this particular site; however, during high precipitation events, the conditions shift. The CO<sub>2</sub> spikes at the end of August, in October, December, and again in January, all coinciding with high precipitation, which may flush whatever soil CO<sub>2</sub>

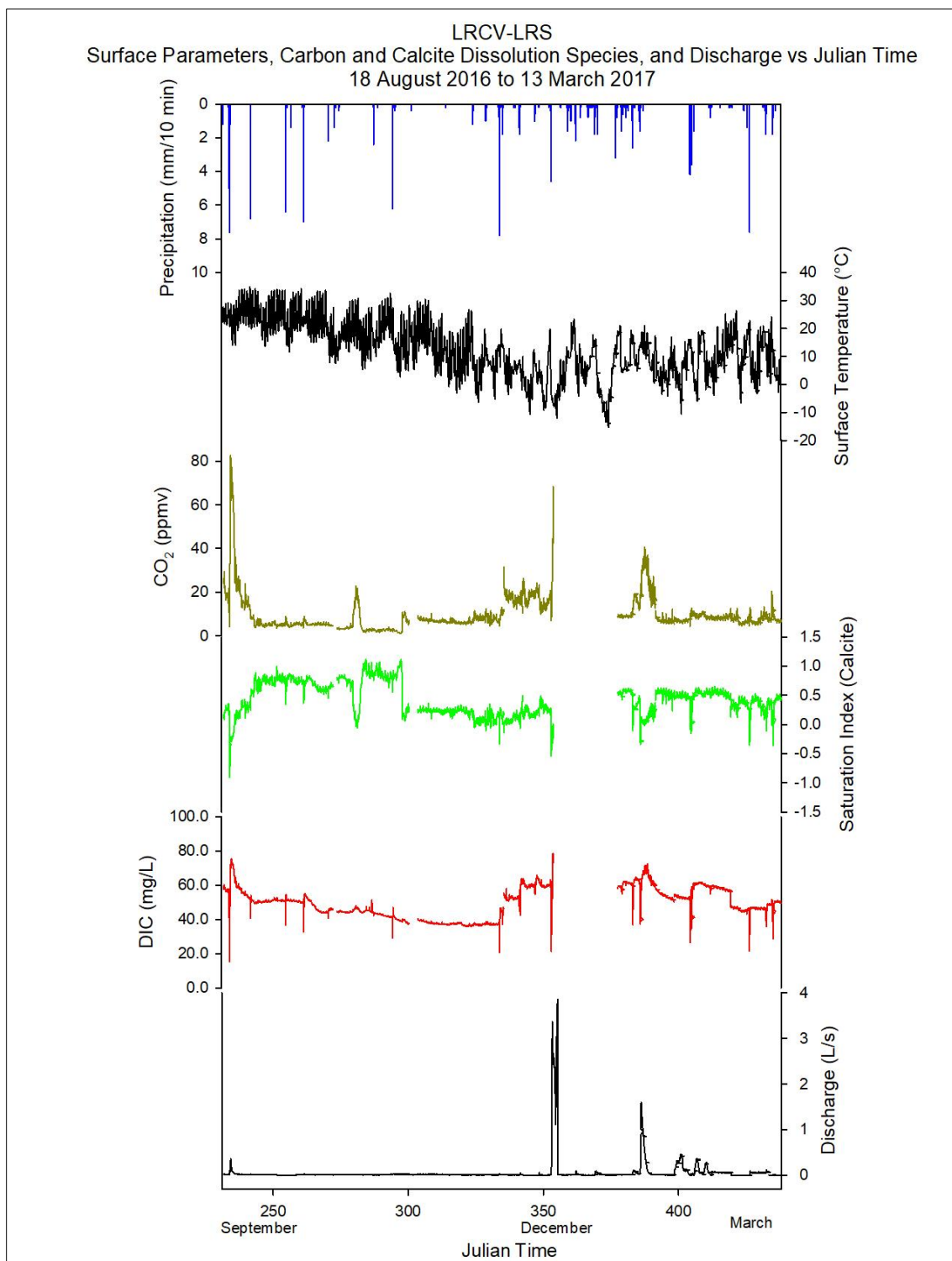


Figure 6.9 DIC coefficient changes at LRCV-LRS. Note the muted responses in DIC components, resulting from a spike in values during the month of January.  
Source: Created by the author.

exists in the epikarst and transfer it to the groundwater, causing spikes in CO<sub>2</sub> readings at the spring. A similar situation was observed at Maolon Spring in China, where rainfall served to dissolve soil CO<sub>2</sub> and transfer it to the epikarst (Liu et al. 2007) during high precipitation events. Likewise, in a different study conducted by Liu et al. (2010), similar behaviors in epikarst springs in China were recorded, driven by piston push effects, which drained the soil of CO<sub>2</sub> concentrations, transferring it to the epikarst, where it was reflected at the spring and correlated with lower values of pH. Groundwater CO<sub>2</sub> concentrations at LRWF are likely influenced from sources governed by an impermeable urban landscape as well, as suggested by minimal seasonal influences on overall CO<sub>2</sub> concentrations (Figure 6.10). Conversely, in areas where soil exists beneath these impermeable surfaces near LRWF, soil microbial activity may be contributing to total CO<sub>2</sub> concentrations on an ongoing basis as opposed to seasonally.

#### *Saturation Index (SIc)*

Calculated values of SIc are proportional to pH values and are also a representation of the saturation of the water with respect to calcite (Hess and White 19923; Drever 1997; Palmer 1991; Palmer 2007a; Yang et al. 2012). In saturated waters, the value is usually zero, while under-saturated water is expressed as a negative number, and supersaturated water is expressed as a positive number. Seasonally, during the summer months, as CO<sub>2</sub> concentrations increase in groundwater, so does dissolution, and, thus, the saturation index should increase; however, because the concentration of CO<sub>2</sub> is often so high, the aggressiveness of the water reduces more slowly, thus, the saturation index will remain below zero, especially if there is minimal water-rock interaction. If the source of CO<sub>2</sub> is either terminated or reduced, then the remaining CO<sub>2</sub> in the system will

have a chance to react, thus causing the saturation index to rise. This is often what is observed as the summer months transition into the winter, as described from studies in Algeria (Chemseddine et al. 2015) and China (Cheng et al. 2005; Li et al. 2007a; Li et al. 2007b; Liu et al. 2007; Yang et al. 2012; Knierim et al. 2015).

At Crumps Cave WF1, the saturation index of calcite mirrors that of pH values, as a representation of the aggressiveness of water with respect to dissolution kinetics (Figure 6.7); thus, during the summer months, SI<sub>c</sub> values follow seasonal variability interspersed with dilution effects from high precipitation events. The same under-saturated values in the summer months, as well as close-to-saturation values in the winter months, were also observed in studies elsewhere (Hess and White 1992; Liu et al. 2007; Yang et al. 2012). During those studies, storm events resulting in severe dilution effects were observed, and the saturation index decreased abruptly before recovering, as a result of high infiltration of precipitation in conjunction with excess dissolved CO<sub>2</sub> (Vesper and White 2004; Cheng et al. 2005; Liu et al. 2007; Li et al. 2008a; Li et al. 2008b).

The seasonal variability, in conjunction with dilution effects during storm events at Crumps Cave, is a product of both conduit flow and possible direct input from surface infiltration, in conjunction with increased CO<sub>2</sub> during the summer and reduced CO<sub>2</sub> during the winter. During the winter transition, the saturation index breaches the zero mark for a short time, indicating that the water was supersaturated. This spike in values is due to the extended dry season extending water-rock interaction during minimal precipitation events, which reduced the number of system flushes and increased the residence time in the system. As the winter storm season set in, the saturation index

dropped below zero as storage water became diluted, system flush frequencies increased, and water-rock interaction decreased, lowering the SIc values.

At Crumps Cave SF, the saturation index mirrors that of the saturation index at WF1; however, values do not show as much seasonal trending nor as much storm event influence (Figure 6.8). These differences could be a result of the lower resolution at SF. Although minimal variability is observed during the summer months, significant variability is observed in the winter months. This variability could be driven by dilution, (low SIc concentrated, infiltrating precipitation, which serves to reduce storage water concentrations), from storm events causing initial reductions in SIc concentrations. Once this freshly diluted water exists the system, higher concentrated water with respect to SIc is reflected in the data (Yang et al. 2012). Likewise, as saturation index values move closer to zero during the winter months after storm events, dilution effects on epikarst water can become more apparent, and thus, appear to have a greater impact on values.

At the LRCV-LRS, the saturation index fluctuates between under-saturated and supersaturated throughout the course of the study, with the majority of the nine months spent in a saturated or supersaturated state (Figure 6.9). During the storm event in December 2016, seasonal variability is also masked; however, overall index values show the water is consistently oversaturated. This response could be a result of extended residence times allowing for prolonged water-rock interaction. Exact CO<sub>2</sub> concentration fluctuations are difficult to ascertain, but the observable responses and trends seem to support the suggestion that supersaturation is a result of the utilization of available CO<sub>2</sub> in the system and, thus, explains the high values of pH in conjunction with the high values of SIc. Similar behaviors were observed at Nongla Spring in China, where the water was

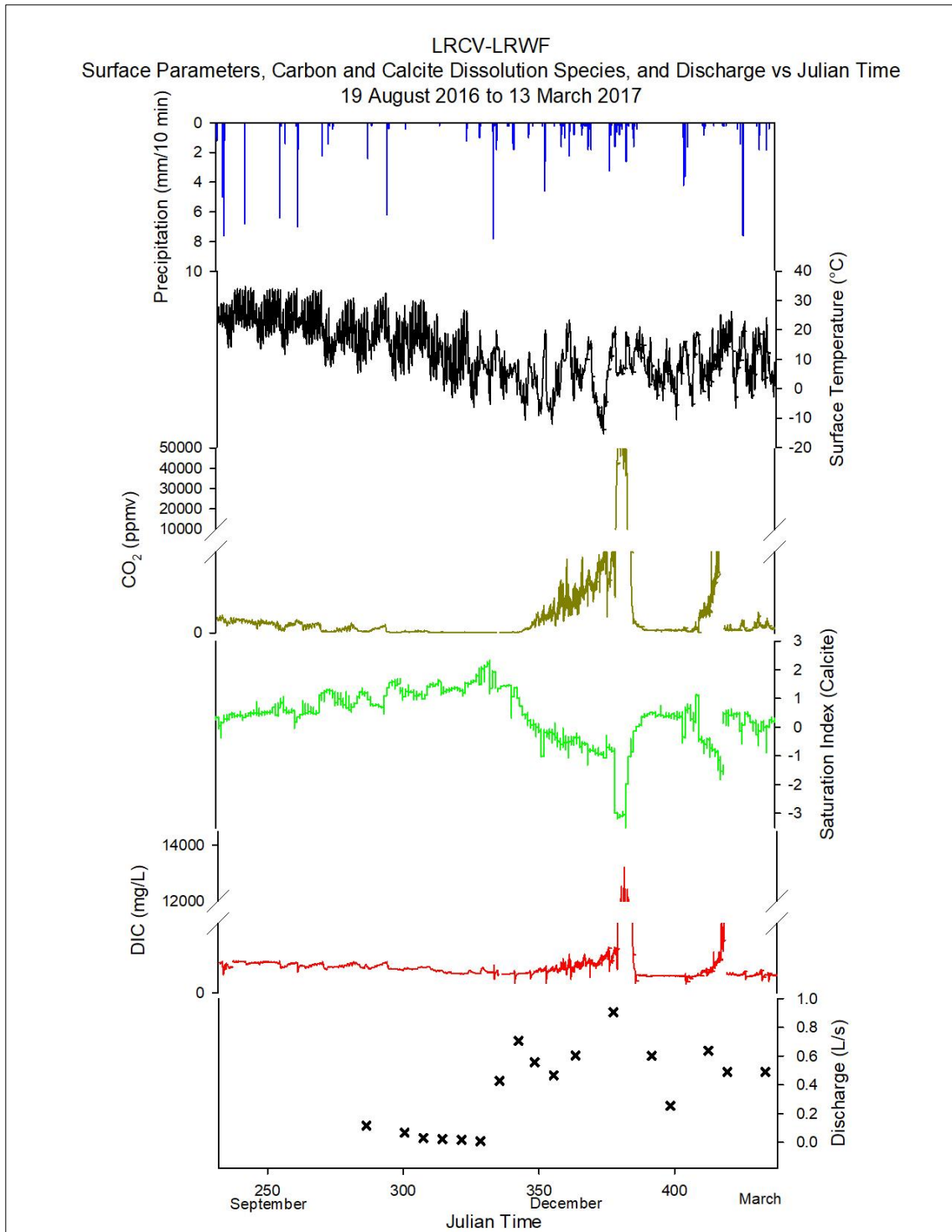


Figure 6.10 DIC coefficient changes at LRCV-LRWF. Note the muted responses in DIC components, resulting from a spike in values during the month of January, possibly a result of multiple storm events generating a high volume of discharge and associated DIC responses. Conversely, saturation indices seem to display seasonal trends.

Source: Created by the author.

consistently saturated or supersaturated, while CO<sub>2</sub> concentrations were consistently low. The authors suggested this relationship was a result of the soil CO<sub>2</sub> effect, where CO<sub>2</sub> concentrations are reduced, due to a lag time in surface and soil temperature equilibrium (Liu et al. 2007; Yang et al. 2012). Likewise, an examination into the behaviors of an aquifer in Algeria suggested that calcite precipitation is a result of increased soil CO<sub>2</sub> derived from open system conditions (Chemseddine et al. 2015).

At the LRCV-LRWF, values are the inverse of typical karst water behavior seen at Crumps, suggesting that minimal dissolved CO<sub>2</sub> exists in the system. This is most likely due to available CO<sub>2</sub> concentrations being used during dissolution until the water was supersaturated (Figure 6.10). At the winter transition, pH values begin to decrease, possibly in conjunction with a surge of CO<sub>2</sub> carried into the epikarst during the winter storms, allowing for dissolution and, thus, driving the saturation index below zero. The process could be a result of two consecutive influences: 1) the dilution effect of excess precipitation infiltrating the system, carrying with it soil derived CO<sub>2</sub>; and 2) that same excess CO<sub>2</sub> in the system reduced the pH and drove further dissolution, thereby causing the saturation of the water to eventually increase as dissolution continues to saturate the water with calcite and CO<sub>2</sub> is used in the reaction.

Palmer (2007a) suggested that this process is ongoing, as dissolution kinetics are a cyclical process that do not proceed to completion, due to open system conditions providing a continuous supply of CO<sub>2</sub>. On the other hand, even if a finite supply of CO<sub>2</sub> existed, dissolution kinetics will reduce or slow depending on the saturation level of the water, which can only contain a certain concentration of calcite. Should levels of saturation reach supersaturated, dissolution will temporarily cease until more water or



CO<sub>2</sub> is added to the system, serving to dilute concentrations and allow dissolved CO<sub>2</sub> to react with the surrounding bedrock again (Palmer 2007a). Pu et al. (2014a) suggested a similar explanation for processes observed in a karst aquifer in China. In that study, dissolved CO<sub>2</sub> in precipitation caused the saturation index to fluctuate between supersaturated before the precipitation, to under-saturated after the precipitation as an influx of fresh water containing highly concentrated CO<sub>2</sub> provided for an increase in dissolution kinetics. Li et al. (2008a) further supported these observations in a different study, where a severe decrease in pH resulted from infiltrating excess CO<sub>2</sub>. That investigation suggested precipitation not only contained excess dissolved CO<sub>2</sub> from microbial activity, but from atmospheric CO<sub>2</sub> as well. Since microbial activity is temperature dependent, and the winter months at both Crumps Cave and LRCV had odd temperature fluctuations, a significant increase in microbial activity could have contributed to the severe decrease in pH, thus showing a similar decline in SI<sub>c</sub> as well (Telmer and Veizer 1999; Peyraube et al. 2014; Milanolo and Gabrovšek 2015; Zhang et al. 2015; Zhao et al. 2015).

#### *Dissolved Inorganic Carbon (DIC)*

Dissolved inorganic carbon is expressed as a concentration, assigned to natural waters, either surface or subsurface, and designed to identify the reaction constituents and/or products within a given system (either CO<sub>2</sub> or dissolved CaCO<sub>3</sub>, respectively) (White 1988; Clark and Fritz 1997; Drever 1997; Palmer 2007a). Several studies have explored the concentrations of DIC in surface and karst spring water (Emblanch et al. 2003; Liu et al. 2010; Shin et al. 2011; Charlier et al. 2012; Faimon et al. 2012a; Faimon et al. 2012b; Yang et al. 2012; Knierim et al. 2013; Osterhoudt 2014; McClanahan 2016;

Salley 2016; Zhang et al. 2016) to determine the seasonal and storm event fluctuations. Their results are mixed, with some karst landscapes showing the possibility of serving as a carbon sink, while other studies show no real link to excess atmospheric CO<sub>2</sub> and karst landscape absorption (Liu et al. 2010). Since DIC is an important reaction product in karst dissolution processes and, thus, karst landscape development, understanding the relationship of DIC with seasonal and storm event variability, as well as the fluctuation of carbon in relation to discharge, can aid in understanding the extent of dissolution at Crumps Cave and LRCV.

At Crumps Cave WF1, DIC concentrations show distinct seasonal variability (Figure 6.7). Generally, values increase during the summer months and decrease during the winter months to coincide with dissolution reactions, with the overall trend mirroring that of CO<sub>2</sub> concentrations. This suggests that DIC values are heavily influenced by CO<sub>2</sub> concentrations in groundwater (Emblanch et al. 2003; Shin et al. 2011; White 2013; Knierim et al. 2015; Zhang et al. 2016) and can exhibit both seasonal and diel cycle variability, as discovered by Gammons et al. (2011) and de Montety et al. (2011). Here, accelerated photosynthetic uptake served to deplete CO<sub>2</sub>-DIC concentrations during the day, while an increase in CO<sub>2</sub>-DIC concentrations occurred during the night from plant respiration, indicating a reduction in <sup>12</sup>C uptake. DIC concentrations at Crumps Cave show responses to high precipitation events as well, with severe depletion as a result of possible dilution effects. High-resolution DIC fluctuations were calculated against total discharge and reflect variability both seasonally and volumetrically, due to high precipitation events. The volume of DIC discharged from the system over the course of

the study period is presented in Table 6.1, along with the respective range of discharged DIC during that time.

At Crumps Cave SF, seasonal variability in DIC concentrations is visible, with highs in the summer and lows in the winter; however, due to weekly resolution, influences from precipitation events are not as clearly defined (Figure 6.8). Overall, concentrations of DIC are higher at SF than at WF1, and mirror higher concentrations of CO<sub>2</sub> observed at SF. The difference in concentrations could be a result of a difference in resolution, as SF weekly resolution did not capture subtle changes to the system, especially during high precipitation events, which can directly influence DIC concentrations (Liu et al. 2010; Yang et al. 2012).

DIC concentrations at LRCV-LRS show minimal seasonal variability, possibly a result of overall low concentrations of CO<sub>2</sub> (Figure 6.9); however, numerous high precipitation events flushed the system of concentrated SIc, but added increased concentrations of CO<sub>2</sub> and DIC. Similar peaks indicating piston effects were observed during the onset of a storm event in China by Pu et al. (2014a; 2014b). They attributed the increase in the values to highly concentrated storage water flushing from the system, which had accumulated during a prior dry season. A similar pattern of precipitation and epikarst responses is at work at the LRS (Li et al. 2008b; Li et al. 2010).

Overall DIC concentrations at LRCV-LRWF are also fairly masked in Figure 6.10 by a spike in concentration during two separate events associated with both a reduction in pH and SIc, as well as an increase in CO<sub>2</sub>. This spike in concentrations, as noted by the maximum value of 13,502 mg/L in Table 5.1 and illustrated in Figure 6.10, is due to an intense flush of CO<sub>2</sub> through the epikarst, caused by the aforementioned dual, high-

volume precipitation events. Although seasonal variability is relatively absent from the data, concentrations of DIC show steep increases, due to increases in precipitation events causing a surge of fresh water to flush storage water with highly concentrated DIC through the system, before being replaced by water lower in DIC concentrations (Li et al. 2008b; Li et al. 2010). SpC and pH values show decreases during these precipitation events, while CO<sub>2</sub> concentrations show increases, suggesting that dissolution may have occurred prior to the storm, leading to an increase in DIC as illustrated in Figure 6.10.

### *6.1.2 Storm Event Hydrogeochemical Variability at WF1 and LRS*

Data for two separate storm events (August and November, 2016), are presented in Figures 6.11 to 6.15, and illustrate changes in surface parameters associated with geochemical responses. Data for Crumps Cave WF1 and LRCV-LRS are presented, as they both contain high-resolution data in all respects, as well as a presumed accurate geochemical depiction of their respective karst landscapes. Both events span a period of three days, and the data presented are intended to characterize baseflow to baseflow conditions, the changes within that timeframe, and highlight the importance of geochemical relationships to surface influences in the epikarst.

#### *STE 1: August 20-August 23, 2016 (JD233-236)*

The first event chosen for deeper scrutiny occurred on August 20, 2016, and lasted until August 23, 2016. Precipitation rates at Crumps Cave were slightly less than precipitation rates at the LRCV, due to the fact that precipitation at the LRCV occurred in two parts, as opposed to a single rainfall event recorded at Crumps Cave during the study (Figures 6.11 and 6.12).

The surface temperature at Crumps Cave WF1 (Figure 6.11) showed distinct diurnal fluctuations over the course of the storm event, with a ~5 °C temperature decrease immediately following the onset of the rainfall (Liu et al. 2007). A short lag time occurred between the onset of the precipitation event and a sudden increase in water temperature, suggesting that conduit flow dominates at WF1, facilitating the transference of warm precipitation to the epikarst (Vanderhoff 2011; Groves et al. 2013). Additionally, while surface temperature exhibited distinct diurnal fluctuations, water temperature did not, suggesting that, during this particular storm, precipitation seems to drive hydrogeochemical responses more so than surface temperature.

Water temperature gradually decreased over the course of the storm event, further suggesting there is a lag time for warmer, infiltrating precipitation to reach equilibrium with cooler, epikarst storage water. The SpC (Figure 6.11) also demonstrates a short lag time between infiltrating precipitation and response in the epikarst, with a strong dilution effect caused by the infiltrating precipitation, further supporting both direct conduit flow and a piston effect, where storage water is sufficiently discharged from the system and replaced with new precipitation (Li et al. 2008a; Li et al. 2008b). The pH values (Figure 6.11) respond minimally to precipitation moving through the system, suggesting that infiltrating precipitation and karst water pH values were at or near equilibrium at the onset of the storm, and, thus, minimally affected. Further, CO<sub>2</sub> values decrease quite steeply, shortly after the onset of precipitation, suggesting that fresh, infiltrating water served to flush concentrated water from the system, before replacing it with diluted water (Pu et al. 2014a; Pu et al. 2014b).

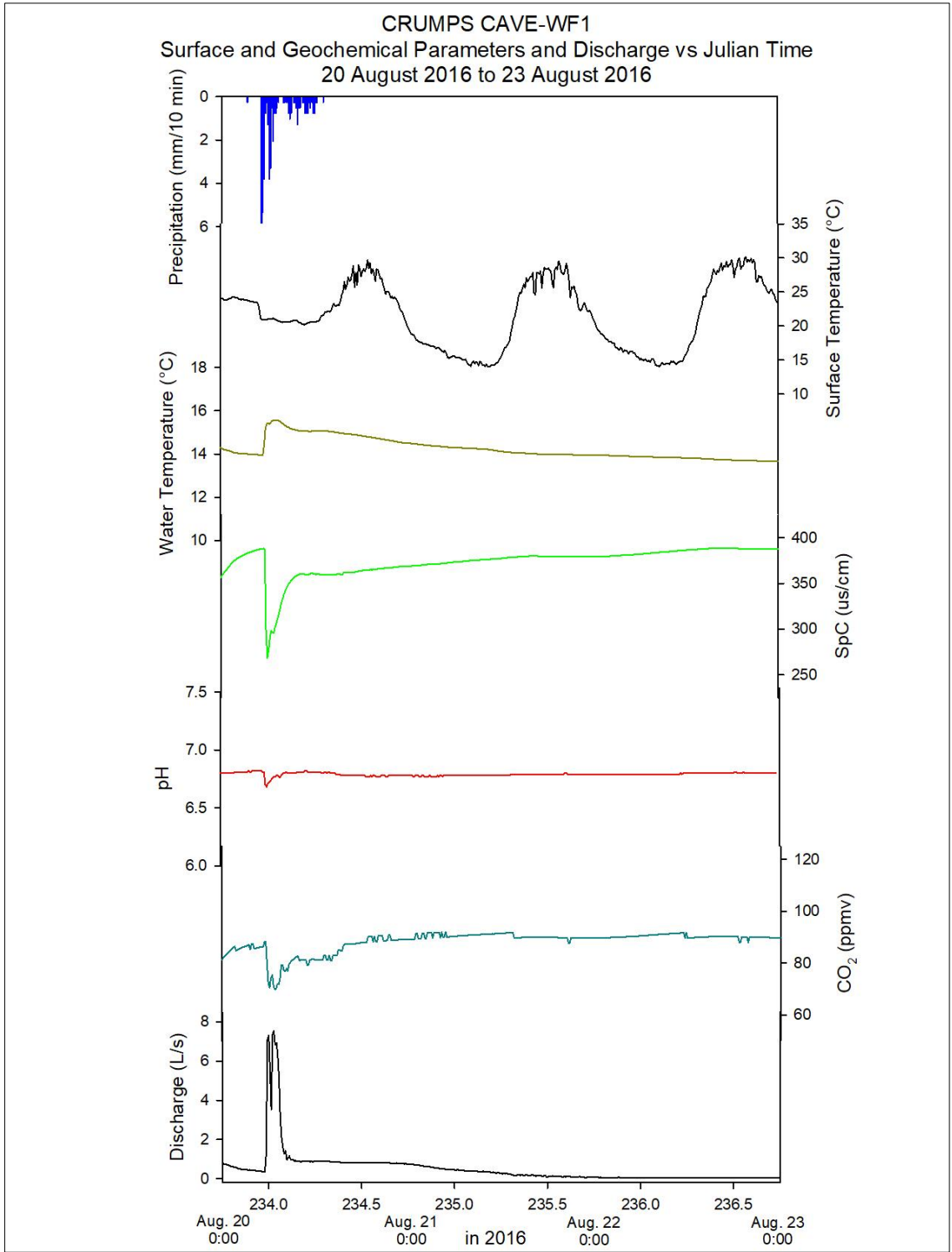


Figure 6.11 Crumps Cave-WF1 Storm Event JD233-236. Note the near immediate response to both discharge and geochemical values, suggesting direct conduit flow occurs from surface to discharge point.

Source: Created by the author.

Discharge at WF1 increased shortly after the onset of precipitation. This increase in discharge is due to the well-developed epikarst facilitating transference of water from the surface to the waterfall (Groves et al. 2005; Vanderhoff 2011; Groves et al. 2015). Short lag times (~25-45 minutes) are observed between the onset of the precipitation, the hydrogeochemical responses, and the return to normalized conditions, which suggest that surface influences have a direct impact on epikarst process. These same behaviors were observed at Crumps Cave in a previous study on contaminant transport through the epikarst (Vanderhoff 2011). In that investigation, the author suggested conduit-dominated flow as the primary facilitator of surface water transference to the aquifer and, thus, near immediate responses in recorded hydrogeochemical parameters (Cheng et al. 2005; Liu et al. 2007; Li et al. 2008a; Li et al. 2008b; Liu et al. 2010; Yang et al. 2012; Pu et al. 2014a; Pu et al. 2014b; Yang et al. 2012; Gulley et al. 2015).

At the LRS (Figure 6.12), precipitation occurred in two phases, with the first event of short duration but high intensity, while the second phase included longer duration rainfall with larger volume and intensity. This had minimal impact on surface temperatures, which displayed diurnal responses following a small decrease after the onset of the second phase of precipitation. As with responses at WF1, diurnal fluctuations are not present in the water temperature, which exhibits distinct responses to infiltrating precipitation, suggesting that, at both sites during intense storm events, surface temperature has minimal impact on hydrogeochemical changes. Geochemical responses to the first phase of precipitation are less pronounced than responses to the second phase of precipitation, indicating a longer lag time between the onset of precipitation and the responses in hydrogeochemical changes (Figure 6.12).

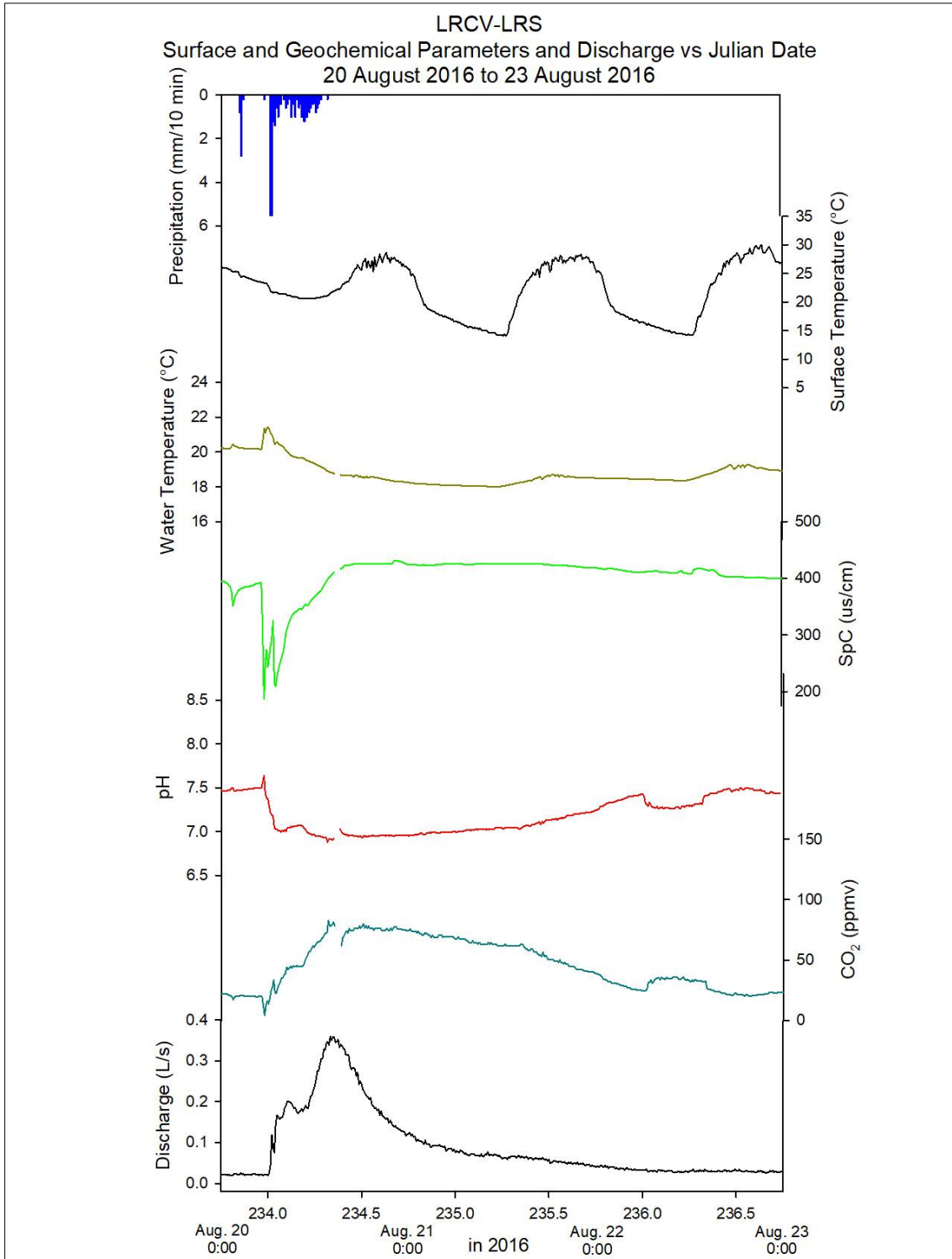


Figure 6.12 LRCV-LRS Storm Event JD233-236. Note the slightly delayed response to both discharge and geochemical values, suggesting a lag time exists from surface to discharge point.

Source: Created by the author.



All parameters respond to the second phase of precipitation, and to rather large degrees, indicating subsequent timing of both precipitation events prevent sufficient recovery period between them, compounding the responses following the second precipitation phase. Water temperature increased slightly, followed by a gradual decrease, which eventually reduced water temperature levels to several degrees cooler than pre-storm levels (Cheng et al. 2005; Liu et al. 2007; Li et al. 2008a; Li et al. 2008b; Liu et al. 2010; Yang et al. 2012; Pu et al. 2014a; Yang et al. 2012; Gulley et al. 2015). SpC responded in two phases, potentially due to the two-phase precipitation, which indicates that a lag time exists from the onset of precipitation to the point at which the logger registers the infiltration of the fresh, less ion-rich water (Figure 6.12). The pH values also decrease quite severely from infiltrating precipitation containing high concentrations of dissolved CO<sub>2</sub> (Figure 6.12) (Cheng et al. 2005; Liu et al. 2010; Yang et al. 2012; Pu et al. 2014b). The pH values never fully recover, possibly due to a substantial influx of CO<sub>2</sub>. CO<sub>2</sub> concentrations increase significantly shortly following the onset of precipitation, suggesting that either storage water with high concentrations of CO<sub>2</sub> was flushed from the system, or that precipitation infiltrating the system contained large concentrations of dissolved CO<sub>2</sub>, from the topsoil (Liu et al. 2007; Liu et al. 2010; Pu et al. 2014b). Discharge volumes demonstrated distinct lag times between the onset of precipitation and the peak of discharge by about 12 hours, indicating that certain thresholds of water volumes within the epikarst must be met before significant discharge is registered at the spring (Figure 6.12). From the study period geochemical data, specifically the calcium, magnesium, bicarbonate, CO<sub>2</sub>, and SiC data (Table 5.1), it would appear that extensive storage is occurring at the LRS, while sufficient storage is occurring

even during drought conditions, at Crumps Cave to facilitate ongoing discharge at all sites. At Crumps Cave, that storage is potentially governed by the presence of the chert layer acting as a leaky perched aquifer. This perched aquifer is recharged during high precipitation events, which also flushes increased concentrations of soil-derived CO<sub>2</sub> through the system during the growing season, thus increasing the propensity for dissolution from highly aggressive water, despite the fast transference. Similar behavior was observed in storm event monitoring by Vesper and White (2004) during an investigation into a Tennessee cave system. Likewise, large volumes of high rainfall intensity over very short periods of time are required to flush the system at both locations.

At the LRCV, precipitation may not transfer to the epikarst as quickly, due to impermeable surface layers derived from urbanization, combined with a general lack of topsoil facilitating downward diffusion. In fact, flooding problems are a large concern for Bowling Green residents, where the landscape has been modified to an extent that most water is directed into the aquifer through injection wells instead of through the epikarst (Crawford 1984a; Crawford 1984b; Crawford 1989; Crawford 2003; Crawford 2005; Brewer and Crawford 2005; Cesin and Crawford 2005). Thus, precipitation diffusion into the epikarst at the LRCV is more heterogeneous, and is influenced by a combination of reduced soil extent and increased surrounding impermeable surfaces. As a consequence, CO<sub>2</sub> diffuses to the epikarst at a slower rate, allowing for study period concentrations of soil CO<sub>2</sub> to remain higher, relative to those concentrations observed at Crumps Cave, where a more natural, less-anthropogenically influenced setting exists.

*STE 2: November 28-December 1, 2016 (JD 333-336)*

The second storm event occurred at the onset of the winter season, after a several-months-long drought with very minimal rainfall in the region. Precipitation for this event occurred in two distinctly separate phases, roughly a day and a half apart, at both Crumps Cave and the LRCV. Surface temperatures at Crumps Cave indicate less diurnal variability and increased responses to surface changes as a consequence of the storm (Figure 6.13).

Slightly higher temperatures resulted from the first rain event, suggesting that precipitation was warmer than surrounding air and, thus, took a short time to equilibrate. Water temperature also increased due to infiltrating precipitation, with a short lag time between the onset of each precipitation phase (Figure 6.13). This behavior is indicative of high volume precipitation driving hydrogeochemical changes during storm events, while surface temperature variability drives seasonal hydrogeochemical responses.

SpC values decrease in response to the onset of the first rain phase, suggesting that large volumes of precipitation flushed the system and that any storage water accumulated during the drought was minimal, as evident by the lack of an increase in SpC preceding the dilution effect. SpC values gradually increase following the first precipitation phase, suggesting that values began to return to pre-storm levels, before decreasing in response to the second phase of precipitation; however, this time the decrease is not as significant, possibly due to the fact that the SpC did not reach pre-storm concentrations before the onset of the precipitation (Figure 6.13) (Li et al. 2008a).

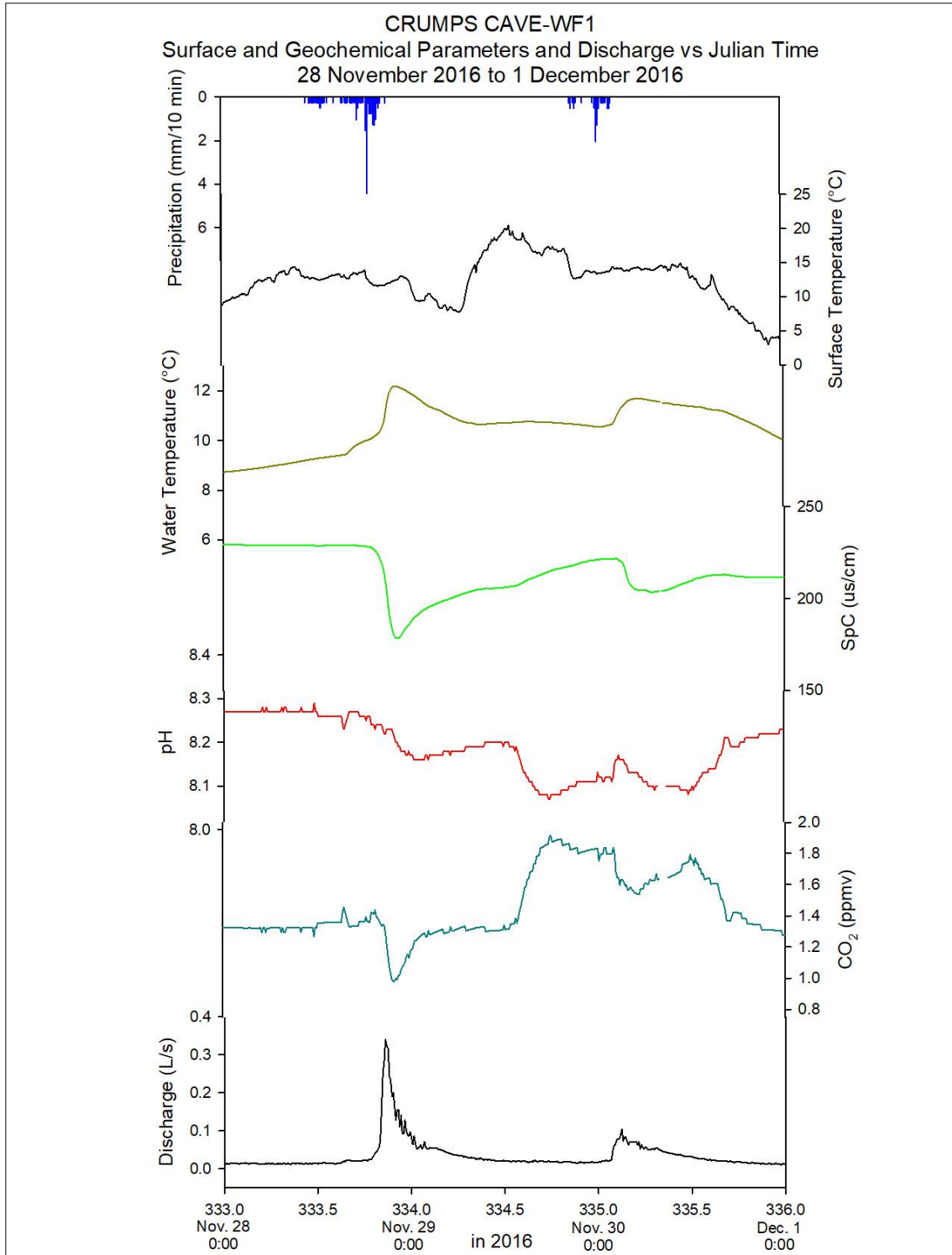


Figure 6.13 Crumps Cave-WF1 Storm Event JD333-336. Note the increase in CO<sub>2</sub> and decrease in pH, opposite of the responses during the summer storm.

Source: Created by the author.

The pH values gradually decrease at the onset of the first precipitation phase, and continue to decrease throughout the course of the storm event, suggesting that high precipitation contained excess dissolved CO<sub>2</sub> from the topsoil. During the August storm, excess antecedent moisture and degassing may have served to reduce the available CO<sub>2</sub> in the soil; however, due to drought conditions, CO<sub>2</sub> buildup in the soil may have occurred prior to this storm, providing an ample supply to diffuse to the epikarst as a dissolved constituent within the precipitation (Figure 6.13) (Pu et al. 2014a; Pu et al. 2014b). Likewise, CO<sub>2</sub> concentrations increased significantly over the course of the storm event, with the shift occurring around the onset of the first precipitation phase, and continuing to increase as the storm progressed. This suggests that, while conduit flow likely dominates at Crumps Cave, a high concentration of CO<sub>2</sub> from the topsoil was still present, which was then transported by the infiltrating precipitation (Figure 6.13). Discharge peaked twice, with very short lag times between the onset of precipitation and peak volume. The first precipitation phase resulted in significant increase in discharge, which gradually decreased following the end of the first precipitation phase. Discharge eventually returned to baseflow before the onset of the second precipitation phase, indicating that water transference at Crumps Cave is conduit dominated, as evidenced by the near immediate response to increased precipitation flushing the system (Figure 6.13).

At the LRCV-LRS (Figure 6.14) precipitation occurred in two separate phases, with the first phase delivering increased precipitation rates versus the second phase. Surface temperature increased as a result of the onset of the first precipitation event, with a significant increase in between rain phases. Shortly following the end of the second precipitation phase, surface temperature began to reduce, indicating that warmer air in

conjunction with the storm may have equilibrated with pre-storm colder air (Figure 6.14). SpC response occurred shortly, following a lag time from the onset of the first precipitation phase. Significant decreases in SpC values at that time indicate that infiltrating water flushed higher concentrated water from the system, followed by a gradual increase to above pre-storm values, which eventually stabilized around 350  $\mu\text{S}/\text{cm}$  until registering the second precipitation phase, where another reduction in SpC occurred, although not as significant (Figure 6.14) (Yang et al. 2012).

The pH gradually decreased over the course of the storm event, but did not show any significant responses to precipitation, suggesting that infiltrating water potentially contained lower concentrations of  $\text{CO}_2$ , as evident by the mirrored response to pH by  $\text{CO}_2$  concentrations over the course the storm. The gradual decrease in pH and the gradual increase in  $\text{CO}_2$ , except for a brief instance immediately, following the start of the November 29 (JD334), when a slight decrease in both pH and  $\text{CO}_2$  occur in response to the onset of the first precipitation phase. Discharge responded quickly to the first precipitation event, with the peak of discharge occurring shortly after the peak rainfall; however, discharge did not respond to the second precipitation phase, possibly due to the fact that the majority of stored water was flushed from the system in the first rain phase, forcing the epikarst to recharge its volumetric water supply (Yang et al. 2012).

Discharge volumes also remained slightly above baseflow for the duration of the storm indicating that large volumes of water from both storage and precipitation were moving through the system, which further suggests that the threshold required for significant discharge response was exceeded.

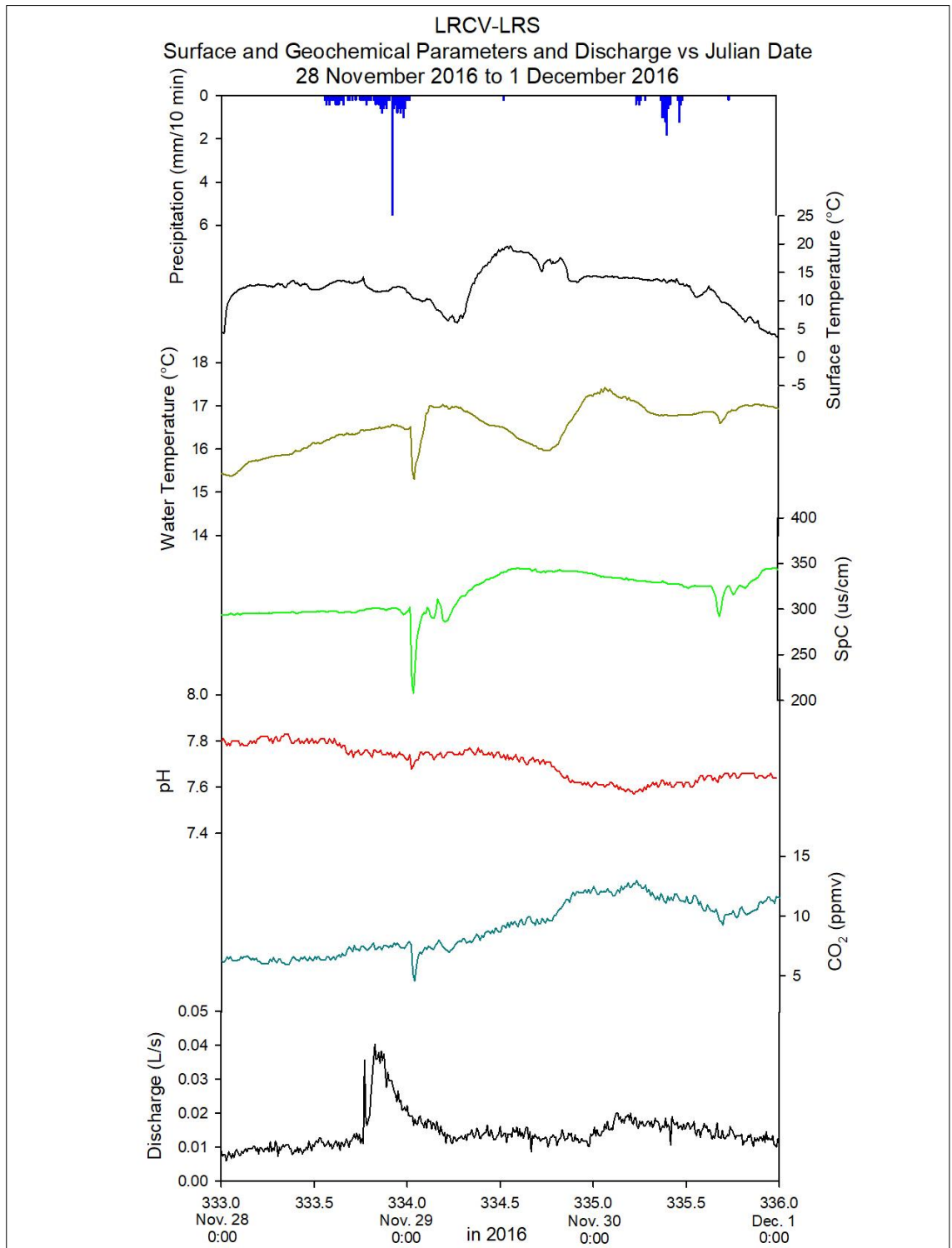


Figure 6.14 LRCV-LRS Storm Event JD333-336. Note the slightly delayed response to geochemical values, suggesting certain volumetric capacity needs to be reached before the spring responds due to drought conditions.

Source: Created by the author.

### 6.1.3 Influences on Epikarst $\delta^{13}\text{C}_{\text{DIC}}$

The evolution of  $\delta^{13}\text{C}_{\text{DIC}}$  in karst systems is influenced by external and internal processes, including vegetation and soil respiration and bedrock dissolution, as discussed and illustrated by Clark and Fritz (1997). Of these primary terrestrial sources, vegetation and soil respiration seem to contribute the most (Li et al. 2010), especially on seasonal scales. The data from this study suggest that seasonal influences from soil  $\text{CO}_2$  contribute to dissolution processes at Crumps Cave, especially during the growing season, while soil  $\text{CO}_2$  influences karst processes year-round at the LRCV. The primary difference between the study sites, agricultural versus urban land use, provides a unique opportunity to understand the sourcing and transport of  $\delta^{13}\text{C}_{\text{DIC}}$  on a regional scale.

The  $\delta^{13}\text{C}_{\text{DIC}}$  values at all four sites (Figures 5.1 and 5.2) indicate that seasonal influences are having a great effect on the enrichment and depletion of  $\delta^{13}\text{C}_{\text{DIC}}$  over the entirety of the study period; however, that enrichment and depletion seem to be occurring irrespective of precipitation, which in other studies is suggested to be a negligible influence (Telmer and Veizer 1999; Lambert and Aharon 2010).

At Crumps Cave (WF1 and SF), seasonal variability is apparent, with values showing greater depletion during the summer and greater enrichment during the wintertime. Similar findings of  $\delta^{13}\text{C}_{\text{DIC}}$  seasonal variability were found in other studies (Telmer and Veizer 1999; Li et al. 2008a; Li et al. 2008b; Lambert and Aharon 2010; Li et al. 2010; Zhao et al. 2015; Knierim et al. 2015; McClanahan et al. 2016), where it appears that soil  $\text{CO}_2$  and vegetation cover contributed the most to  $\delta^{13}\text{C}_{\text{DIC}}$  depletion, especially due to fractionation effects within the topsoil from microbial activity being more active during the summer months than during the winter. Over the course of the fall



months,  $\delta^{13}\text{C}_{\text{DIC}}$  values enrich, with substantial enrichment occurring near the fall to winter transition, and continuing until the end of the study. This increasing enrichment, especially near the end of the study period and at the onset of the spring transition, suggests that a certain lag time exists between vegetation root respiration and subsequent microbial activity, depletion of  $\delta^{13}\text{C}_{\text{DIC}}$  values, and registry of that depleted signal by epikarst water (Li et al. 2010).

At the LRCV (LRS and LRWF), seasonal influences are slightly less apparent than at Crumps Cave. While depletion of  $\delta^{13}\text{C}_{\text{DIC}}$  values during the summer months seems to trend similarly to the isotopic signatures at Crumps Cave, they diverge greatly at the onset of the winter transition. The  $\delta^{13}\text{C}_{\text{DIC}}$  values remain in a depleted state, which could be a result of an urban environment masking the signal response (Li et al. 2010).

A substantial enrichment occurred at three of the four sites in the month of September (JD 225) following a series of high precipitation events. Crumps Cave-WF1 and LRCV-LRWF showed higher enrichment compared to LRCV-LRS, while Crumps Cave-SF showed the least enrichment. Knierim et al. (2015) suggested that, based on similar findings in an investigation of Jack's Cave in Arkansas, the magnitude of different source inputs changes seasonally. For example, surface temperature is a proxy for soil respiration (Clark and Fritz 1997; Knierim et al. 2015), and at lower temperatures soil respiration rates are lower. For temperatures at or higher than 10 °C, more microbial activity is likely to occur, thus producing increased concentrations of soil  $\text{CO}_2$ . Likewise, more microbial activity is also responsible for the ongoing fractionation of  $^{13}\text{C}$  relative to  $^{12}\text{C}$ , causing increasingly depleted values of  $^{13}\text{C}$  (Clark and Fritz 1997; Knierim et al.

2015). The enrichment occurring at three of the four sites could be a result of a reduction in fractionation effects derived from a reduction in plant root respiration.

### *Soil Respiration*

Soil CO<sub>2</sub> concentrations are a function of soil respiration, microbial activity, and mineral weathering, and concentrations are partly contingent on soil thickness – thicker soils equal increased concentrations of CO<sub>2</sub> (Zhao et al. 2015). Thus, mineral weathering is a product of soil CO<sub>2</sub> concentrations after diffusion to the bedrock layer via infiltrating precipitation and the presence of sufficient antecedent moisture, facilitates dissolution (Pu et al. 2014a; Pu et al. 2014b; Knierim et al. 2015). Natural vegetation in temperate and mid-latitude climate zones often operates using the C<sub>3</sub> pathway, while certain agricultural crops, such as corn and sugarcane, utilize the C<sub>4</sub> pathway (Clark and Fritz 1997). As vegetation dies, microbial activity breaks down the decayed matter and generates CO<sub>2</sub>; thus soil CO<sub>2</sub> is higher in concentrations than the atmosphere on average (Clark and Fritz 1997; Pu et al. 2014a; Pu et al. 2014b; Zhao et al. 2015).

### *Bedrock Dissolution*

Carbonate rocks are generally derived from marine sediments and have a  $\delta^{13}\text{C}$  value close to zero (Clark and Fritz 1997). Carbonate dissolution processes are heavily dependent on the amount of CO<sub>2</sub> available to react with the bedrock via carbonic acid, which should yield a  $\delta^{13}\text{C}_{\text{DIC}}$  value of  $-11.5\text{‰}$  (Pu et al. 2014a; Pu et al. 2014b). According to Clark and Fritz (1997), if completely open conditions exist, the  $\delta^{13}\text{C}$  value will be controlled by the soil CO<sub>2</sub>, due to an ongoing replenishment interacting with the bedrock. On the other hand, if the system is closed, then a finite supply of CO<sub>2</sub> is

available, and eventually the  $\delta^{13}\text{C}$  will be diluted with DIC purely from carbonate dissolution. Understanding the relationship values between  $\text{pCO}_2$ , DIC, and  $\delta^{13}\text{C}$  can provide insight into the conditions of the system, be it open or closed, or a combination of both. Further, in open conditions, regardless of the type of vegetation ( $\text{C}_3$  or  $\text{C}_4$ ), final groundwater values of  $\delta^{13}\text{C}_{\text{DIC}}$  will be enriched by about 7‰ from the original soil  $\text{CO}_2$ . This enrichment is primarily due to the fact that  $\text{CO}_2$  and DIC have reached equilibrium at increasing values of pH. In closed systems, similar enrichments occur; however, those enrichments reflect a direct, linear one-to-one relationship between  $\delta^{13}\text{C}_{\text{DIC}}$  and  $\text{CO}_2$  dissolved during recharge (Cerling 1984; Fritz et al. 1989; Cerling et al. 1991; Clark and Fritz 1997; Cane and Clark 1999).

#### *$\delta^{13}\text{C}_{\text{DIC}}$ Sourcing at Crumps Cave (WF1 and SF)*

Results from carbon source identification using mixing model software with inputs from the atmosphere, soil water, and carbonate bedrock were compared to identify specific  $\text{CO}_2$  sources seasonally. At Crumps Cave WF1 and SF (Figure 5.3 and 5.4), carbon isotopic sourcing indicates soil  $\text{CO}_2$  dominates during the summer months, shifting to atmospheric  $\text{CO}_2$  dominating during the winter months. As vegetation cover reduces and microbial activity turns dormant during the winter months, the majority of  $\text{CO}_2$  in the system is derived from the atmosphere, simply due to the reduction in soil derived  $\text{CO}_2$  signals.

The trends and seasonal shift of carbon sourcing align with isotopic trends of  $\delta^{13}\text{C}$ , as illustrated in Figure 5.1. Seasonal shifts from soil  $\text{CO}_2$  to atmospheric  $\text{CO}_2$  coincides with the completion of the growing season, indicating that supplies of soil  $\text{CO}_2$  have significantly reduced, no longer contributing as greatly to epikarst waters (Knierim

et al. 2015) (Figures 5.3 and 5.4). Likewise, carbonate weathering sources during the summer months were relatively low, suggesting that, while dissolution is occurring, an increased soil CO<sub>2</sub> signal is masking all other signals (Bakalowicz 2004; Klimchouk 2004) (Figures 5.3 And 5.4). However, atmospheric and carbonate bedrock weathering sources increased during the winter months, while the soil CO<sub>2</sub> signal was much weaker. Atmospheric CO<sub>2</sub> dominance versus carbonate weathering is a result of the overall minimal residence times and less available CO<sub>2</sub> to react with the bedrock (Figures 5.3 and 5.4; Figure 6.1).

In a study conducted by Li et al. (2010), seasonally fluctuating soil CO<sub>2</sub> suggested similar drivers are at work in karst landscapes in China. The authors found that this increase in soil CO<sub>2</sub> drives carbonate weathering and increases dissolution, and that the shift in soil CO<sub>2</sub> resulting from vegetation and microbial activity is responsible for the evident seasonal pattern associated with carbonate sourcing. Likewise, Zhao et al. (2015) found that an investigation into three catchment basins with varying soil thickness and land uses rendered similar seasonal shifting in carbon sources. In that investigation, the catchment used primarily for agricultural purposes and contained relatively thick soils; however, bedrock dissolution was reduced, due to the fact that the groundwater flow path was short and well developed, facilitating fairly easy transference to the aquifer with minimal water-rock interaction. In both of those investigations, the reduction of soil CO<sub>2</sub> contributions during the wintertime allowed for atmospheric and carbonate dissolution signals to become more pronounced over time.

Similarly, an investigation into speleothem growth by Lambert and Aharon (2010) suggested that, in karst landscapes with relatively quick water transport through

the epikarst, chemical equilibrium with  $^{13}\text{C}$ -depleted soil  $\text{CO}_2$  may retain a higher atmospheric  $\text{CO}_2$  signal. This phenomenon would explain why atmospheric  $\text{CO}_2$  dominates during the wintertime, when depleted soil  $\text{CO}_2$  signals exist, due to the reduction in vegetation cover and microbial activity combined with winter storms facilitating the movement of water through the epikarst.

#### $\delta^{13}\text{C}_{\text{DIC}}$ Sourcing at LRCV (LRS and LRWF)

Carbon sourcing at LRS and LRWF (Figures 5.5 and 5.6) is dominated by soil  $\text{CO}_2$  throughout the majority of the study period. Atmospheric contributions at both sites are heavily masked by the strong soil  $\text{CO}_2$  signal, while the bedrock weathering signal shows the least contributions over the course of the study period. Although residence times at LRS and LRWF are significantly higher throughout the study period, allowing for more soil  $\text{CO}_2$  equilibrium and water-rock interaction, certain high precipitation events serve to flush the system with fresh meteoric water, mixing end members and disrupting the signal (Lambert and Aharon 2010).

The masking of all other source signals could result from the fact that the LRCV is located within Bowling Green, KY, a large urban environment (Figures 5.5 and 5.6). Seasonal contributions from agricultural practices are relatively absent, which can influence soil  $\text{CO}_2$  signals during the summer months. Cuezva et al. (2011) found, through an investigation of both wet and dry periods, that soil moisture has a direct effect on  $\text{CO}_2$  exchange between the atmosphere and the epikarst (Figure 6.20). They discovered that increased moisture in the soil facilitates transference of  $\text{CO}_2$  into the epikarst while preventing degassing to the atmosphere. Further, a lack of moisture during the dry period actually allows for more atmospheric exchange of  $\text{CO}_2$  with the epikarst.

This is most likely the case during the dry season and in between rain events over the winter months at Crumps Cave, where soil moisture is reduced or nearly absent, allowing for facilitation of CO<sub>2</sub> transference to the atmosphere and a greater atmospheric CO<sub>2</sub> sourcing signal; however, despite similar seasonal soil conditions at the LRCV, this atmospheric exchange may not be occurring, due to the presence of an impermeable surface layer above the soil layer trapping CO<sub>2</sub> in the soil throughout the study period.

This impermeable surface trapping of CO<sub>2</sub> in the soil could also be responsible for the dominant soil CO<sub>2</sub> sourcing signal rendered in the *IsoSource* analysis. Likewise, Zhao et al. (2015) discovered that agricultural land use practices continue to enhance signals during the summer months and degrade signals during the winter months. Without this contribution at LRCV, soil CO<sub>2</sub> signal attenuation is less skewed. Lastly, due to the dual porosity nature of the LRCV (Charlier et al. 2012), combined with more direct runoff injection to the aquifer and less precipitation based soil CO<sub>2</sub> transference to the epikarst, CO<sub>2</sub> signals experience a lag time in registry at the spring, as suggested by the overall higher soil CO<sub>2</sub> signal throughout the course of the study period at both sites.

Bedrock dissolution and atmospheric signals make up relatively small percentages at both sites over the course of the study period and especially during the summer. At LRWF (Figure 5.6) atmospheric contributions increase to over 40% at the onset of the winter season for roughly the months of November and December, before decreasing again in the month of February and March (Figures 5.5 and 5.6). The variability of surface temperatures during the month of January, combined with a relatively warm winter season, could result in a reactivation of soil microbial activity, despite an absence of vegetation growth.

The increase in soil CO<sub>2</sub> values in the month of February and March could be a reflection of lag time between the generation of soil CO<sub>2</sub> and its transference to the spring, further supporting a slow diffusion through the epikarst. Precipitation appears as a negligible influence on the transport of CO<sub>2</sub>, especially through the soil zone, similar to studies that suggest precipitation can serve to generate disequilibrium between end members (Lambert and Aharon 2010). Additionally, Knierim et al. (2015) found that during the transition between dry and wet seasons, disequilibrium is greatest between CO<sub>2</sub> and DIC. The possibility of most precipitation being channeled through injection wells in Bowling Green means it would bypass the soil zone; thus, soil CO<sub>2</sub> concentrations would remain high even during the wintertime (Figures 5.5 and 5.6).

#### *6.1.4 Conduit Dissolution and DIC Flux*

Dissolution rates and individual conduit wall retreats were calculated (Eq. 4.1 and 4.2) to better determine the extent of epikarst development that may be occurring at all four sites (Table 6.1). Likewise, mass DIC fluctuation over the study period was calculated (Eq. 4.3) for WF1 and LRS utilizing high-resolution discharge (Table 6.1; Figure 6.15). Wall retreats were calculated for each site to provide a general idea of the extent of conduit growth; however, the results are limited by the fact that the Palmer equation yields values referenced to a single conduit, not the extent of conduit development throughout the entire epikarst. Since identifying specific conduits that may or may not be growing is impossible without further geophysical investigations, dissolution rates, which are expressed as a volume of material removed during a specific time period, are more representative of the extent of epikarst development occurring at each site during the study period.

Wall retreats at Crumps Cave (WF1 and SF) indicate that conduit growth rate is greater at WF1, at 1,224.17 cm over the study period, and lower at SF at 1.36 cm over the study period. Total dissolution, or volume of calcite material removed over the study period, is higher at WF1 as well, with a total calculated volume of  $0.18 \text{ kg/m}^3$  over the study period, while much lower at SF, at  $0.000396 \text{ kg/m}^3$  of total calculated volume over the study period.

At the LRCV (LRS and LRWF), wall retreat values are significantly different from one another, and considerably higher than at Crumps Cave, on average 841 cm over the study period at LRS and 105,205 cm over the study period at the LRWF. Higher saturation indexes at LRS and LRWF suggest that more precipitation is occurring than dissolution, as evident by the presence of a flowstone and rimstone dam near LRWF, and indicated by a negative value for the total calculated dissolution over the study period at both sites. Conversely, since maximum calculated values of dissolution yielded positive numbers,  $0.00121 \text{ kg/m}^3$  at LRS and  $0.00274 \text{ kg/m}^3$  at LRWF, respectively, at least some dissolution of calcite is occurring at both sites. On the other hand, Covington et al. (2015), found that dissolution rates are, at best, a rough estimate of conduit evolution, primarily due to the suggestion that mechanical weathering has a greater impact on material removal than chemical weathering. In that study, the PWP equation was applied to over 59 surface stream study sites, where more variability from surface process were observed, as opposed to dominant chemical weathering processes in the epikarst, which can be partially buffered from surface influences by depth. Covington et al. (2015) explained that low value variability of calcite dissolution can derive from several influences, with low  $\text{CO}_2$  concentrations governing increased pH values as the primary



influence. Since dissolved CO<sub>2</sub> concentrations have the strongest control on dissolution rates, dissolution rates at each of the four study sites should increase during the growing season and decrease during the dormant season.

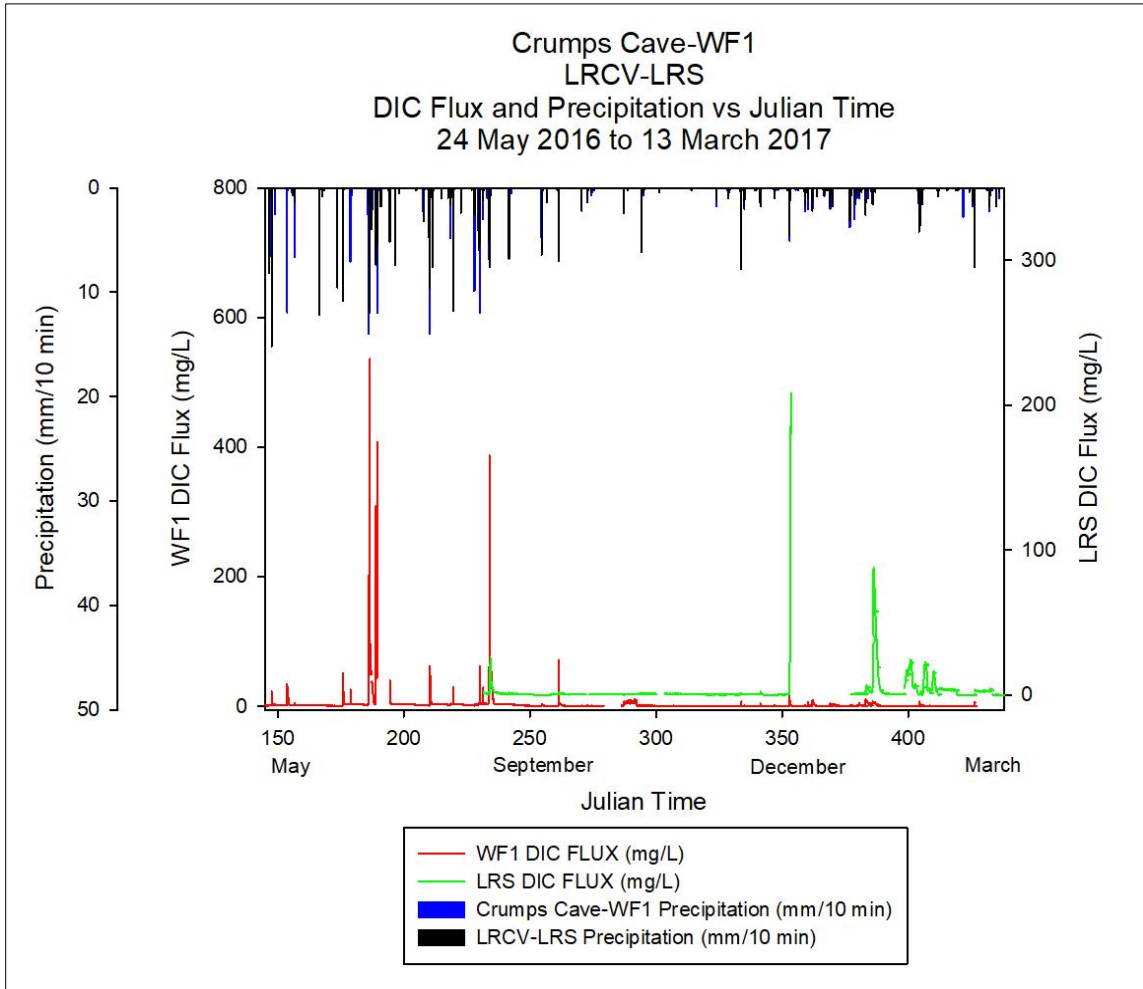


Figure 6.15 Time Series DIC Fluctuations at WF1 and LRS. Note that peak DIC fluctuations at Crumps Cave seem higher relative to LRS, while a pronounced lag time at LRS occurs before responses are observed, suggesting storage thresholds need to be met before increases in DIC are recorded in conjunction with increased discharges. Source: Created by the author.

Hydrogeochemical data indicate the processes at WF1 and SF are both driven by soil CO<sub>2</sub> transferred to the epikarst via seasonal and storm event processes, so the possibility for the difference in values could be attributed to a difference in resolution.

WF1 values were calculated from 10-minute resolution data; therefore, they are assumed to be a more accurate representation of the actual dissolution and wall retreat values at Crumps Cave. The difference in calculated values at LRS and LRWF could possibly be attributed to the thickness of the epikarst with respect to the emergence of water at the spring. Although the epikarst thickness at the LRCV is relatively shallow compared to Crumps Cave, LRS emerges from the bedrock at less than five meters from the surface, whereas water emerging from the bedrock at the LRWF is more than 10 meters from the surface, suggesting a longer flow path from the surface to the spring and, thus, increased potential for water-rock interaction and drainage basin size. Likewise, with increased residence times and higher  $SIC$  values at LRWF, the presence of a flowstone and rimstone dam at the mouth of the waterfall further supports that at least some net bedrock removal is occurring in the epikarst zone.

Carbon flux, or the fluctuation of DIC concentrations with varying discharge, is a measurement of the extent of carbonate rock weathering with respect to  $CO_2$  being consumed during the dissolution process. Carbon flux can aid in delineating  $CO_2$  uptake in karst systems versus the amount that is discharged from the system (Knierim et al. 2015). Values were calculated (Eq. 4.3) over the course of the study period. Figure 6.15 presents the fluctuation of DIC at both WF1 and LRS over the course of the study period. From high-resolution discharge and DIC data, DIC flux calculations were completed for two of the four sites (WF1 and LRS).

Calculated mass DIC flux for the entirety of the study period for WF1 is 109,468 mg/study period, while LRS rendered a mass DIC flux of 364,186 mg/study period. Although it would seem the mass DIC flux for LRS removes and transports more DIC

over the course of the study period, the calculated value represented above includes a storm event during the month of December in which the highest recorded discharge volume occurred at LRS. Considering LRS discharge is driven by large volume storm events that exceed epikarst thresholds and, thus, evacuate the system of storage water, this number is most likely an accurate representation of mass DIC flux over the course of the study. Likewise, DIC concentrations and fluctuations appear to be influenced by increased values of certain hydrogeochemical data, such as SpC, and lower values of pH and CO<sub>2</sub> during storm events, which corroborate the suggestion that storm event variability drives DIC fluctuations at LRS. Further, increased residence times at LRS and LRWF would also contribute to increased dissolution rates and DIC fluctuations.

**Table 6.1.** Summary Statistics of DIC flux, conduit enlargement, and dissolution rates.

		DIC Flux (mg/ study period)	Wall Retreat (cm/study period)	Dissolution Rate (kg/m <sup>3</sup> /study period)
WF1**	Total	109,468	1,224.17	0.18
	Min	0.21	0.00	-1.34x10 <sup>-5</sup>
	Max	536	0.14	1.24x10 <sup>-5</sup>
SF*	Total	-	1.36	0.000396
	Min	-	0.00	-1.19x10 <sup>-5</sup>
	Max	-	0.13	2.81x10 <sup>-5</sup>
LRS**	Total	364186	481.07	-0.699
	Min	0.00	0.00	-0.00138
	Max	208	123.24	0.00121
LRWF**	Total	-	105,205.90	-1.810
	Min	-	0.00	-0.00229
	Max	-	347.86	0.00274

\*Low-resolution

\*\*High-resolution

Source: Created by the author.

### *6.1.5 Low-Resolution $\delta^{13}\text{C}_{\text{DIC}}$ , $\text{CO}_2$ , $\text{SIc}$ , $\text{DIC}$ Site Comparisons*

The data for low-resolution calculated  $\text{CO}_2$  and  $\text{DIC}$  versus  $\delta^{13}\text{C}_{\text{DIC}}$  on a temporal basis are presented in Figures 6.16 to 6.19 for both Crumps Cave (WF1 and SF) and LRCV (LRS and LRWF). These data are presented to illustrate the statistical robustness of both the measured weekly resolution of geochemical data and the calculated high-resolution of geochemical data reported earlier in the thesis. Data illustrating individual low-resolution versus time series for  $\text{CO}_2$ ,  $\text{SIc}$ , and  $\text{DIC}$  concentrations, and  $\delta^{13}\text{C}_{\text{DIC}}$  values, at each site, are in Appendix 5.

For Crumps Cave (WF1 and SF), both  $\text{CO}_2$  and  $\text{DIC}$  (Figures 6.16 and 6.17) values track with  $\delta^{13}\text{C}_{\text{DIC}}$  values during the summertime, indicating that ongoing root respiration and soil  $\text{CO}_2$  production are causing a depletion in  $\delta^{13}\text{C}_{\text{DIC}}$  values while driving  $\text{CO}_2$  and  $\text{DIC}$  concentrations in the epikarst (Jiang 2013). During the wintertime, as vegetation and microbial activity decreases, due to surface changes, the tracking of  $\text{CO}_2$ ,  $\text{DIC}$ , and  $\delta^{13}\text{C}_{\text{DIC}}$  diverge. The  $\delta^{13}\text{C}_{\text{DIC}}$  values become more enriched as  $\text{CO}_2$  production and  $\text{DIC}$  concentrations severely reduce. This is indicative of the reduction in fractionation of the  $^{12}\text{C}/^{13}\text{C}$  isotope caused by root respiration and microbial activity and thus, a shifting in carbon sourcing from soil to atmosphere (Faimon et al. 2012a; 2012b).

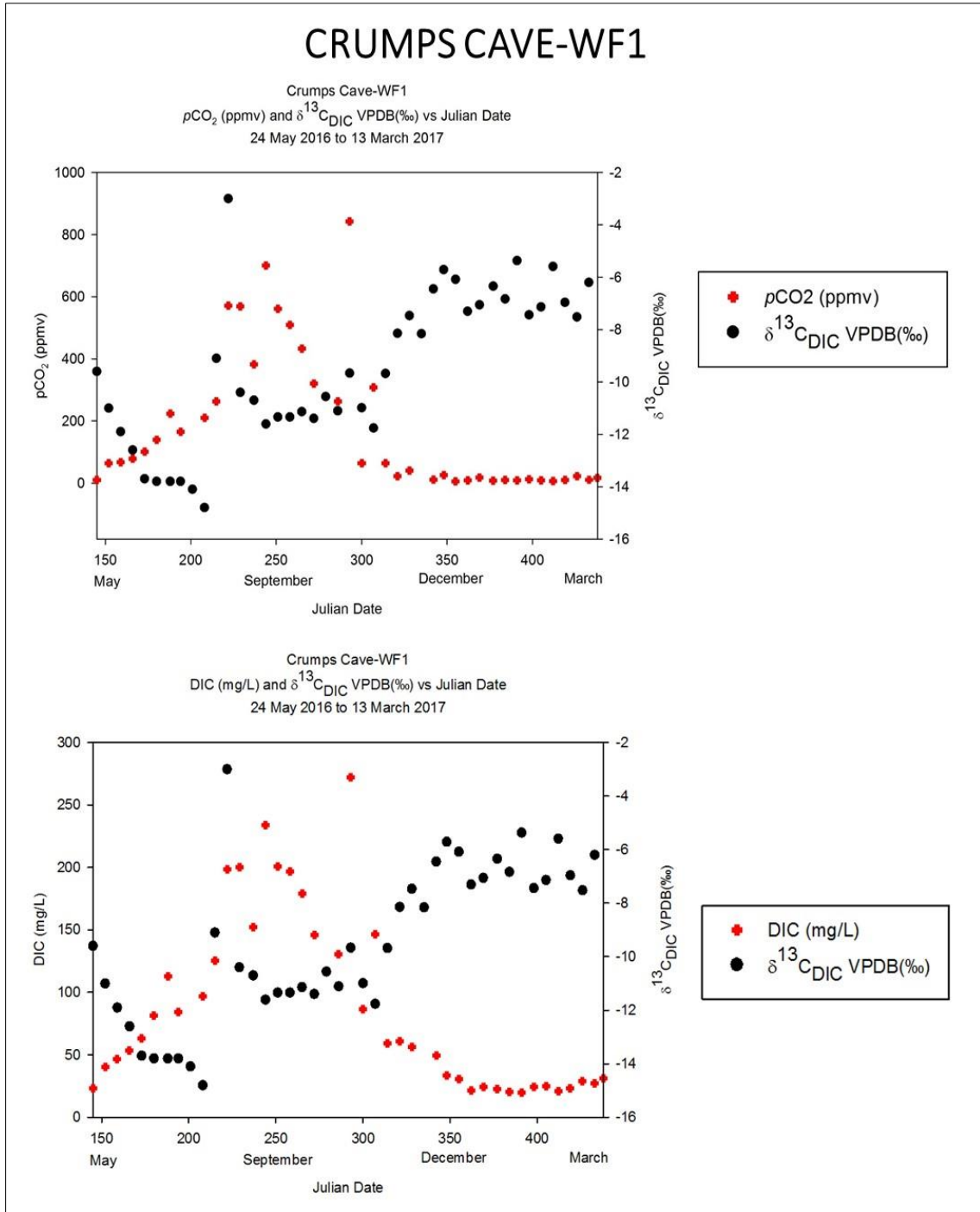


Figure 6.16 Time series of  $\text{CO}_2$ , DIC, and  $\delta^{13}\text{C}_{\text{DIC}}$  at Crumps Cave-WF1. Note the tracking of variables, suggesting that soil derived  $\text{CO}_2$  is the dominant component of DIC at Crumps Cave during the summer. Additionally, the  $\delta^{13}\text{C}$  values shift to enriched values based on seasonal shifts.

Source: Created by the author.

At the LRCV (LRS and LRWF), values of CO<sub>2</sub>, DIC and  $\delta^{13}\text{C}_{\text{DIC}}$  indicate clear seasonal trending during the summer months (Figures 6.18 and 6.19), suggesting that increased summertime fractionation, soil CO<sub>2</sub> production, and increase in DIC concentrations are at work. However, as the summer season transitions to winter, the divergence of  $\delta^{13}\text{C}_{\text{DIC}}$  observed at Crumps Cave does not occur at LRCV, indicating that  $\delta^{13}\text{C}_{\text{DIC}}$  values remain in a depleted state (Figures 5.5 and 5.6). The lack of wintertime enrichment may actually be a result of a masked signal by the presence of extensive impermeable surfaces preventing identification of an alternative carbon source. Likewise, any soil CO<sub>2</sub> that is diffused to the epikarst remains as a dissolved constituent in epikarst water, allowing for additional water-rock interaction, and the potential for precipitation should supersaturated water encounter an open atmosphere. Considering that LRS is extremely shallow, the likelihood of epikarst-derived water interacting with the surface is greater. Should precipitation occur *in situ*, affecting the isotopic signature, water reaching the spring could reflect an inaccurate representation of sourcing.

This phenomenon of prior calcite precipitation (PCP) is most readily described in research examining the influences on speleothem growth, which, according to Sinclair et al. (2012), is heavily driven by multiple factors, including changes in water-rock residence times, hydrologic variability, temperature, and soil zone processes. The possibility that secondary mineralization is occurring *in situ* at LRS may influence the signal detected at the spring. This process would be reflective of dominant soil zone CO<sub>2</sub>, primarily because bedrock CO<sub>2</sub> has already run through an entire cycle, from dissolution to precipitation to degassing, and no longer exists as a dissolved constituent.

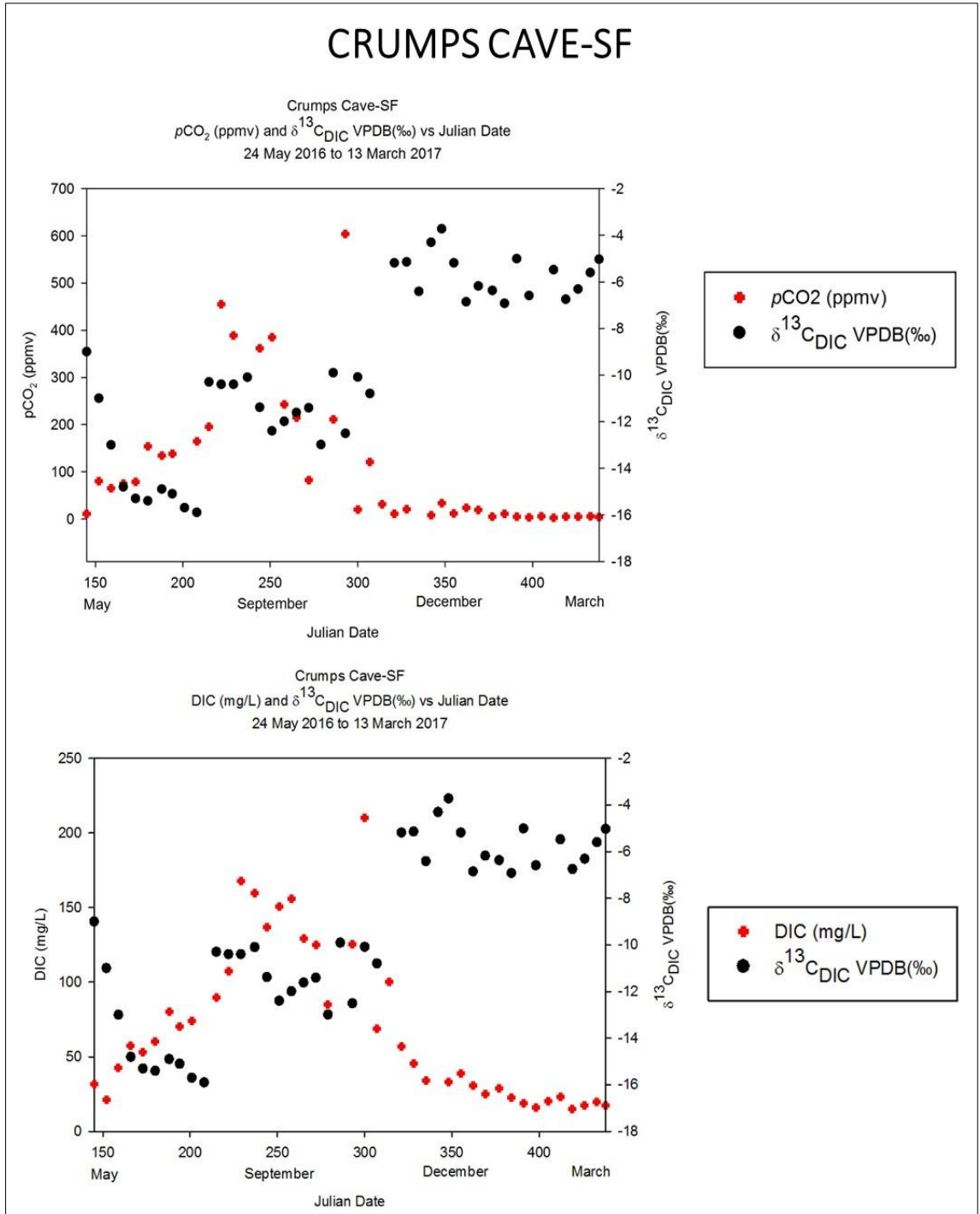


Figure 6.17 Time series of  $\text{CO}_2$ , DIC, and  $\delta^{13}\text{C}_{\text{DIC}}$  at Crumps Cave-SF. Note the tracking between variables, suggesting that seasonal  $\text{CO}_2$  is the dominant component of DIC. Additionally, the  $\delta^{13}\text{C}$  values shift to enriched states based on seasonal shifts.  
 Source: Created by the author.

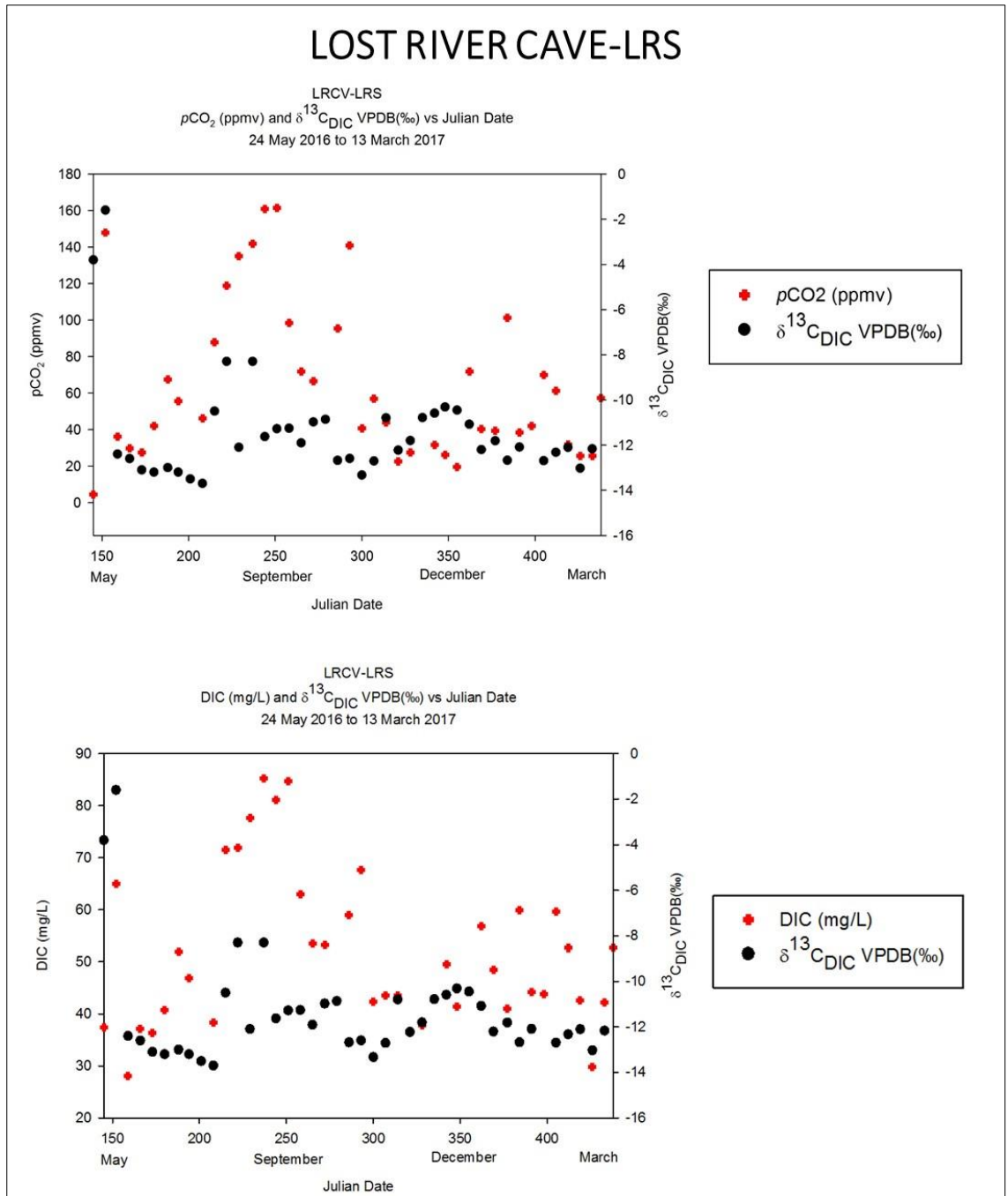


Figure 6.18 Time series of  $\text{CO}_2$ , DIC, and  $\delta^{13}\text{C}_{\text{DIC}}$  at LRCV-LRS. Note the ongoing tracking of variables, suggesting that  $\text{CO}_2$  is the dominant component at LRCV over the course of the study. Additionally, the  $\delta^{13}\text{C}$  values remain in a depleted state during the winter months, with  $\text{CO}_2$  and DIC trending closely.  
 Source: Created by the author.



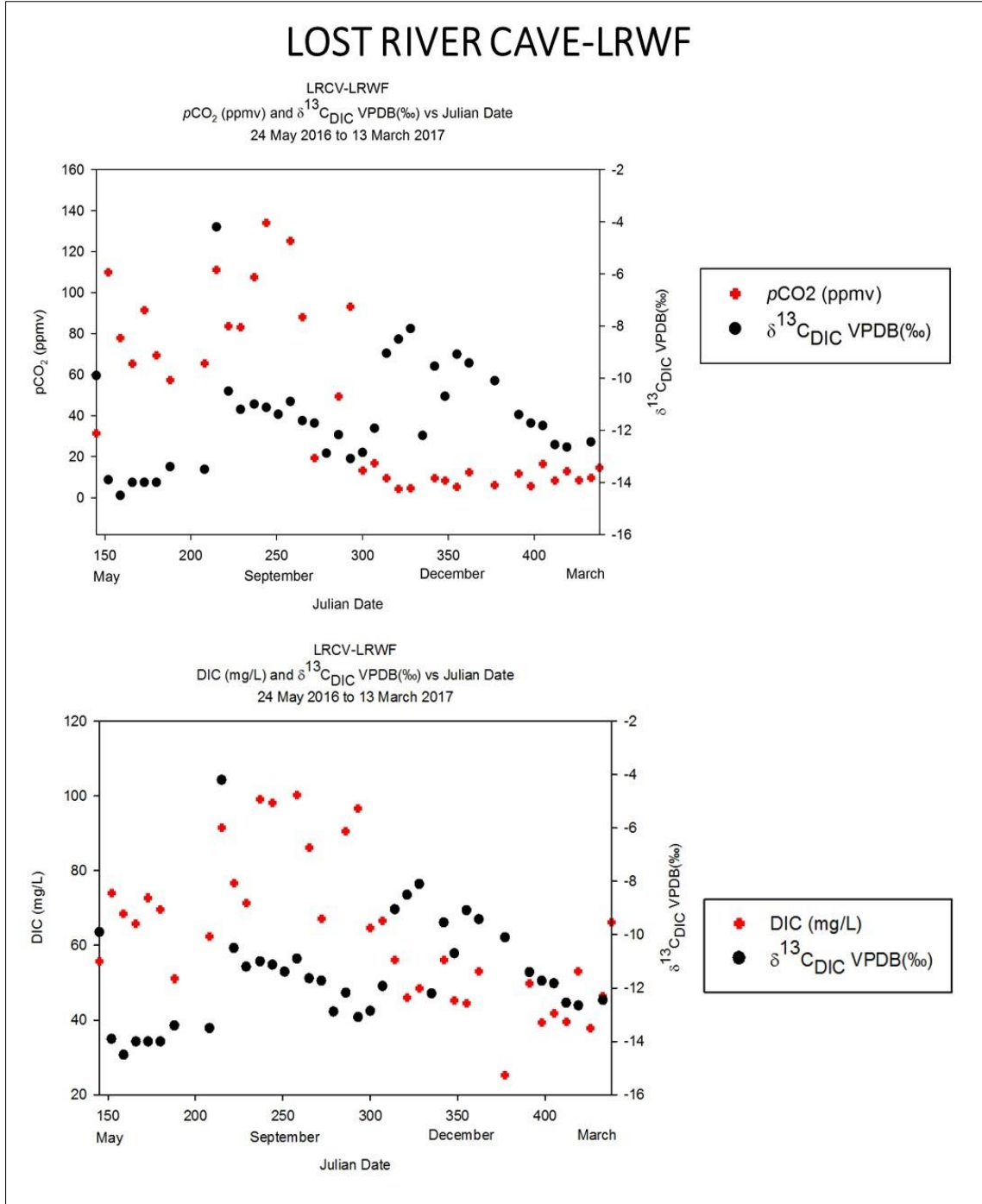


Figure 6.19 Time series of  $\text{CO}_2$ , DIC, and  $\delta^{13}\text{C}_{\text{DIC}}$  at LRCV-LRWF. Note the tracking between variables, suggesting that  $\text{CO}_2$  is the dominant component of DIC at the LRCV over the course of the study. Additionally, the  $\delta^{13}\text{C}$  values briefly shift to enriched states during the month of December, before showing depletion during the remainder of the winter.

Source: Created by the author.

Secondly, increased soil CO<sub>2</sub> is possibly trapped in the soil during the winter months due to excess artificial impermeable surfaces preventing atmospheric exchange (Cuezva et al. 2011). Likewise, the majority of high volume precipitation bypasses the epikarst in favor of direct injection to the aquifer through numerous injection wells (Crawford 1984a; Crawford 1984b; Crawford 1989).

## **6.2 Hydrogeochemical Site Comparisons**

### *6.2.1 Regional Scope*

The vertical extent of the epikarst and its associated geochemical gradient are a major debate in the karst literature (Williams 1983; White 1988; Clemens et al. 1999; Martin and Dean 2001; Vacher and Mylroie 2002; Bakalowicz 2004; Klimchouk 2004; White and White 2005; Florea and Vacher 2006; Petrella et al. 2007; Trček 2007; Williams 2008; Gulley et al. 2015; White 2015). Most telogenetic karst landscapes are driven by influences from the surface (i.e., precipitation, surface temperature, vegetation cover and root respiration, and soil microbial activity), which contribute to CO<sub>2</sub> production and transfusion through the epikarst and into the aquifer, especially during the growing season. The means of sourcing, diffusion, and exchange of CO<sub>2</sub> from atmosphere, to the soil layer, to the epikarst, under different surface and hydrological conditions are presented in Figure 6.20.

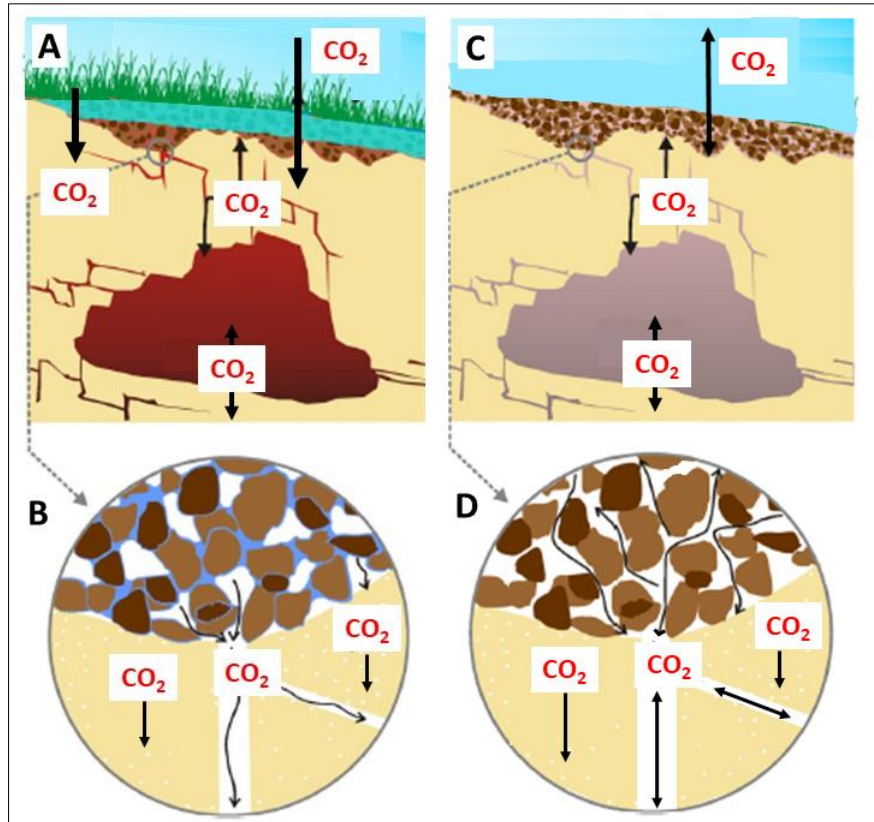


Figure 6.20 Illustration of CO<sub>2</sub> exchange in the epikarst. A) Diffusion to the epikarst during the growing season; B) Close-up image of the way in which soil distributes CO<sub>2</sub> through pore spaces during high moisture conditions; C) Diffusion of atmospheric dominant CO<sub>2</sub> during the dormant season; D) Close-up of the way in which CO<sub>2</sub> diffuses through soil pore space during low moisture conditions. Note that most CO<sub>2</sub> is derived from a combination of atmospheric CO<sub>2</sub>, microbial activity in the soil, and root respiration. Some CO<sub>2</sub> derived from atmospheric sources is primarily injected into the epikarst through direct recharge, while the rest infiltrates the soil layer first, mixing with soil CO<sub>2</sub> concentrations. Also note that depending on the season, CO<sub>2</sub> sourcing shifts between soil and atmospheric/carbonate rock dominance.

Source: Modified from Cuezva et al. (2011).

At Crumps Cave, the hydrogeochemical data indicate that a combination of seasonal changes and storm event variability serve to influence the cave on both long- and short-term scales. Seasonally, hydrogeochemical responses are influenced by the gradual changes in surface temperature driving vegetation growth and, thus, soil CO<sub>2</sub>

production, especially during the summer months. Groves et al. (2005) found storage at Crumps Cave exists within the epikarst, governed by the thin layer of chert, which potentially creates a leaky, perched aquifer. This perched aquifer could partially inhibit direct flow from the surface to the vadose zone, except during times of high precipitation when the system is discharged of storage water. The near immediate responses in all hydrogeochemical data at both WF1 and SF during storm events further indicate that ongoing storage is occurring, which is then flushed through the system during those storm events. Further, increased seasonal DIC fluctuations and dissolution rates, as well as reduced overall wall retreat, suggest that conduit development in the epikarst has reached a critical slow point during the winter months, as discussed in Palmer (1991; 2007a; 2007b), where development is relatively contingent on continuous aggressive water-rock interaction in a dissolvable medium.

In this respect, dissolution rates are higher during the growing season, due to increased water aggressiveness from an increased supply of soil CO<sub>2</sub>. Rates slow during the dormant season as soil CO<sub>2</sub> sourcing shifts to atmospheric CO<sub>2</sub> sourcing. This shift in CO<sub>2</sub> sourcing serves to slowdown dissolution. Further, despite colder water being capable of holding more dissolved CO<sub>2</sub>, the reduction in a highly concentrated supply of CO<sub>2</sub> negates that capability, also providing for a reduction in dissolution kinetics. Likewise, as calcite saturation approaches saturated to supersaturated levels, the rate of dissolution slows further, even when increased water-rock interaction occurs during the dry season. On the other hand, during the growing season, despite high volume precipitation events transferring water quickly through the epikarst, thus reducing residence time, the water is supersaturated with soil CO<sub>2</sub> concentrations, driving aggressive dissolution.

The LRCV sites exhibit different responses than Crumps Cave sites, primarily due to the urban environment governing soil and vegetation extent, CO<sub>2</sub> sourcing and diffusion in the epikarst, and seasonal variability in hydrogeochemical data. The presence of a heavily paved (and rather impermeable) urban landscape on the surface, in conjunction with an impermeable chert layer at the water table, contributes to a unique development of the epikarst at both the LRS and LRWF. This unique situation is derived from the potential trapping of soil CO<sub>2</sub> in the soil layer beneath the paved surface layer, which diffuses to the epikarst at a much slower rate overall, due to a reduction in infiltrating precipitation and antecedent moisture conditions.

The hydrogeochemical data indicate that, while seasonal variability is less apparent, responses to storm events drive the movement of epikarst water. It is during these high precipitation events that soil CO<sub>2</sub> diffusion to the epikarst increases. Further, the presence of the chert layer at the water table (Groves 1987), which significantly slows further reductions in the water table, may potentially contribute to an upward diffusion of CO<sub>2</sub> at LRS, generating heterogeneous pockets of increased CO<sub>2</sub> concentrations (which diffuse to areas of lower CO<sub>2</sub> concentrations) providing for increased dissolution in a lateral and vertical gradient, as observed in eogenetic karst systems by Gulley et al. (2005). As a consequence, certain volumetric thresholds are required to be met before increases in discharge are observed. The epikarst at LRCV behaves similarly to that of eogenetic karst, as observed by Gulley et al. (2015), where heterogeneous CO<sub>2</sub> diffusion causes conduits to form independent of telogenetic governed hydraulic conductivity. This unique combination of governing characteristics serves to increase dissolution rates and wall retreats, as well as DIC fluxes, over the course of the study period; however,

calcite saturation at both LRCV sites is continuously high, as evident by the presence of a growing flowstone at LRWF. This suggests that dissolution kinetics are governed by the extent of saturation, as well as the contribution of CO<sub>2</sub>, and that CO<sub>2</sub> sourcing is an important driver of this process.

As mentioned earlier and shown in previous studies, the presence of a chert layer at both locations may be governing water storage and transference and, thus, water-rock interaction and residence times. A comparison of mean discharges and their respective ranges at the four study sites in this investigation, as well as other springs around the world, is presented in Table 6.2. Precipitation and recharge time series analysis for all four sites are presented in graphical form in Appendix 6. The majority of aquifer discharges at different sites around the world render slightly higher volumes in averages, peak flows, and baseflows, compared to epikarst discharges, suggesting that the epikarst can serve to store water, but volumetrically it does not equate to primary aquifer storage. On the other hand, although discharge in the epikarst is reduced comparatively to the main aquifer, CO<sub>2</sub> flux and dissolution processes are greater in the epikarst, due to the open system nature of most landscapes with surface influences. These processes drive dissolution kinetics throughout the aquifer, with the majority of those processes occurring at relatively shallow depths (between 10 to 30 meters) (Bakalowicz 2004; Klimchouk 2004). Thus, aquifer development and karst landscape evolution are highly contingent on the status of dissolution kinetics and CO<sub>2</sub> fluctuations in the epikarst.

Table 6.2. Comparison of world epikarst and aquifer spring discharges to this investigation.

Spring	Discharge (Q)			Reference
	Mean	Max Flow	Baseflow	
Ewers Alley (USA)	0.056 L/s		0.142 L/s	Jackson (2012)
Barton Spring (USA)	1.42 m <sup>3</sup> /s	2.7 m <sup>3</sup> /s	0.28 m <sup>3</sup> /s	Wong et al. (2012)
Milandre Test Site (France)				
Saivu Spring		200 L/s	20 L/s	Perrin et al. (2003)
Hubelj (SW Slovenia)		24.9 m <sup>3</sup> /s	0.12 m <sup>3</sup> /s	Trček (2007)
Acqua dei Faggi (S Italy) *	0.04 m <sup>3</sup> /s	0.065 m <sup>3</sup> /s	0.005 m <sup>3</sup> /s	Petrella et al. (2007)
Fontaine de Vaucluse (SE France)		70 m <sup>3</sup> /s	10 m <sup>3</sup> /s	Emblanch et al. (2003)
Beaver Spring (USA)		127 L/s	30 L/s	Vesper and White (2004)
Guangxi (SW China) *		156.4 L/s	149.5 L/s	Zhang et al. (2016)
Cent-Fonts (S of France) *		12.2 m <sup>3</sup> /s	1.0 m <sup>3</sup> /s	Aquilina et al. (2004)
Edwards Aquifer (USA)				Worthington (2003)
Comal Springs		442 (cfs)	270 (cfs)	
San Marcos Springs		403 (cfs)	215 (cfs)	
Wilkins Bluehole (USA)			0.56 m <sup>3</sup> /s	Ray and Blair (2005)
Lost River Rise (USA)			0.35 m <sup>3</sup> /s	
Crumps-WF1*	0.07 L/s	11.5 L/s	0.013 L/s	<i>Current study</i>
Crumps-SF*	0.16 L/s	0.46 L/s	0.06 L/s	
Lost River Cave and Valley-LRS*	0.06 L/s	3.84 L/s	0.01 L/s	
Lost River Cave and Valley-LRWF*	0.39 L/s	0.39 L/s	0.009 L/s	

\*epikarst spring

Source: Created by the author.

Hydrogeochemical processes at Crumps Cave and at locations in China, Italy, and France all exhibit certain responses to surface influences driving dissolution kinetics governed by seasonal and storm event variability. At the LRCV, the presence of an urban landscape plays a vital role on the development of the epikarst with respect to carbon sourcing and diffusion, and dissolution kinetics and DIC fluctuations.

Previous karst investigations focused primarily on aquifer processes, where it is assumed that the influences governing the majority of karst development are the greatest, and thus require the most attention (Veni et al. 2001; Aquilina et al. 2004; Palmer 2007a; Worthington 2007; De Waele et al. 2009; Anaya et al. 2014). As a consequence, the epikarst is often overlooked as a large contributor to karst landscape development. Those investigations that do focus on the epikarst suggest that the upper layer of the karst system plays a vital role in geochemical influences (White 1988; Emblanch et al. 2003; Bakalowicz 2004; Klimchouk 2004); however, the majority of those investigations are limited to single cave systems under similar conditions such as land use, epikarst thickness, and climate. Further, only a handful of those investigations have examined epikarst processes in high resolution to characterize immediate changes as a way to delineate the primary and secondary hydrogeochemical drivers to aquifer development (Zhongcheng and Daoxian 1999; Bakalowicz 2004; Palmer 2007a; Petrella et al. 2007; Trček 2007; White 2007; Jacob et al. 2009; Liu et al. 2010; Yang et al. 2012; Peyraube et al. 2014; Milanolo and Gabrovšek 2015; Zhang et al. 2016). This investigation aimed to combine those elements (epikarst hydrogeochemical high-resolution monitoring in multiple karst systems under various land uses) to further delineate the influence of those



variables on epikarst processes and their extent of impact on aquifer evolution in telogenetic karst systems.

The results of this investigation indicate that under natural and agricultural settings, dissolution kinetics in the epikarst are driven by surface viability, such as precipitation and temperature, which govern the availability of soil CO<sub>2</sub> and its subsequent diffusion to the epikarst. Seasonal changes are the most prominent driving factor for increased production of CO<sub>2</sub>, while high-volume storm events facilitate the diffusion of these large concentrations of CO<sub>2</sub> to the epikarst where dissolution can actually occur.

While concentrations of CO<sub>2</sub> and DIC at Crumps Cave and the LRCV are relatively similar, the methods by which they diffuse to the epikarst are different. Likewise, the way the epikarst processes these constituents is also different. While a natural landscape may seem more conducive to karst development, in this study the data suggest that an urban environment can facilitate dissolution and supersaturation, redistributing bedrock and possibly contributing to potential karst landscape hazards, such as water containment storage and transport. Thus, urban landscapes, it would seem, have relatively important impacts on hydrogeochemical processes in karst systems. Those impacts can have negative effects on the human population as urban sprawl becomes more and more of a contributor to the way that the epikarst responds and to any subsequent influences on aquifer development and drinking water quality.

## Chapter 7: Conclusions

Understanding the hydrogeochemical relationships with storage and flow propensity in various karst settings is crucial to tying together certain fundamental concepts about the primary functionality of the epikarst with respect to deeper geochemical processes. Further, tracking carbon through the epikarst as a means to understand dissolution kinetics and the propensity for karst systems to serve as carbon sinks is extremely important, especially considering the growing concern over the accumulation of atmospheric carbon dioxide released from anthropogenic activities. Additionally, DIC fluctuations can illustrate how carbon is utilized by karst systems, further illuminating the extent to which vast deposits of terrestrial limestone may serve as carbon sinks (Zhang et al. 2015).

The Pennyroyal Sinkhole Plain in southcentral Kentucky has been the focus of karst research for decades (Crawford 1984a; Crawford 1984b; Crawford 1989; Crawford 2003; Crawford 2005; Brewer and Crawford 2005; Cesin and Crawford 2005; Vanderhoff 2011; Nedvidek 2014). Of those studies, the majority addressed cave development and aquifer processes at varying resolutions (Palmer 2007a; Vanderhoff 2011; Lawhon 2014; Nedvidek 2014). Examinations into individual caves and their hydrogeochemical processes have left a gap in the literature, allowing for a comparative study with respect to multiple karst systems as a means to understand how those same processes operate on a regional scale.

This investigation examined two cave systems under different land use conditions, with a focus on epikarst hydrogeochemical processes and how those processes serve to influence dissolution rates and conduit development in the epikarst.

Further, tracking carbon from inception to discharge can better infer both carbon uptake in karst systems and a karst landscape's role in the global carbon flux calculation. This investigation yielded the following findings:

- Seasonal, diurnal, and storm event variability serve to influence hydrogeochemical dissolution processes through the diffusion of soil CO<sub>2</sub>. Surface influences, such as temperature and precipitation, contribute to CO<sub>2</sub> production and diffusion during the growing period; however, CO<sub>2</sub> diffusion to the epikarst is variable by location, with Crumps Cave sites experiencing dominant seasonal diffusion, while the LRCV sites experienced dominant storm event diffusion once certain antecedent moisture thresholds were met. The dissimilarity in diffusion is due to land use differences, soil coverage, epikarst thicknesses, and stages of epikarst development.
- At Crumps Cave, storm event variability drives immediate hydrogeochemical responses and facilitates movement of water through the epikarst, while seasonal variability drives long-term changes, which influence dissolution processes via the diffusion of CO<sub>2</sub> as both a dissolved constituent in infiltrating, low-precipitation events and antecedent moisture seepage.
- At the LRCV, storm event variability is less pronounced, due to the urban landscape interfering with natural recharge of the epikarst. This is in direct contrast to the LRCV aquifer, which responds quite heavily to storm events (Lawhon 2014). Seasonal changes are also less apparent, but longer residence times and slower soil CO<sub>2</sub> diffusion increase the rate of dissolution and subsequent supersaturation.

- Carbon uptake is heavily driven by soil CO<sub>2</sub> in the summer months at both locations, while primarily driven by atmospheric CO<sub>2</sub> at Crumps Cave and soil CO<sub>2</sub> at the LRCV in the winter. This is primarily due to a difference in land use at both locations, with Crumps Cave influenced by seasonal agricultural use and the LRCV influenced by an urban setting, which aids in the reduction in the rate of soil CO<sub>2</sub> diffusion to the epikarst.
- Telogenetic epikarst thickness and its internal conduit development are highly contingent on the aforementioned dissolution rates. Crumps Cave epikarst appears to be better developed than the LRCV, as evident by the near immediate response to even minimal rainfall events, while LRCV sites require certain capacity thresholds to be met before an increase in discharge is registered. This implies that storage is occurring at both sites, with Crumps Cave' capacity being greater and able to transport more volume in shorter time periods, while the LRCV experiences more matrix dominated flow. At the LRS, this matrix-dominated flow could be a result of an extremely thin epikarst, while epikarst thickness at the LRWF is less than that of Crumps Cave, but accommodating of water transference at a volume greater than the LRS.
- The differences in epikarst thickness and the presence of a rather impermeable chert layer at both locations govern water residence times and, thus, the extent of dissolution. As described by Williams (1983; 2008), Bakalowicz (2004), and Klimchouk (2004), epikarst dissolution kinetics reduce and eventually cease at depths between 10 to 30 meters, due to a shift from open system conditions to closed system conditions. A shift from open system conditions to relatively closed

system conditions may be occurring at Crumps Cave, where 18 meters of epikarst thickness exist between surface and epikarst drains. DIC concentrations and flux, and saturation indexes, are lower at Crumps Cave versus the LRCV. Epikarst thickness at the LRS is less than five meters and epikarst thickness at the LRWF is roughly 13 meters. Likewise, isotopic soil signals at both LRCV sites are stronger throughout the year, as well as increased dissolution rates, and greater DIC fluctuations. DIC fluctuation calculations are a workable approach to understanding how carbon sequestration and utilization in karst environments operates, provided that similarities between examination sites exist, such as the defining geology of the region. Conversely, even if land use and hydrological differences are present (i.e. variability in storage and flow), the DIC fluctuation calculations will illuminate the impact of these differences on overall carbon utilization, further providing for insight into global carbon uptake in karst regions.

Generally, the investigation yielded many similarities between all sites, such as hydrogeochemical responses driven primarily by soil CO<sub>2</sub> seasonal influences and secondarily by storm events; however, certain site specific characteristics, such as land use cover and epikarst thickness, indicate that, indeed, the extent of epikarst development and its associated hydrogeochemical processes are reliant on both geology and thickness of the epikarst, for storage and flow variability were evident and unique to all sites (Williams 1983; Worthington et al. 2000; Worthington 2003; Worthington 2007; Bakalowicz 2004; Klimchouk 2004; Williams 2008).

Certain limitations of this project prohibit a more accurate representation of the processes at work and, as such, assumptions were made, including the following:

- Dissolution processes and carbon flux were contingent on discharge and geochemical parameters. All values were calculated based on assumed sizes of recharge basins, however, the exact area of recharge for all sites were unknown for this study. Thus, it is important that future work address this issue to ensure an exact quantitative assessment can be drawn with respect to the impact that the size of the recharge basin has on each site's DIC fluctuations and extent of storage.
- At SF, low resolution of the collected data generated assumptions about responses during events that occurred between collection dates.
- At LRS, placement of the loggers was downstream from the sample collection site; thus assumptions that the reach of the stream posed a negligible influence on geochemical evolution were made.
- At LRWF, failed access to the site on certain collection dates due to inclement weather meant lost data, while low-resolution discharge required an assumption regarding volumetric responses from precipitation influences. Lastly, the time period for the study was short of a full year, primarily due to funding and investigation timeline modifications due to extraneous circumstances. Thus, only the onset of the spring transition was captured.

This investigation serves to contribute to the scientific understanding of epikarst dissolution processes in mid-latitude regions, specifically southcentral Kentucky, with a focus on hydrogeochemical and carbon isotope evolution. Further investigations along similar lines could include continued high-resolution sample collection in all respects, with an inclusion of technological monitoring at all sites. A closer examination of the impact of an urban setting on carbon sourcing and transport at the LRCV, plus use of soil

CO<sub>2</sub> utilization, with an emphasis on multi-year collection and monitoring, could increase conceptual understanding on the processes at work in karst systems related to carbon flux in varied land use settings around the world. Lastly, comparative analyses between eogenetic karst systems and telogenetic epikarst systems are severely lacking in the literature. The data from this investigation suggest that they exhibit similar behaviors and thus, closer examinations are vital to understanding both epikarst and aquifer development, especially in an ever-growing urban landscape.

## References

- Amundson, R., Stern, L., Baisden, T., Wang, Y. 1998. The isotopic composition of soil and soil-respired CO<sub>2</sub>. *Geoderma* 82, 83-114.
- Allen, D.M. 2004. Sources of groundwater salinity on islands using <sup>18</sup>O, <sup>2</sup>H, and <sup>34</sup>S. *Groundwater* 42(1), 17–31.
- Anaya, A., Padilla, I., Macchiavelli, R., Vesper, D.J., Meeker, J.D., Alshawabkeh, A.N. 2014. Estimating preferential flow in karstic aquifers using statistical mixed models. *Groundwater* 52(4), 584-596.
- Aquilina, L., Ladouche, B., Dorfliger, N. 2004. Water storage and transfer in the epikarst of karstic systems during high flow periods. *Journal of Hydrology* 327, 472-485.
- Bakalowicz, M. 2004. The epikarst, the skin of karst. *Karst Waters Institute Special Publication* 9, 16-22. Accessed on March 25, 2015 from:  
[https://www.researchgate.net/publication/267426221\\_THE\\_EPIKARST\\_THE\\_SKIN\\_OF\\_KARST](https://www.researchgate.net/publication/267426221_THE_EPIKARST_THE_SKIN_OF_KARST)
- Baldini, J.U.L., Baldini, L.M., McDermott, F., Clipson, N. 2006. Carbon dioxide sources, sinks, and spatial variability in shallow temperate zone caves: Evidence from Ballynamintra Cave, Ireland. *Journal of Cave and Karst Studies* 68(1), 4–11.
- Blecha, M., Faimon, J. 2014a. Karst soils: dependence of CO<sub>2</sub> concentrations on pore dimension. *Acta Carsologica* 43(1), 55-64.
- Blecha, M., Faimon, J. 2014b. Spatial and temporal variations in carbon dioxide (CO<sub>2</sub>) concentrations in selected soils of the Moravian Karst (Czech Republic). *Carbonates Evaporites* 29, 395-408.
- Brewer, J., Crawford, N. 2005. *Groundwater basin catchment delineation and generalized flow routes through the karst aquifer beneath Bowling Green, Kentucky, USA*. Paper presented at the 14th International Congress of Speleology, Athens, August 21-28. Hellenic Speleological Society P-15, 594-597. Available online at:  
[http://www.esse.edu.gr/media/lipes\\_dimosiefsis/14isc\\_proceedings/p/15.pdf](http://www.esse.edu.gr/media/lipes_dimosiefsis/14isc_proceedings/p/15.pdf).
- Cane, G., Clark, I.D. 1999. Tracing groundwater recharge in an agricultural watershed with isotopes. *Groundwater* 37, 133-139.



- Cerling, T.E. 1984. The stable isotope composition of soil carbonate and its relationship to climate. *Earth and Planetary Science Letters* 71, 229-240.
- Cerling, T.E., Solomon, D.K., Quade, J., Bowman, J.R. 1991. On the isotopic composition of carbon in soil carbon dioxide. *Geochimica et Cosmochimica Acta* 55, 3403-3405.
- Cesin, G.L., Crawford, N.C. 2005. *Urban storm management for cities built upon karst: Bowling Green, Kentucky, USA*. Paper presented at the 14th International Congress of Speleology, Athens, August 21-28. Hellenic Speleological Society O-12, 66-70. Available online at: [http://www.esse.edu.gr/media/lipes\\_dimosiefsis/14isc\\_proceedings/o/012.pdf](http://www.esse.edu.gr/media/lipes_dimosiefsis/14isc_proceedings/o/012.pdf)
- Charlier J-B., Bertrand, C., Mudry, J. 2012. Conceptual hydrogeological model of flow and transport of dissolved organic carbon in a small Jura karst system. *Journal of Hydrology* 460-461, 52-64.
- Chemseddine, F., Dalila, B., Fethi, B. 2015. Characterization of the main karst aquifers of the Tez bent Plateau, Tebessa Region, Northeast of Algeria, based on hydrochemical and isotopic data. *Environmental Earth Science* 74, 241-250.
- Cheng, Z., Daoxian, Y., Jianhua, C. 2005. Analysis of the environmental sensitivities of a typical dynamic epikarst system at the Nongla monitoring site, Guangxi, China. *Environmental Geology* 47, 615-619.
- Clark, I., Fritz, P. 1997. *Environmental Isotopes in Hydrogeology*, Boca Raton, FL: CRC Press.
- Clemens, T., Huckinghaus, D., Liedl, R., Sauter, M. 1999. Simulation of the development of karst aquifers: role of epikarst. *International Journal of Earth Sciences* 88, 157-162.
- Covington, M.D., Gulley, J.D., Gabrovšek, F. 2015. Natural variations in calcite dissolution rates in streams: Controls, implications, and open questions. *Geophysical Research Letters* 42, 2836-2843.
- Crawford, N. 1984a. Sinkhole flooding associated with urban development upon karst terrain: Bowling Green, Kentucky. In Balkema, A.A. (ed.) *Proceedings of the First Multidisciplinary Conference on Sinkholes, Orlando, Florida, October 15-17*, 283-292.

- Crawford, N. 1984b. Toxic and explosive fumes rising from carbonate aquifers: A hazard for residents of sinkhole plains. In Balkema, A.A. (ed.) *Proceedings of the First Multidisciplinary Conference on Sinkholes, Orlando, Florida, October 15-17, 297-304.*
- Crawford, N. 1989. *The Karst Landscape of Warren County.* Bowling Green, KY: Technical Report 23, City-County Planning Commission of Warren County.
- Crawford, N. 2003. *Lazy Acres mobile home park ~ Lost River Cave dye tracing investigation.* Bowling Green, KY: Technical Report, Bowling Green–Warren County Health Department.
- Crawford, N. 2005. Ground-Water basin catchment delineation by dye tracing, water table mapping, cave mapping, and geophysical techniques: Bowling Green, Kentucky. In: Beck, B.F. (ed.), *Proceedings of the Tenth Multidisciplinary Conference on Sinkholes and the Engineering Impacts of Karst, San Antonio, TX, September 24-28.* 394-402.
- Cuezva, S. Fernandez-Cortes, A., Benavente, D., Serrano-Ortiz, P., Kowalski, A.S., Sanchez-Moral, S. 2011. Short-term CO<sub>2</sub>(g) exchange between a shallow karstic cavity and the external atmosphere during summer: Role of the surface soil layer. *Atmospheric Environment* 45, 1418-1427.
- Davidson, E.A., Belk, E., Boone, R.D. 1998. Soil water content and temperature as independent or confounded factors controlling soil respiration in a temperate mixed hardwood forest. *Global Change Biology* 4(2), 217-227.
- de Montety, V., Martin, J.B., Cohen, M.J., Foster, C., Kurz, M.J. 2011. Influence of diel biogeochemical cycles on carbonate equilibrium in a karst river. *Chemical Geology* 283, 31-43.
- De Waele, J., Plan, L., Audra, P. 2009. Recent developments in surface and subsurface karst geomorphology: An introduction. *Geomorphology* 106(1-2), 1-8.
- Doctor, D.H., Kendall, C., Sebestyen, S.D., Shanley, J.B., Ohte, N., Boyer, E.W. 2008. Carbon Isotope Fractionation of Dissolved Inorganic Carbon (DIC) due to Outgassing of Carbon Dioxide from a Headwater Stream. *Hydrological Processes* 22, 2410-2423.

- Drever J.I. 1997. *The Geochemistry of Natural Waters*. Upper Saddle River, NJ: Pearson Prentice Hall.
- Emblanch, C., Zuppi, G.M., Mudry J., Blavoux, B., Batiot, C. 2003. Carbon 13 of T<sub>DIC</sub> to quantify the role of the unsaturated zone: the example of the Vaucluse karst systems (Southeastern France). *Journal of Hydrology* 279, 262-274.
- Faimon, J., Licbinksa, M., Zajicek, P., Sracek, O. 2012a. Partial pressures of CO<sub>2</sub> in epikarstic zone deduced from hydrogeochemistry of permanent drips, the Moravian Karst, Czech Republic. *Acta Carsologica* 41(1), 47-57.
- Faimon, J., Licbinksa, M., Zajicek, P. 2012b. Relationship between carbon dioxide in Balcarka Cave and adjacent soils in the Moravian Karst region of the Czech Republic. *International Journal of Speleology* 41(1), 17-28.
- Fierer, N., Allen, A.S., Schimel, J.P., Holden, P.A. 2003. Controls on microbial CO<sub>2</sub> production: a comparison of surface and subsurface soil horizons. *Global Change Biology* 9(9), 1322-1332.
- Florea, L.J. 2013. Isotopes of carbon in a karst aquifer of the Cumberland Plateau of Kentucky, USA. *Acta Carsologica* 42(2-3), 277-289.
- Florea, L.J., Vacher, H.L. 2006. Springflow hydrographs: eogenetic vs telogenetic karst. *Groundwater* 44(3), 352-361.
- Fritz, P., Fontes, J.C., Frappe, S.K., Louvant, D., Michelot J.L. 1989. The isotope geochemistry of carbon in groundwater at Stripa. *Geochimica et Cosmochimica Acta* 53, 1765-1775.
- Gammons, C.H., Babcock, J.N., Parker, J.N., Poulson, S.R. 2011. Diel cycling and stable isotopes of dissolved oxygen, dissolved inorganic carbon, and nitrogenous species in a stream receiving treated municipal sewage. *Chemical Geology* 283, 44-55.
- Gebbinck, C.D.K., Kim, S-T., Knyf, M., Wyman, J. 2014. A new online technique for the simultaneous measurement of the  $\delta^{13}\text{C}$  value of dissolved inorganic carbon and the  $\delta^{18}\text{O}$  value of water from a single solution sample using continuous-flow isotope ratio mass spectrometry. *Rapid Communications in Spectrometry* 28, 553-562.

- Godoy, J.M., Godoy, M.L.D.P., Neto, A. 2012. Direct determination of  $\delta(D)$  and  $\delta(^{18}O)$  in water samples using cavity ring down spectrometry: Application to bottled mineral water. *Journal of Geochemical Exploration* 119-120, 1-5.
- Gorka, M. Sauer, P.E., Lewicka-Szczebak, D., Jedrysek, M-O. 2011. Carbon isotope signature of dissolved inorganic carbon (DIC) in precipitation and atmospheric CO<sub>2</sub>. *Environmental Pollution* 159, 294-301.
- Groves, C. 1987. *Lithologic controls on karst groundwater flow, Lost River groundwater basin, Warren County, Kentucky*. M.S. in Geography, Department of Geography and Geology, Western Kentucky University, Bowling Green, KY. Accessed on April 22, 2016, from <http://digitalcommons.wku.edu/theses/1554/>
- Groves, C., Meiman, J. 2001. Inorganic carbon flux and aquifer evolution in the south-central Kentucky karst. In Kuniansky, E.L. (ed), *U.S. Geological Survey Interest Group Proceedings, Water-Resources Investigations*, Reston, VA: USGS Report 01-4011, 99-105.
- Groves, C., Bolster, C., Meiman, J. 2005. *Spatial and Temporal Variations in Epikarst Storage and Flow in South Central Kentucky's Pennyroyal Plateau Sinkhole Plain*. Reston, VA: U.S. Geological Survey Karst Interest Group Proceedings, 64-73. Available online at [http://digitalcommons.wku.edu/geog\\_fac\\_pub/28/](http://digitalcommons.wku.edu/geog_fac_pub/28/).
- Groves, C., Polk, J., Miller, B., Kambesis, P., Bolster, C., Vanderhoff, S., Tyrie, B., Ruth, M., Ouellette, G., Osterhoudt, L., Nedvidek, D., McClanahan, K., Lawhon, N., Hall, H. 2013. *The Western Kentucky University Crumps Cave Research and Education Preserve*. Paper presented at the 20<sup>th</sup> National Cave and Karst Management Symposium, Carlsbad, NM, October 4-9, 105-110. Available online at: [http://scholarcommons.usf.edu/nckms\\_2013/Proceedings/ShowCaves\\_Interpretation\\_and\\_Biology/7/](http://scholarcommons.usf.edu/nckms_2013/Proceedings/ShowCaves_Interpretation_and_Biology/7/)
- Gulley, J.D., Martin, J.B., Moore, P.J., Murphy, J. 2012. Formation of phreatic caves in an eogenetic karst aquifer by CO<sub>2</sub> enrichment at lower water tables and subsequent flooding by sea level rise. *Earth Surface Processes and Landforms* 38(11), 1210-1224.

- Gulley, J.D., Martin, J.B., Moore, P.J., Brown, A., Spellman, P.D., Ezell, J. 2015. Heterogeneous distributions of CO<sub>2</sub> may be more important for dissolution and karstification in coastal eogenetic limestone than mixing dissolution. *Earth Surface Processes and Landforms* 40, 1057-1071.
- Hatcher, B.E. 2013. *Sources of CO<sub>2</sub> controlling the carbonate chemistry of the Logsdon River, Mammoth Cave, Kentucky*. M.S. Geoscience thesis, Department of Geography and Geology, Western Kentucky University, Bowling Green, KY. Accessed April 1, 2016, from <http://digitalcommons.wku.edu/theses/1311/>
- Hess, J.W., White, W.B. 1992. Groundwater geochemistry of the carbonate karst aquifer, southcentral Kentucky, U.S.A. *Applied Geochemistry* 8, 189-204.
- Hoefs, J. 2010. *Stable Isotope Geochemistry* (6<sup>th</sup> Edn.). Berlin, Germany: Springer-Verlag.
- Huang, F., Zhang, C., Xie, Y., Li, L., Cao, J. 2015. Inorganic carbon flux and its source in the karst catchment of Maocun, Guilin, China. *Environmental Earth Science* 74, 1079-1089.
- Hunkeler, D. Mudry, J. 2007. Hydrochemical Methods. In Goldschieder, N., Drew, D. (eds.) *Methods in Karst Hydrogeology*. London, U.K.: Taylor and Francis, 93-122.
- Hursh, A., Ballantyne, A., Cooper, L., Maneta, M., Kimball, J., Watts, J. 2017. The sensitivity of soil respiration to soil temperature, moisture, and carbon supply at the global scale. *Global Change Biology* 23, 2090-2103.
- Jackson, P.E. 2000. Ion chromatography in Environmental Analysis. In Meyers, R.A. (ed.) *Encyclopedia of Analytical Chemistry*. Chichester, U.K.: John Wiley and Sons, 2779-2801
- Jackson, D. 2012. An evaluation of physical and chemical discharge parameters at a spring that drains the epikarst: Kentucky, USA. *Carbonates and Evaporites* 27, 173-184.
- Jacob, T., Chery, J., Bayer, R., Le Moigne, N., Boy, J-P., Vernant., P., Boudin, F. 2009. Time-lapse surface to depth gravity measurements on a karst system reveal the dominant role of the epikarst as a water storage entity. *Geophysical Journal International* 177, 347-360.

- Jiang, Y. 2013. The contribution of human activities to dissolved inorganic carbon fluxes in a karst underground river system: Evidence from major elements and  $\delta^{13}\text{C}_{\text{DIC}}$  in Nandong, Southwest China. *Journal of Contaminant Hydrology* 152, 1-11.
- Jiang, G., Guo, F., Wu, J. 2007. The threshold value of epikarst runoff in forest karst mountain area. *Environmental Geology* 55, 87-93.
- Klimchouk, A. 2004. Towards defining, delimitating and classifying epikarst: Its origin, processes and variants of geomorphic evolution. In: Jones, W.K., Culver, D.C. Herman, J. (eds.) *Karst Waters Institute Special Publication* 9, 23-35.
- Knierim, K.J., Pollock, E., Hays, P.D. 2013. Using isotopes of dissolved inorganic carbon species and water to separate sources of recharge in a cave spring, northwestern Arkansas, USA. *Acta Carsologica* 42(2-3), 261-276.
- Knierim, K.J., Pollock, E., Hays, P.D., Khojasteh, J. 2015. Using stable isotopes of carbon to investigate the seasonal variation of carbon transfer in a northwestern Arkansas cave. *Journal of Cave and Karst Studies* 77(1), 12-27.
- Lambert, W.J. Aharon, P. 2010. Controls on dissolved inorganic carbon and  $\delta^{13}\text{C}$  in cave waters from DeSoto Caverns: Implications for speleothem  $\delta^{13}\text{C}$  assessments. *Geochimica et Cosmochimica Acta* 75, 753-768.
- Lawhon, N. 2014. *Investigating telogenetic karst aquifer processes and evolution in South-Central Kentucky, U.S., using high-resolution storm hydrology and geochemistry monitoring*. M.S. Geoscience thesis, Department of Geography and Geology, Western Kentucky University, Bowling Green, KY. Accessed April 1, 2016, from <http://digitalcommons.wku.edu/theses/1324/>.
- LeGrand, H. 1983. Perspective on karst hydrology. *Journal of Hydrology* 61(1-3), 343-355.
- Li, Q., Sun, H., Han, J., Liu, Z., Yu, L. 2008a. High resolution study on hydrochemical variations caused by the dilution of precipitation in the epikarst spring: an example spring in Landiantang at Nongla, Mashan, China. *Environmental Geology* 54, 347-354.
- Li, S-L., Liu, C-Q., Lang, Y-C., Tao, F., Zhao, Z., Zhou, Z. 2008b. Stable carbon isotope biogeochemistry and anthropogenic impacts on karst ground water, Zunyi, Southwest China. *Aquatic Geochemical* 14, 211-221.

- Li, S-L., Liu, C-Q., Li, J., Lang, Y-C., Ding, H., Li, L. 2010. Geochemistry of dissolved inorganic carbon and carbonate weathering in a small typical karstic catchment of Southwest China: Isotopic and chemical constraints. *Chemical Geology* 277, 301-309.
- Liu, Z., Li, Q., Sun, H., Wang, J. 2007. Seasonal, diurnal and storm-scale hydrochemical variations of typical epikarst springs in subtropical karst areas of SW China: Soil CO<sub>2</sub> and dilution effects. *Journal of Hydrology* 337, 207-223.
- Liu, Z., Dreybrodt, W., Wang, H. 2010. A new direction in effective accounting for the atmospheric CO<sub>2</sub> budget: Considering the combined action of carbonate dissolution, the global water cycle and photosynthetic uptake of DIC by aquatic organisms. *Earth-Science Reviews* 99, 162-172.
- Martin, J.B., Dean, R.W. 2001. Exchange of water between conduits and matrix in the Floridan aquifer. *Chemical Geology* 179, 145-165.
- McClanahan, K., Polk, J.S., Groves, C., Osterhoudt, L., Grubbs, S. 2016. Dissolved Inorganic Carbon Sourcing using  $\delta^{13}\text{C}_{\text{DIC}}$  from a Karst Influenced River System. *Earth Surface Processes and Landforms* 41(3), 392-405.
- Michaud, J.P., Wierenga, M. 2005. *Estimating discharge and stream flows: a guide for sand and gravel operations*. Olympia, WA: Washington State Department of Ecology 05-10-070. Accessed August 1, 2016, from: [fortress.wa.gov/ecy/publications/documents/0510070.pdf](http://fortress.wa.gov/ecy/publications/documents/0510070.pdf)
- Milanolo, S., Gabrovšek, F. 2015. Estimation of carbon dioxide flux degassing from percolating waters in a karst cave: case study from Bijambare cave, Bosnia and Herzegovina. *Chemie der Erde* 75, 465-474.
- Myroie, J.E. 2013. Coastal karst development in carbonate rocks. In: Lace, M.J., Myroie, J.E. (eds.), *Coastal Karst Landforms*. New York, NY: Coastal Research Library 5, Springer Science and Business Media, 77-109.
- Neal, C. 2001. Alkalinity measurements within natural waters: towards a standardized approach. *The Science of the Total Environment* 265, 99-113.

- Nedvidek, D. 2014. *Evaluating the effectiveness of regulatory stormwater monitoring protocols on groundwater quality in urbanized karst regions*. M.S. Geoscience thesis, Department of Geography and Geology, Western Kentucky University, Bowling Green, KY. Accessed April 1, 2016, from: <http://digitalcommons.wku.edu/theses/1407/>.
- NOAA (National Oceanic and Atmospheric Administration). 2016. *Current rates of atmospheric carbon dioxide in parts per million*. Washington, D.C.: NOAA. Accessed April 1, 2016, from [www.esrl.noaa.gov/gmd/ccgg/trends/global.html](http://www.esrl.noaa.gov/gmd/ccgg/trends/global.html)
- Osterhoudt, L.L. 2014. *Impacts of carbonate mineral weathering on hydrochemistry of the Upper Green River Basin, Kentucky*. M.S. Geoscience thesis, Department of Geography and Geology, Western Kentucky University, Bowling Green, KY. Accessed April 26, 2016, from: <http://digitalcommons.wku.edu/theses/1337/>
- Palmer, A.N. 1991. Origin and morphology of limestone caves. *Geological Society of America Bulletin* 103, 1-21.
- Palmer, A.N. 2003a. Speleogenesis in carbonate rocks. *Speleogenesis and Evolution of Karst Aquifers* 1(1), 1-11 (republished article available online at: <http://www.speleogenesis.info/journal/issue/?issue=1>).
- Palmer, A.N. 2003b. Dynamics of cave development by allogenic water. *Speleogenesis and Evolution of Karst Aquifers* 1(1), 1-11 (republished article available online at: <http://www.speleogenesis.info/journal/issue/?issue=1>).
- Palmer, A.N. 2007a. *Cave Geology*. Dayton, OH: Cave Books.
- Palmer, A.N. 2007b. Variation in rates of karst processes. *Acta Carsologica* 36(1), 15-24.
- Paylor, R.L., Currens, J.C. 2002. *Karst Occurrence in Kentucky*. Lexington, KY: Kentucky Geological Survey, University of Kentucky, Map and Chart 33, Series XII.
- Perrin, J., Jeannin, P-Y., Zwahlen, F. 2003. Epikarst storage in a karst aquifer: a conceptual model based on isotopic data, Milandre test site, Switzerland. *Journal of Hydrology* 279, 106-124.
- Petrella, E., Capuano, P., Celico, F. 2007. Unusual behavior of epikarst in the Acqua dei Faggi carbonate aquifer (Southern Italy). *Terra Nova* 19, 82-88.



- Peyraube, N., Lastennet, R., Denis, A. 2012. Geochemical evolution of groundwater in the unsaturated zone of a karstic massif, using the  $P_{CO_2}$ - $SI_C$  relationship. *Journal of Hydrology* 430-431, 13-24.
- Peyraube, N., Lastennet, R., Denis, A., Malaurent, P. 2013. Estimation of epikarst air  $P_{CO_2}$  using measurements of water  $\delta^{13}C_{TDIC}$ , cave air  $P_{CO_2}$  and  $\delta^{13}C_{CO_2}$ . *Geochimica et Cosmochimica Acta* 118, 1-17.
- Peyraube, N., Lastennet, A., Denis, A., Malaurent, P., Villanueva, J.D. 2014. Interpreting  $CO_2$ - $SI_C$  relationship to estimate  $CO_2$  baseline in limestone aquifers. *Environmental Earth Science* 72, 4207-4215.
- Phillips D.L., Jillion W.G. 2003. Source partitioning using stable isotopes: coping with too many sources. *Oecologia* 136, 261–269.
- Pu, J., Cao, M., Zhang, Y., Yuan, D., Zhao, H. 2014a. Hydrochemical indications of human impact on karst groundwater in a subtropical karst area, Chongqing, China. *Environmental Earth Science* 72, 1683-1695.
- Pu, J., Yuan, D., Zhao, H., Shen, L. 2014b. Hydrochemical and  $P_{CO_2}$  variations of a cave stream in a subtropical karst area, Chongqing, SW China: piston effects, dilution effects, soil  $CO_2$  and buffer effects. *Environmental Earth Science* 71, 4039-4049.
- Ray, J.A., Blair, R.J. 2005. Large perennial springs in Kentucky: Their identification, base flow, catchment, and classification. In: Beck, B.F. (ed.) *Sinkholes and the Engineering and Environmental Impacts of Karst*, Reston, VA: Geotechnical Special Publication No. 144, American Society of Civil Engineers, 410-422.
- Ritter, D.F., Kochel, R.C., Miller, J.R. 2002. *Process Geomorphology* (4<sup>th</sup> Edn.). Boston, MA: McGraw Hill Higher Education.
- Salley, C. Groves, C. 2016. Measurement of inorganic carbon fluxes from large river basins in south-central Kentucky karst. In: Trimboli, S.R., Dodd, L.E., Young, D. (eds.) *Proceedings for Celebrating the Diversity of Research in the Mammoth, Cave Region*. Park City, KY: 11th Research Symposium at Mammoth Cave National Park, 123-127.
- Schulte, P., Geldern, R.V., Freitag, H., Karim, A., Negrel, P., Petelet-Giraud, E., Probst, A., Probst, J., Telmer, K., Veizer, J., Barth., J.A.C. 2011. Applications of stable water and carbon isotopes in watershed research: Weathering carbon cycling and water balances. *Earth Science Reviews* 109, 20-31.

- Shen, L., Deng, X., Jiang, Z., Li, T. 2013. Hydroecogeochemical effects of an epikarst ecosystem: case study of the Nogla Landiantang Spring catchment. *Environmental Earth Science* 68, 667-677.
- Shin, W.J., Chung, G.S., Lee, D., Lee, K.S. 2011. Dissolved inorganic carbon export from carbonate and silicate catchments estimated from carbonate chemistry and  $\delta^{13}\text{C}_{\text{DIC}}$ . *Hydrology and Earth System Sciences* 15, 2551-2560.
- Sinclair, D.J., Banner, J.L., Taylor, F.W., Partin, J., Jenson, J., Mylroie, J., Goddard, E., Quinn, T., Jocson, J., Miklavič, B. 2012. Magnesium and strontium systematics in tropical speleothems from the Western Pacific. *Chemical Geology* 294-295, 1-17.
- Singh, V.B., Ramanathan, A., Pottakkal, J.G., Sharma, P., Linda, A., Azam, M.F., Chatterjee, C. 2012. Chemical characterization of meltwater draining from Gangotri Glacier, Garhwal Himalaya, India. *Journal of Earth System Science* 121(3), 625-636.
- Stefansson, A., Gunnarsson, I., Giroud, N. 2007. New methods for the direct determination of dissolved inorganic carbon, organic and total carbon in natural waters by Reagent-Free<sup>TM</sup> Ion Chromatography and inductively coupled plasma atomic emission spectrometry. *Analytical Chimica Acta* 582, 69-74.
- Telmer, K., Veizer, J. 1999. Carbon fluxes,  $p\text{CO}_2$  and substrate weathering in a large northern river basin, Canada: carbon isotope perspectives. *Chemical Geology* 159, 61-86.
- Trček, B. 2007. How can the epikarst zone influence the karst aquifer hydraulic behavior? *Environmental Geology* 51, 761-765.
- USDA (United States Department of Agriculture). 2017. Custom soil resource report for Warren County, Kentucky. Washington, D.C.: USDA, Natural Resources Conservation. Accessed April 2, 2017, from: [websoilsurvey.sc.egov.usda.gov/App/HomePage.htm](http://websoilsurvey.sc.egov.usda.gov/App/HomePage.htm)
- USDOE (United States Department of Energy). 2008. *The Carbon Cycle*. Washington, D.C. Office of Science. Accessed on June 30, 2017, from: <http://genomicscience.energy.gov/carboncycle/index.shtml>
- Vacher, H.L., Mylroie, J.E. 2002. Eogenetic karst from the perspective of an equivalent porous medium. *Carbonates and Evaporites* 17(2), 182-196.

- Vanderhoff, S. 2011. *Multiple storm event impacts on epikarst storage and transport of organic soil amendments in South-Central Kentucky*. M.S. Geoscience thesis, Department of Geography and Geology, Western Kentucky University, Bowling Green, KY. Accessed April 1, 2016, from: <http://digitalcommons.wku.edu/theses/1128/>
- Veni, G., DuChene, H., Crawford, N., Groves, C., Huppert, G., Kastning, E., Olson, R., Wheeler, B. 2001. *Living with Karst: A Fragile Foundation*. Alexandria, VA: American Geological Institute, AGI Environmental Awareness Series.
- Vesper, D.J. White, W.B. 2004. Storm pulse chemographs of saturation index and carbon dioxide pressure: implications for shifting recharge sources during storm events in the karst aquifer at Fort Campbell, Kentucky/Tennessee, USA. *Hydrogeology Journal* 12, 135-143.
- Wagner, R.J., Boulger, R.W., Jr., Oblinger, C.J., Smith, B.A. 2006. *Guidelines and standard procedures for continuous water-quality monitors—Station operation, record computation, and data reporting*. Reston, VA: U.S. Geological Survey Techniques and Methods 1–D3, 1-51. Accessed on March 18, 2017 from: <http://pubs.water.usgs.gov/tm1d3>
- White, W.B. 1988. *Geomorphology and Hydrology of Karst Terrains*. New York, NY: Oxford University Press.
- White, W.B. 2003. Conceptual models for karst aquifers. *Speleogenesis and Evolution of Karst Aquifers* 1(1), 2. Re-published by permission from: Palmer, A.N., Palmer, M.V., and Sasowsky, I.D. (eds.), *Karst Modeling: Special Publication 5, The Karst Waters Institute*, Charles Town, West Virginia (USA), 11-16.
- White, W.B. 2007. A brief history of karst hydrogeology: contributions of the NSS. *Journal of Cave and Karst Studies* 69(1), 13-26.
- White, W.B. 2013. Carbon fluxes in karst aquifers: sources, sinks, and the effect of storm flow. *Acta Carsologica* 42(2-3), 177-186.
- White, W.B. 2015. Carbon fluxes in karst aquifers: sources, sinks, and the effect of storm flow. *Acta Carsologica* 42(2), 177-186.
- White, W.B., White, E.L. 1989. *Karst Hydrology: Concepts from the Mammoth Cave Area*. New York, NY: Van Nostrand Reinhold.

- White, W.B., White, E.L. 2005. Groundwater flux distribution between matrix, fractures, and conduits: constraints on modeling. *Speleogenesis and Evolution of Karst Aquifers* 3(2), 2-6.
- Wilde, F.D., Sandstrom, M.W., Skrobialowski, S.C. 2015. *National field manual for the collection of water-quality data*. Reston, VA: U.S. Geological Survey, Techniques of Water-Resources Investigations, Book 9. Accessed December 9, 2016, from: [water.usgs.gov/owq/FieldManual/](http://water.usgs.gov/owq/FieldManual/)
- Williams, P.W. 1983. The role of the subcutaneous zone in karst hydrology. *Journal of Hydrology* 61, 45-67.
- Williams, P.W. 2008. The role of the epikarst in karst and cave hydrogeology: a review. *International Journal of Speleology* 37(1), 1-10.
- Wong, C.I., Mahler, B.J., Musgrove, M. Banner, J.L. 2012. Change in sources and storage in a karst aquifer during a transition from drought to wet conditions. *Journal of Hydrology* 468-469, 159-172.
- Worthington, S.R.H. 2003. *Conduits and turbulent flow in the Edwards aquifer*. San Antonio, TX: Edwards Aquifer Authority.
- Worthington, S.R.H. 2007. Groundwater residence times in unconfined carbonate aquifers. *Journal of Cave and Karst Studies* 69(1), 94-102.
- Worthington, S.R.H., Ford, D.C., Davis, G.J. 2000. Matrix, fracture and channel components of storage and flow in a Paleozoic limestone aquifer. In Sasowsky, I.D., Wicks, C.M. (eds.) *Groundwater Flow and Contaminant Transport in Carbonate Aquifers*. New York, NY: Taylor and Francis, 113-128
- Yang, R.Y., Liu, Z., Min Zhao, C.Z. 2012. Response of epikarst hydrochemical changes to soil CO<sub>2</sub> and weather conditions at Chenqi, Puding, SW China. *Journal of Hydrology* 468-469, 151-158.
- YSI (Yellow Springs Instrument). 2013. 6-Series Multi-Parameter Water Quality Sondes User Manual. Yellow Springs, OH: YSI Incorporated. Accessed January 27, 2016, from: [www.ysi.com/File%20Library/Documents/Manuals/069300-YSI-6-Series-Manual-RevJ.pdf](http://www.ysi.com/File%20Library/Documents/Manuals/069300-YSI-6-Series-Manual-RevJ.pdf)

- Zaihua, L., Daoxian, Y., Shiyi, H. 1997. Stable carbon isotope geochemical and hydrochemical features in the system of carbonate – H<sub>2</sub>O-CO<sub>2</sub> and their implications-evidence from several typical karst areas of China. *Acta Geologica Sinica* 71(4), 446-454.
- Zeng, C. Liu, A., Zhao, M., Yang, R. 2016. Hydrologically-driven variations in the karst-related carbon sink fluxes: Insights from high-resolution monitoring of three karst catchments in Southwest China. *Journal of Hydrology* 533, 74-90.
- Zhang, J., Quay, P.D., Wilbour, D.O. 1995. Carbon isotope fractionation during gas-water exchange and dissolution of CO<sub>2</sub>. *Geochemica et Cosmochemica Acta* 59, 107-114.
- Zhang, L., Qin, X., Liu, P., Huang, Q., Lan, F., Ji, H. 2015. Estimation of carbon sink fluxes in the Pearl River basin (China) based on a water-rock-gas-organism interaction model. *Environmental Earth Science* 74, 945-952.
- Zhang, C., Wang, J., Yan, J., Pei, J. 2016. Diel cycling and flux of HCO<sub>3</sub> in a typical karst spring-fed stream of southwestern China. *Acta Carsologica* 45(1), 107-122.
- Zhao, M., Liu, Z., Li, H-C., Zeng, C., Yang, R., Chen, B., Yan, H. 2015. Response of dissolved inorganic carbon (DIC) and  $\delta^{13}\text{C}_{\text{DIC}}$  to changes in climate and land cover in SW China karst catchments. *Geochimica et Cosmochimica Acta* 165, 123-136.
- Zhongcheng, J., Daoxian, Y. 1999. CO<sub>2</sub> source-sink in karst processes in karst areas of China. *Episodes* 22(1), 33-35.
- Zogg, G.P., Zak, D.R., Ringelberg, D.B., White, D.C., MacDonald, N.W., Pregitzer, K.S. 1995. Compositional and functional shifts in microbial communities due to soil warming. *Alliance of Crop, Soil, and Environmental Science Societies* 61(2), 475-481.

## Appendix 1: Crumps-WF1 Mixing Model Results

Mixture Date	N Value	Relative Contributions by Source %											
		Atmosphere				Soil				Bedrock			
		Mean	Min	Max	Std	Mean	Min	Max	Std	Mean	Min	Max	Std
5/24/2016	269	24.5	0.0	54.0	14.6	65.6	46.0	82.0	8.9	9.9	0.0	22.0	6.1
5/31/2016	269	24.5	0.0	54.0	14.6	65.6	46.0	82.0	8.9	9.9	0.0	22.0	6.1
6/7/2016	228	21.6	0.0	48.0	12.9	69.1	52.0	83.0	7.6	9.3	0.0	21.0	5.7
6/14/2016	184	17.2	0.0	39.0	10.5	75.6	61.0	88.0	6.3	7.2	0.0	17.0	4.6
6/21/2016	62	5.8	0.0	16.0	4.2	92.2	84.0	98.0	3.4	2.0	0.0	6.0	1.7
6/28/2016	113	11.0	0.0	26.0	6.9	84.4	74.0	93.0	4.4	4.6	0.0	11.0	3.0
7/6/2016	133	12.8	0.0	30.0	7.9	81.7	70.0	91.0	4.8	5.5	0.0	13.0	3.6
7/12/2016	147	14.5	0.0	33.0	8.9	79.0	67.0	89.0	5.2	6.5	0.0	15.0	4.2
7/19/2016	115	11.1	0.0	26.0	6.9	84.1	74.0	92.0	4.3	4.8	0.0	12.0	3.2
7/26/2016	75	7.3	0.0	18.0	4.8	89.7	82.0	96.0	3.3	3.1	0.0	8.0	2.2
8/2/2016	399	38.7	0.0	82.0	22.8	44.0	18.0	67.0	12.6	17.3	0.0	37.0	10.3
8/9/2016	327	31.7	0.0	67.0	18.7	17.1	0.0	36.0	10.2	51.2	33.0	68.0	8.7
8/16/2016	319	31.5	0.0	67.0	18.6	54.5	33.0	74.0	10.4	14.0	0.0	30.0	8.4
8/24/2016	308	29.8	0.0	64.0	17.6	56.9	36.0	75.0	9.9	13.3	0.0	29.0	8.0
8/31/2016	275	30.3	0.0	64.0	17.8	54.1	36.0	70.0	8.8	15.6	0.0	33.0	9.2
9/7/2016	286	34.1	0.0	71.0	20.2	46.5	29.0	64.0	9.1	19.0	0.0	40.0	11.2
9/14/2016	267	26.3	0.0	57.0	15.6	62.0	43.0	78.0	8.8	11.7	0.0	26.0	7.1
9/21/2016	283	27.5	0.0	59.0	16.2	60.3	41.0	77.0	9.1	12.2	0.0	27.0	7.4
9/28/2016	264	26.0	0.0	56.0	15.4	62.5	44.0	79.0	8.7	11.5	0.0	25.0	7.0
10/5/2016	317	30.6	0.0	66.0	18.1	55.7	34.0	75.0	10.1	13.7	0.0	30.0	8.3
10/12/2016	286	27.7	0.0	60.0	16.4	60.1	40.0	77.0	9.2	12.3	0.0	27.0	7.5
10/19/2016	367	35.7	0.0	76.0	21.0	48.4	24.0	70.0	11.6	15.9	0.0	34.0	9.5
10/26/2016	287	28.3	0.0	61.0	16.8	59.1	39.0	77.0	9.4	12.6	0.0	27.0	7.6
11/2/2016	126	10.6	0.0	27.0	7.0	85.9	73.0	96.0	5.3	3.5	0.0	9.0	2.5
11/9/2016	354	30.5	0.0	67.0	18.1	58.1	33.0	79.0	11.5	11.4	0.0	25.0	6.9
11/16/2016	487	41.8	0.0	90.0	24.6	42.7	10.0	71.0	15.3	15.5	0.0	34.0	9.3
11/23/2016	539	47.1	0.0	100.0	27.7	34.8	0.0	66.0	17.1	18.1	0.0	39.0	10.8
11/30/2016	493	40.7	0.0	88.0	24.0	45.2	12.0	74.0	15.8	14.1	0.0	31.0	8.5
12/7/2016	560	47.6	0.0	99.0	27.9	29.8	0.0	62.0	17.5	22.6	1.0	43.0	10.9
12/13/2016	563	44.1	0.0	92.0	25.8	29.3	0.0	61.0	17.2	26.6	8.0	44.0	8.9
12/20/2016	463	46.0	0.0	96.0	26.9	24.8	0.0	52.0	14.7	29.1	4.0	52.0	12.4
12/27/2016	498	48.4	0.0	100.0	28.3	29.6	0.0	58.0	15.6	22.0	0.0	46.0	12.9
1/3/2017	504	49.0	0.0	100.0	28.6	28.0	0.0	57.0	15.7	22.9	0.0	47.0	13.1
1/11/2017	483	47.2	0.0	98.0	27.6	25.5	0.0	53.0	15.1	27.3	2.0	51.0	12.7
1/18/2017	503	48.9	0.0	100.0	28.6	27.0	0.0	56.0	15.6	24.1	0.0	48.0	13.1
1/25/2017	432	42.6	0.0	89.0	25.0	23.1	0.0	48.0	13.6	34.3	11.0	56.0	11.5
2/1/2017	579	46.4	0.0	100.0	27.6	38.1	0.0	72.0	18.6	15.5	0.0	34.0	9.3
2/8/2017	584	48.4	0.0	100.0	28.3	34.0	0.0	68.0	18.4	17.5	0.0	37.0	10.1
2/15/2017	528	43.6	0.0	91.0	25.5	28.1	0.0	59.0	16.5	28.4	9.0	46.0	9.3
2/22/2017	568	48.8	0.0	100.0	28.5	31.5	0.0	64.0	17.8	19.7	0.0	41.0	10.9
3/1/2017	559	46.2	0.0	99.0	27.1	37.8	1.0	70.0	17.9	16.0	0.0	35.0	9.6
3/8/2017	887	47.2	0.0	97.0	26.7	47.6	0.0	100.0	27.8	5.2	0.0	12.0	2.9
3/13/2017													



## Appendix 2: Crumps-SF Mixing Model Results

Mixture Date	N Value	Relative Contributions by Source %											
		Atmosphere				Soil				Bedrock			
		Mean	Min	Max	Std	Mean	Min	Max	Std	Mean	Min	Max	Std
5/24/2016	410	37.7	0.0	80.0	22.1	46.9	20.0	71.0	13.1	15.5	0.0	33.0	9.3
5/31/2016	269	24.5	0.0	54.0	14.6	65.5	46.0	82.0	8.9	9.9	0.0	22.0	6.1
6/7/2016	162	15.3	0.0	35.0	9.3	78.2	65.0	89.0	5.6	6.5	0.0	15.0	4.1
6/14/2016	49	4.8	0.0	13.0	3.5	93.7	87.0	99.0	2.9	1.7	0.0	5.0	1.5
6/21/2016													
6/28/2016	21	2.8	0.0	8.0	2.4	96.9	92.0	100.0	2.1	1.0	0.0	3.0	1.0
7/6/2016	69	6.8	0.0	17.0	4.3	9.4	83.0	96.0	3.2	2.8	0.0	8.0	2.1
7/12/2016	80	7.8	0.0	19.0	5.1	88.9	81.0	95.0	3.4	3.3	0.0	9.0	2.4
7/19/2016	25	2.8	0.0	8.0	2.4	96.0	92.0	100.0	2.0	1.2	0.0	4.0	1.2
7/26/2016	16	2.1	0.0	6.0	1.9	97.0	94.0	100.0	1.6	0.9	0.0	3.0	1.0
8/2/2016	330	32.0	0.0	68.0	18.9	53.7	32.0	73.0	10.5	14.3	0.0	31.0	8.8
8/9/2016	319	31.5	0.0	67.0	18.6	54.5	33.0	74.0	10.4	14.0	0.0	30.0	8.4
8/16/2016	319	31.5	0.0	67.0	18.6	54.5	33.0	74.0	10.4	14.0	0.0	30.0	8.4
8/24/2016	342	33.2	0.0	71.0	19.5	52.1	29.0	72.0	10.9	14.8	0.0	32.0	8.9
8/31/2016	283	31.2	0.0	66.0	18.5	52.7	34.0	70.0	9.1	16.1	0.0	34.0	9.5
9/7/2016	254	30.5	0.0	64.0	18.0	52.8	36.0	68.0	8.1	16.7	0.0	35.0	10.0
9/14/2016	233	22.7	0.0	50.0	13.5	67.3	50.0	82.0	7.7	10.0	0.0	22.0	6.1
9/21/2016	252	24.8	0.0	54.0	14.8	64.2	46.0	80.0	8.3	11.0	0.0	24.0	6.7
9/28/2016	268	25.9	0.0	56.0	15.4	62.5	44.0	79.0	8.7	11.5	0.0	25.0	7.0
10/5/2016	179	17.2	0.0	39.0	10.4	75.3	61.0	87.0	6.1	7.5	0.0	17.0	4.7
10/12/2016	347	34.3	0.0	73.0	20.2	50.4	27.0	71.0	11.2	15.3	0.0	33.0	9.2
10/19/2016	206	19.9	0.0	44.0	11.9	71.3	56.0	84.0	6.9	8.8	0.0	20.0	5.4
10/26/2016	337	33.3	0.0	71.0	19.6	51.9	29.0	72.0	10.9	14.9	0.0	32.0	8.9
11/2/2016	226	18.7	0.0	44.0	11.4	75.1	56.0	90.0	8.0	6.3	0.0	15.0	4.0
11/9/2016													
11/16/2016	487	41.7	0.0	87.0	24.4	25.8	0.0	54.0	15.2	32.4	13.0	51.0	9.5
11/23/2016	473	41.5	0.0	87.0	24.4	25.2	0.0	53.0	14.9	33.2	13.0	52.0	9.7
11/30/2016	575	47.5	0.0	99.0	27.8	30.5	0.0	64.0	18.0	22.1	1.0	41.0	10.0
12/7/2016	444	37.7	0.0	79.0	22.1	23.6	0.0	50.0	13.5	38.8	21.0	55.0	8.5
12/13/2016	448	35.0	0.0	74.0	20.5	23.1	0.0	49.0	13.7	41.5	26.0	56.0	7.2
12/20/2016	423	41.8	0.0	87.0	24.5	22.6	0.0	47.0	13.4	35.6	13.0	57.0	11.3
12/27/2016	503	48.9	0.0	100.0	28.6	27.1	0.0	56.0	15.6	24.0	0.0	48.0	13.1
1/3/2017	478	46.8	0.0	97.0	27.2	25.1	0.0	52.0	14.8	28.4	3.0	52.0	12.5
1/11/2017	478	47.3	0.0	98.0	27.7	25.6	0.0	53.0	15.1	27.1	2.0	51.0	12.7
1/18/2017	504	49.0	0.0	100.0	28.6	27.4	0.0	56.0	15.7	23.6	0.0	48.0	13.1
1/25/2017	423	41.0	0.0	86.0	24.1	22.2	0.0	47.0	13.1	36.8	14.0	58.0	11.1
2/1/2017	596	48.8	0.0	100.0	28.1	31.6	0.0	66.0	18.6	19.8	0.0	39.0	9.7
2/8/2017													
2/15/2017	444	43.2	0.0	90.0	25.3	23.3	0.0	49.0	13.8	33.5	10.0	55.0	11.7
2/22/2017	566	48.7	0.0	100.0	28.4	30.4	0.0	63.0	17.7	20.9	0.0	42.0	11.0
3/1/2017	570	47.0	0.0	98.0	27.5	30.2	0.0	63.0	17.8	22.8	2.0	42.0	10.0
3/8/2017	854	43.8	0.0	91.0	25.4	45.7	0.0	96.0	26.7	10.8	4.0	17.0	3.0
3/13/2017	446	41.0	0.0	86.0	24.1	23.7	0.0	50.0	14.0	35.3	14.0	55.0	10.3

### Appendix 3: LRCV-LRS Mixing Model Results

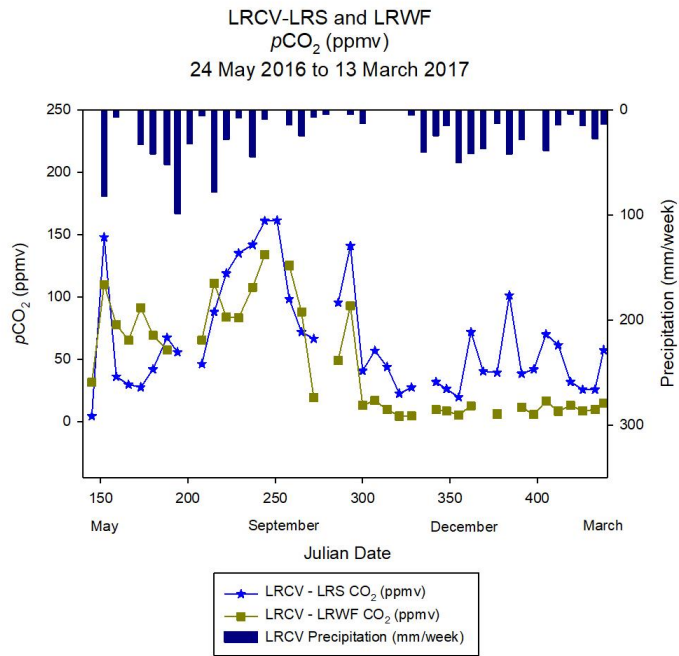
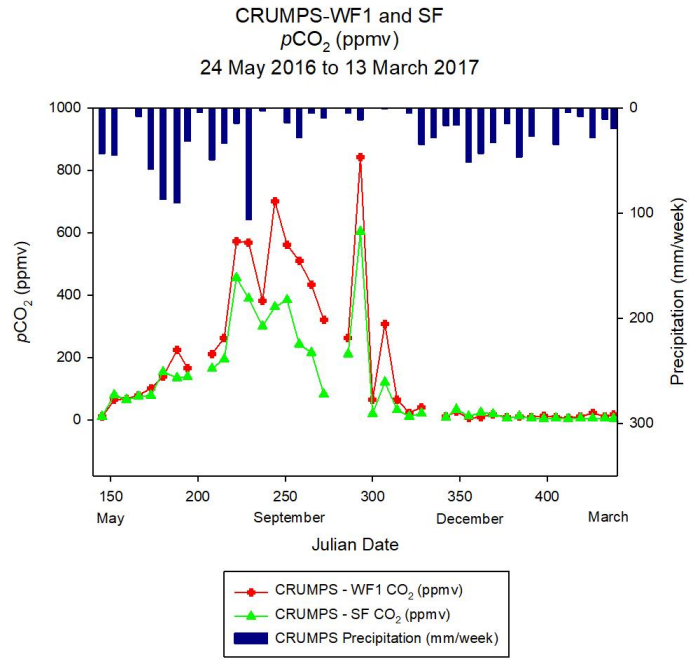
Mixture Date	N Value	Relative Contributions by Source %											
		Atmosphere				Soil				Bedrock			
		Mean	Min	Max	Std	Mean	Min	Max	Std	Mean	Min	Max	Std
5/24/2016	366	35.6	0.0	75.0	20.9	19.1	0.0	40.0	11.4	45.4	25.0	64.0	9.7
5/31/2016	257	25.3	0.0	54.0	15.0	13.6	0.0	29.0	8.2	61.2	46.0	75.0	7.1
6/7/2016	208	20.4	0.0	45.0	12.3	70.6	53.0	84.0	7.0	9.0	0.0	20.0	5.6
6/14/2016	197	19.3	0.0	43.0	11.6	72.2	57.0	85.0	6.7	8.5	0.0	19.0	5.3
6/21/2016	158	15.5	0.0	35.0	9.4	77.8	65.0	88.0	5.6	6.8	0.0	16.0	4.3
6/28/2016	166	16.0	0.0	36.0	9.7	77.0	64.0	88.0	5.7	7.0	0.0	16.0	4.4
7/6/2016	177	17.1	0.0	38.0	10.3	75.4	62.0	87.0	6.0	7.5	0.0	17.0	4.7
7/12/2016	166	16.0	0.0	36.0	9.7	77.0	64.0	88.0	5.7	7.0	0.0	16.0	4.4
7/19/2016	147	14.4	0.0	33.0	8.8	79.4	67.0	89.0	5.3	6.3	0.0	15.0	4.0
7/26/2016	138	13.3	0.0	31.0	8.2	81.0	69.0	90.0	4.9	5.7	0.0	14.0	3.7
8/2/2016	319	30.9	0.0	66.0	18.3	55.3	34.0	74.0	10.2	13.8	0.0	30.0	8.3
8/9/2016	444	43.1	0.0	91.0	25.3	37.6	9.0	63.0	14.0	19.3	0.0	41.0	11.5
8/16/2016	228	22.0	0.0	48.0	13.1	68.2	52.0	82.0	7.5	9.8	0.0	22.0	6.0
8/24/2016	444	43.1	0.0	91.0	25.3	37.6	9.0	63.0	14.0	19.3	0.0	41.0	11.5
8/31/2016	255	24.7	0.0	54.0	14.7	64.4	46.0	80.0	8.3	10.9	0.0	24.0	6.7
9/7/2016	276	26.7	0.0	58.0	15.8	61.5	42.0	78.0	8.9	11.8	0.0	26.0	7.2
9/14/2016	277	26.7	0.0	58.0	15.9	61.4	42.0	78.0	8.9	11.9	0.0	26.0	7.2
9/21/2016	240	23.2	0.0	51.0	13.8	66.6	49.0	81.0	7.8	10.2	0.0	23.0	6.3
9/28/2016	287	28.3	0.0	61.0	16.8	59.1	39.0	77.0	9.4	12.6	0.0	27.0	7.6
10/5/2016	299	28.9	0.0	62.0	17.1	58.2	38.0	76.0	9.6	12.9	0.0	28.0	7.8
10/12/2016	196	18.9	0.0	42.0	11.4	72.8	58.0	85.0	6.6	8.3	0.0	19.0	5.2
10/19/2016	197	19.3	0.0	43.0	11.6	72.2	57.0	85.0	6.7	8.5	0.0	19.0	5.3
10/26/2016	160	15.3	0.0	35.0	9.4	78.0	65.0	89.0	5.6	6.7	0.0	16.0	4.3
11/2/2016	194	18.7	0.0	42.0	11.2	73.1	58.0	85.0	6.5	8.2	0.0	19.0	5.1
11/9/2016	297	29.3	0.0	63.0	17.3	57.7	37.0	76.0	9.7	13.0	0.0	28.0	7.9
11/16/2016	221	21.4	0.0	47.0	12.8	69.2	53.0	83.0	7.3	9.4	0.0	21.0	5.8
11/23/2016	246	23.8	0.0	52.0	14.2	65.7	48.0	81.0	8.0	10.5	0.0	23.0	6.4
11/30/2016	303	29.3	0.0	63.0	17.4	57.6	37.0	76.0	9.7	13.1	0.0	28.0	7.9
12/7/2016	314	30.4	0.0	65.0	18.0	56.0	35.0	75.0	10.1	13.6	0.0	29.0	8.2
12/13/2016	324	32.0	0.0	68.0	18.9	53.8	32.0	73.0	10.5	14.3	0.0	31.0	8.6
12/20/2016	322	31.3	0.0	67.0	18.4	54.8	33.0	74.0	10.3	13.9	0.0	30.0	8.4
12/27/2016	287	27.7	0.0	60.0	16.5	59.9	40.0	77.0	9.2	12.3	0.0	27.0	7.5
1/3/2017	222	21.5	0.0	47.0	12.8	69.0	53.0	83.0	7.3	9.5	0.0	21.0	5.8
1/11/2017	243	23.7	0.0	52.0	14.1	65.8	48.0	81.0	8.0	10.4	0.0	23.0	6.4
1/18/2017	196	18.9	0.0	42.0	11.4	72.8	58.0	85.0	6.6	8.3	0.0	19.0	5.2
1/25/2017	230	22.2	0.0	49.0	13.2	68.0	51.0	82.0	7.5	9.8	0.0	22.0	6.0
2/1/2017													
2/8/2017	192	18.8	0.0	42.0	11.3	72.9	58.0	85.0	6.6	8.3	0.0	19.0	5.1
2/15/2017	216	20.9	0.0	46.0	12.5	69.9	54.0	83.0	7.2	9.2	0.0	21.0	5.7
2/22/2017	228	22.0	0.0	48.0	13.1	68.2	52.0	82.0	7.5	9.8	0.0	22.0	6.0
3/1/2017	176	17.0	0.0	38.0	10.3	75.5	62.0	87.0	6.0	7.5	0.0	17.0	4.7
3/8/2017	225	21.7	0.0	48.0	13.0	68.8	52.0	83.0	7.4	9.6	0.0	21.0	5.9
3/13/2017													



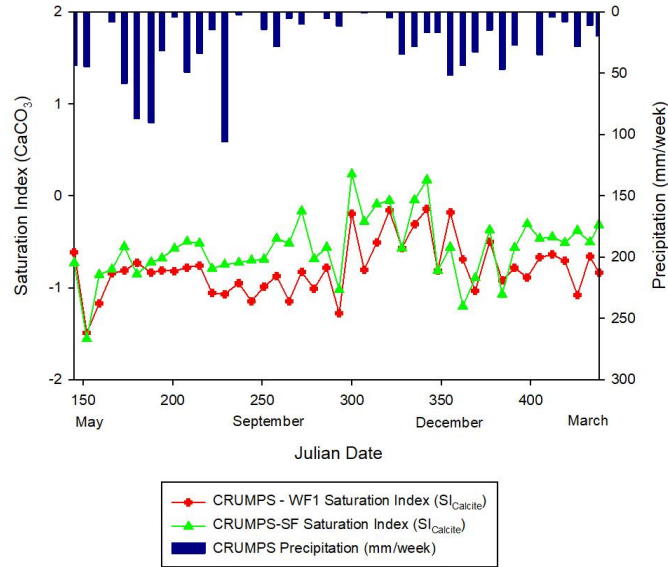
**Appendix 4: I-DCV-I-PWE Mixing Model Results**

Mixture Date	N Value	Relative Contributions by Source %											
		Atmosphere				Soil				Bedrock			
		Mean	Min	Max	Std	Mean	Min	Max	Std	Mean	Min	Max	Std
5/24/2016	347	34.3	0.0	73.0	20.2	50.4	27.0	71.0	11.2	15.3	0.0	33.0	9.2
5/31/2016	128	12.1	0.0	28.0	7.5	82.6	71.0	91.0	4.6	5.3	0.0	13.0	3.4
6/7/2016	93	9.0	0.0	22.0	5.8	87.2	78.0	94.0	3.8	3.8	0.0	10.0	2.6
6/14/2016	119	11.6	0.0	27.0	7.2	83.4	73.0	92.0	4.3	5.0	0.0	12.0	3.3
6/21/2016	119	11.6	0.0	27.0	7.2	83.4	73.0	92.0	4.3	5.0	0.0	12.0	3.3
6/28/2016	119	11.6	0.0	27.0	7.2	83.4	73.0	92.0	4.3	5.0	0.0	12.0	3.3
7/6/2016	153	15.0	0.0	34.0	9.1	78.5	66.0	89.0	5.4	6.5	0.0	15.0	4.1
7/12/2016													
7/19/2016													
7/26/2016	147	14.4	0.0	33.0	8.8	79.4	67.0	89.0	5.3	6.3	0.0	15.0	4.0
8/2/2016	384	37.3	0.0	78.0	21.9	20.1	0.0	42.0	11.9	42.6	22.0	62.0	10.1
8/9/2016	319	30.9	0.0	66.0	18.3	55.3	34.0	74.0	10.2	13.8	0.0	30.0	8.3
8/16/2016	279	27.0	0.0	58.0	16.0	61.0	42.0	78.0	9.0	12.0	0.0	26.0	7.3
8/24/2016	292	28.2	0.0	61.0	16.7	59.3	39.0	77.0	9.4	12.5	0.0	27.0	7.6
8/31/2016	279	27.5	0.0	59.0	16.3	60.3	41.0	77.0	9.1	12.2	0.0	27.0	7.4
9/7/2016	264	26.0	0.0	56.0	15.4	62.5	44.0	79.0	8.7	11.5	0.0	25.0	7.0
9/14/2016	293	28.8	0.0	62.0	17.0	58.5	38.0	76.0	9.5	12.8	0.0	28.0	7.7
9/21/2016	253	24.7	0.0	54.0	14.7	64.4	46.0	80.0	8.3	10.9	0.0	24.0	6.7
9/28/2016	250	24.2	0.0	53.0	14.4	65.1	47.0	80.0	8.1	10.7	0.0	24.0	6.5
10/5/2016	183	17.8	0.0	40.0	10.8	74.4	60.0	86.0	6.3	7.8	0.0	18.0	4.9
10/12/2016	223	21.7	0.0	48.0	13.0	68.8	52.0	83.0	7.4	9.6	0.0	21.0	5.9
10/19/2016	172	16.6	0.0	37.0	10.0	76.1	63.0	87.0	5.9	7.3	0.0	17.0	4.6
10/26/2016	183	17.9	0.0	40.0	10.8	74.2	60.0	86.0	6.3	7.9	0.0	18.0	4.9
11/2/2016	234	23.0	0.0	50.0	13.7	66.8	50.0	81.0	7.8	10.2	0.0	23.0	6.3
11/9/2016	432	41.9	0.0	88.0	24.6	39.2	12.0	64.0	13.6	18.8	0.0	40.0	11.2
11/16/2016	432	41.9	0.0	88.0	24.6	39.2	12.0	64.0	13.6	18.8	0.0	40.0	11.2
11/23/2016	447	44.3	0.0	93.0	25.9	35.9	7.0	62.0	14.3	19.9	0.0	42.0	11.8
11/30/2016	219	21.5	0.0	47.0	12.9	69.0	53.0	83.0	7.3	9.5	0.0	21.0	5.8
12/7/2016	367	36.3	0.0	77.0	21.3	47.5	23.0	69.0	11.8	16.2	0.0	35.0	9.7
12/13/2016	308	29.8	0.0	64.0	17.6	56.9	36.0	75.0	9.9	13.3	0.0	29.0	8.0
12/20/2016	392	38.8	0.0	82.0	22.8	43.9	18.0	67.0	12.6	17.3	0.0	37.0	10.4
12/27/2016	380	36.9	0.0	78.0	21.7	46.6	22.0	69.0	12.0	16.5	0.0	35.0	9.5
1/3/2017													
1/11/2017	342	33.2	0.0	71.0	19.5	52.1	29.0	72.0	10.9	14.8	0.0	32.0	8.9
1/18/2017													
1/25/2017	268	25.8	0.0	56.0	15.4	62.5	44.0	79.0	8.7	11.5	0.0	25.0	7.0
2/1/2017	250	24.2	0.0	53.0	14.4	65.1	47.0	80.0	8.1	10.7	0.0	24.0	6.5
2/8/2017	243	23.7	0.0	52.0	14.1	65.8	48.0	81.0	8.1	10.4	0.0	23.0	6.4
2/15/2017	203	19.5	0.0	43.0	11.7	71.8	57.0	85.0	6.8	8.7	0.0	19.0	5.3
2/22/2017	194	19.0	0.0	42.0	11.4	72.6	58.0	85.0	6.6	8.4	0.0	19.0	5.2
3/1/2017													
3/8/2017	210	20.2	0.0	45.0	12.1	70.9	55.0	84.0	7.0	8.9	0.0	20.0	5.5
3/13/2017													

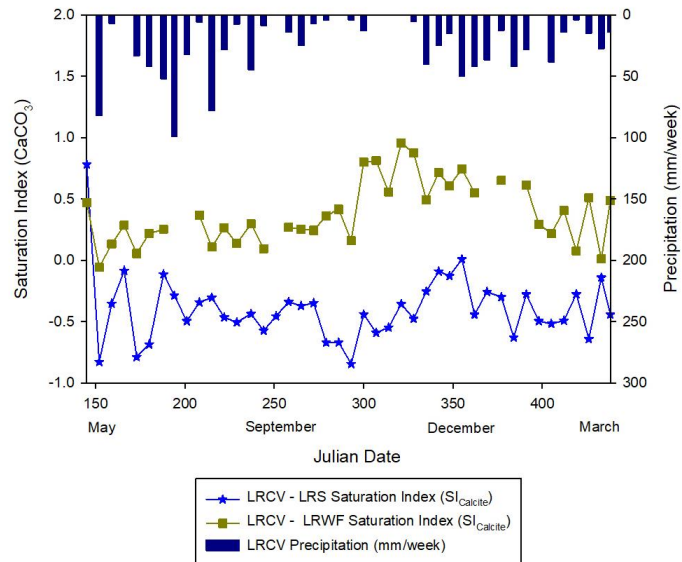
## Appendix 5: Low Resolution Geochemical Time Series



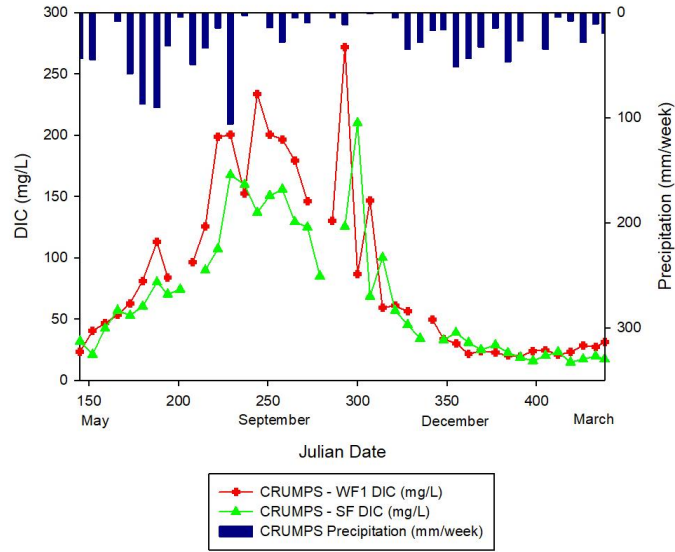
CRUMPS-WF1 and SF  
Saturation Index ( $SI_{\text{Calcite}}$ )  
24 May 2016 to 13 March 2017



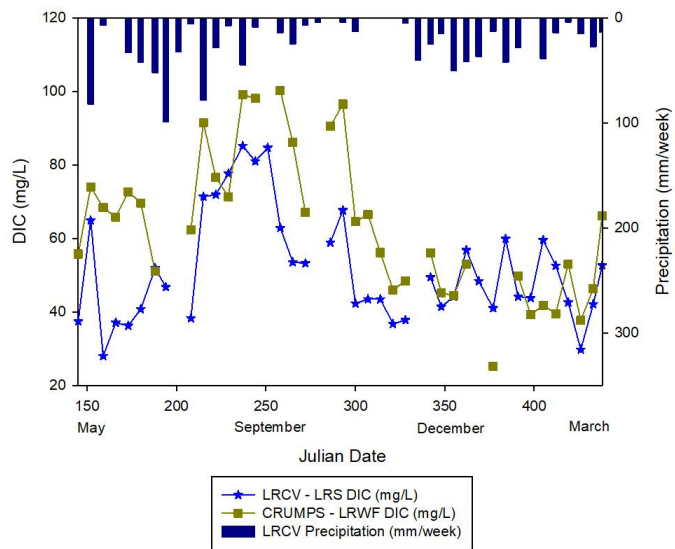
LRCV-LRS and LRWF  
Saturation Index ( $SI_{\text{Calcite}}$ )  
24 May 2016 to 13 March 2017



CRUMPS-WF1 and SF  
Dissolved Inorganic Carbon (DIC)  
24 May 2016 to 13 March 2017



LRCV-LRS and LRWF  
Dissolved Inorganic Carbon (DIC)  
24 May 2016 to 13 March 2017



## Appendix 6: Recharge versus Discharge at Each Site

